Master's thesis

NTNU
Norwegian University of Science and Technology
Faculty of Engineering
Department of Geoscience and Petroleum

Wilson Wiranda

Simulation of Pre-ACT Injection and Development of Proxy Model for Svelvik CO2 Field Laboratory

Master's thesis in Petroleum Engineering
Supervisor: Ashkan Jahanbani Ghahfarokhi
Co-supervisor: Cathrine Ringstad
June 2022

NTNU
Kunnskap for en bedre verden

Wilson Wiranda

Simulation of Pre-ACT Injection and Development of Proxy Model for Svelvik CO2 Field Laboratory

Master's thesis in Petroleum Engineering
Supervisor: Ashkan Jahanbani Ghahfarokhi
Co-supervisor: Cathrine Ringstad
June 2022

Norwegian University of Science and Technology
Faculty of Engineering
Department of Geoscience and Petroleum

NTNU
Norwegian University of
Science and Technology

"All models are wrong, but some are useful" - (Box, 1976)

Abstract

A small-scale CO_2 field laboratory was established in Svelvik, Norway, from 2009 to 2013. The site was characterized during 2009 and 2010, starting from drilling, sampling and logging from Svelvik#1 exploration well. In 2012, Svelvik#2 was drilled as the main CO_2 injector with the completed interval on the depth of 64-65m.

The main objectives of this study are: to build a history match model based on the Pre-ACT 2019 injection data, understand the uncertainties and finally develop a proxy model that can mimic the numerical simulation result of the Svelvik CO_2 field laboratory. The proxy model can be used to design the CO_2 injection rate for the next injection campaign and be input for updating the reservoir model. With the proxy model availability, the previous numerical simulation of Svelvik CO_2 injection that requires hours to obtain results can be reduced to seconds.

After the model is history matched, the prediction scenario is designed as two cycles of injections with the duration of 1 week of injection and 1 week of shut-in period for each cycle. The CO_2 injection rate is designed by using a modified fractional factorial sampling. 18 different injection cases were simulated and the results are used for training proxy models. A proxy model is defined as a function that approximates the response of the full physics model for a given set of input values. The proxy models used in this study are response surface proxy and universal kriging proxy. The inputs for the proxy models are 1^{st} and 2^{nd} CO_2 injection rate, and several outputs are predicted, from bottomhole pressure, average field pressure, dissolved CO_2 in water and CO_2 in gas phase. The validity of the proxy models is evaluated by percent error and correlation coefficient (R^2).

The results of this study show that, there is still no simulation case that successfully matches the measured data. The best history match case, which requires the absolute permeability multiplied by 5, has an average percent error of 0.22% (0.016 bar) and maximum percent error of 1.01% (0.074 bar) with respect to the measured injection well bottomhole pressure. It implies that the permeability in the current geo-model needs to be improved in the permeability model. The history match result also shows the requirement to modify the previously interpreted mud layer (50.7m to 61.2m) to a non-continuous mud layer that contains sand lobes due to the fact that in the monitoring results, the CO_2 is able to migrate to the upper layer which requires a pathway to reach (~38m depth).

The proxy models from the response surface and universal kriging method show a promising result from the validation cases and evaluation cases. All predicted results have R^2 over 0.99, which means that the proxy models are highly correlated to the simulation results. The universal kriging proxy shows a better performance than the response surface due to the limitation of the response surface in following the polynomial regression model, while the universal kriging has the potential to minimize the error through the Gaussian process.

Overall, this study provides a better understanding of the Svelvik CO_2 field laboratory and successfully developed the proxy models to be implemented for designing the next injection campaign or optimization cases in further work.

Keywords: Svelvik CO_2 field laboratory; CO_2 storage; History Matching; Proxy Model; Response surface; Universal Kriging

Preface

This thesis is written to fulfil the partial requirements for the MSc degree in Petroleum Engineering with Reservoir Engineering and Petrophysics at the Department of Geoscience and Petroleum (IGP) – Norwegian University of Science and Technology (NTNU).

I would like to express my gratitude to my supervisor, Associate Professor Ashkan Jahanbani Ghahfarokhi, who introduced me to the topic and gave excellent guidance to complete this study. I would like to thank Cathrine Ringstad, Alv-Arne Grimstad, and SINTEF Industri AS, that have allowed me to learn more about the Svelvik CO2 Field Laboratory; thank you very much for the guidance and discussions to build a better understanding in the field of CO2 injection in Svelvik and the simulation of the Pre-ACT injection. Special thanks to Anja Sundal, who provided two geological scenarios with the detailed properties distribution. In addition, I would like to thank Cuthbert Shang Wui Ng for the suggestions and feedback on the proxy modelling.

Finally, thank you very much to everyone that has been supporting this study until complete.

Trondheim, June 2022

Wilson Wiranda

Table of Contents

List of Figures

List of Tables

List of Abbreviations and Symbols

CCUS	Carbon Capture Utilization and Storage
LHS	Latin Hypercube Sampling
mD	Unit of permeability (millidarcy)
Pre-ACT	Pressure control and conformance management for safe and efficient CO2 storage - Accelerating CCS Technologies
pVT	Pressure, Volume and Temperature
$y(x)$	Output response for the proxy model
β_o	Main coefficient (response surface proxy)
β_i	Linear terms coefficient for response surface proxy or universal kriging proxy
β_{ij}	First order interaction terms coefficient (response surface proxy)
β_{ii}	Quadratic terms coefficient (response surface proxy)
x_i	Vector input first variable
x_j	Vector input second variable
N	Number of input variables
B_i	Linear basis over experimental domain (universal kriging proxy)
$z(x)$	Random error (universal kriging proxy)
θ	Smoothing parameter (universal kriging proxy)
σ_i	Variance
p	Power-exponential selector (universal kriging proxy)
R^2	Correlation coefficient [-]
$k_{r,w}$	Wetting phase relative permeability [-]
$k_{r,nw}$	Non-wetting phase relative permeability [-]
S_w	Wetting phase saturation [-]
S_{wr}	Wetting phase residual saturation [-]
λ	Grain size distribution index [-]
k_{rl}	Liquid relative permeability [-]
k_{rg}	Gas relative permeability [-]
P_c	Capillary Pressure [bar]
P_{sim}	Simulation data point result
P_{proxy}	Proxy data point result

1 Introduction

1.1 Background

Svelvik CO_2 Field Laboratory is part of the European Research Infrastructure for the CO_2 field of Carbon Capture, Utilization, Transport and Storage (CCUS). The CO_2 Field Lab project is a consortium of industry and research institutes that have a strong involvement in CO_2 storage in multiple areas from site management, monitoring and certification from the early stages (Bakk, et al., 2012).

The establishment of the CO_2 Field Laboratory was conducted to answer the EU directives on the geological storage of CO_2 and create specific instructions on monitoring that have not been developed yet. The objectives and research areas provided in Svelvik CO_2 Field Laboratory are mainly related to CO_2 monitoring and leakage detection using various methods with the aim of providing a validated monitoring system through a protocol and certification scheme (Bakk, et al., 2012).

From September to November 2019, through Pre-ACT (Pressure control and conformance management for safe and efficient CO_2 storage – Accelerating CCS Technologies) project, the re-establishment of the Svelvik CO_2 Field Laboratory is successfully done by performing the first experimental campaign at the lab and disseminating the experimental results of the campaign. The new data obtained from the injection campaign are the geophysical monitoring of the CO_2 plume, the water and CO_2 injection rate and the bottomhole pressure of the injection well and monitoring wells. Using the new conceptual geo-model with more detailed properties in the Svelvik site, history matching towards the data obtained and the CO_2 plume observation is conducted in this study. The new model suffers a high computational time due to the dimension of the Svelvik CO_2 Field Laboratory and the details required to study the CO_2 migration in the subsurface.

To solve the high computational time, proxy models are built to mimic the results of the CO_2 injection simulation, where the proxy models are capable of predicting the dissolved CO_2 in water and free CO_2 in the site for each layer for the next injection campaign. Two types of proxy models were built in this project for each geological scenario. The main algorithms of the proxy models that are studied in this project are Response Surface Proxy and Universal Kriging Proxy. The proxy models are capable of reducing the running time from 2 – 6 hours of injection simulation depending on the time steps to a matter of seconds.

1.2 Objectives

The main research objectives are to history match the geo-model with the improved understanding of CO_2 migration and to develop proxy models for the Svelvik CO_2 Field Laboratory. The proxy models will be used as a complement to the conventional numerical simulation model that offers the capability of predicting the injection well bottomhole pressure, dissolved CO_2 in water and free CO_2 with the input of surface gas injection rate.

The research is performed on two geological scenarios in the same field. Several points are being studied in this research:

1. Understanding the CO_2 migration and leakage on 2019 Svelvik CO_2 Injection
2. History Matching with the Pre-ACT 2019 injection campaign data
3. Built proxy models that can mimic the CO_2 injection simulation for the next injection campaign

1.3 Thesis Outline

The outline of the thesis report consists of the introduction of the study, a literature review that consists of an introduction to Svelvik CO_2 Field Laboratory and proxy modelling, methodology from the geological model, dynamic model, history matching until the proxy model development, results and discussion, and conclusion from the study with the further work that can be continued from this study.

2 Literature Review

2.1 Svelvik CO_2 Field Laboratory

2.1.1 Overview

Svelvik CO_2 Field Laboratory located in the Svelvik ridge about 50 km south-west of Oslo and forms the sill of the Drammensfjord. The Svelvik ridge depositional environment is glaciofluvial-glaciomarine terminal deposit formed suring the Ski stage of the Holocene deglaciation (Sørensen, 1981) (Melø, 2011). This site was chosen as a field laboratory on the assumption that the sand ridge contains homogeneous, unconsolidated, highly permeable sand, which offers well constrained conditions for controlled gas injection experiments (Bakk, et al., 2012).

Figure 2.1: Aerial view of the sand and gravel ridge (the Svelvik ridge) where the Field Laboratory is located (Eliasson, 2020)

The main objective of the CO_2 Field Lab project is to assure and increase carbon storage safety by obtaining valuable knowledge about monitoring of CO_2 migration in geological formations. This will enable detection of possible CO_2 leakage at the earliest possible stage (SINTEF, 2010).

Currently the Svelvik CO_2 Field Laboratory has Svelvik#1 as the exploratory well, Svelvik#2 as the injection well, and four monitoring wells (M1 – M4). Overview of the drone photo can be seen in Figure 2.2. The Svelvik#2 injection well is connected to the water tank and CO_2 tank that is designed to enable the injection in the depth of 64-65 meters depth through a gravel pack completion. A pumping test in 2013 showed that the layer is suitable for CO2 injections with a permeability of approximately 123–170 mD. The four monitoring wells are 100m deep and located at the corners of a rhombus with the Svelvik#2 injection well in the centre. The monitoring wells are located 9.9m (M3 and M4) and 16.5 m (M1 and M2) from the Svelvik#2 well.

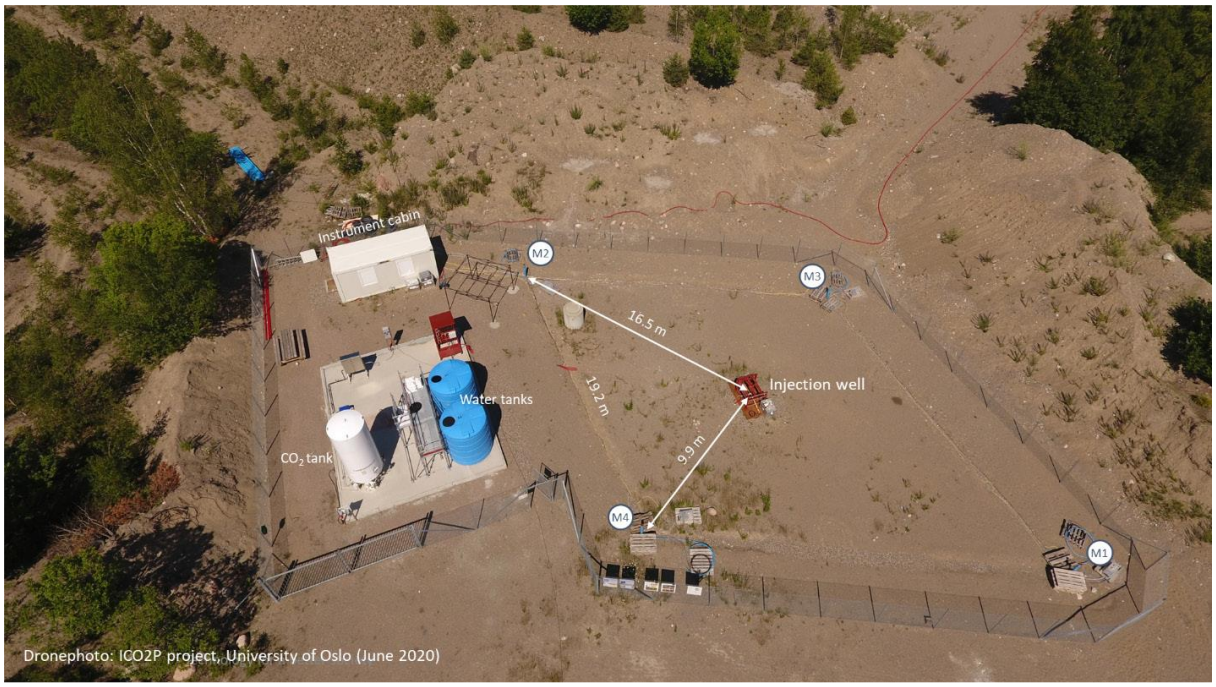

Figure 2.2: Dronephoto of Svelvik CO2 Field Lab Overview (Eliasson, et al., 2017 - 2020)

2.1.2 Geological Setting of Svelvik Ridge

Svelvik ridge was deposited approximately 10000 years ago during the Ski stage. During this period, the glacier readvanced and stay in its position for a significant time (Sørensen, 1981). The deposit forms a seal that act as a blockage between the inner and outer fjord as shown in Figure 2.3. The location of the Svelvik CO_2 field laboratory located in the glaciofluvial deposit. It is deposited in pro-glacial fluvial and marine environments during the suspension in the ice retreat. The ice retreat was the result from a period of warming after Younger Dryas cool period (Hagby, 2018). In the beach deposits, the grains are well sorted, washed and reformed by waves and currents in the shoreface (Sørensen, et al., 1990).

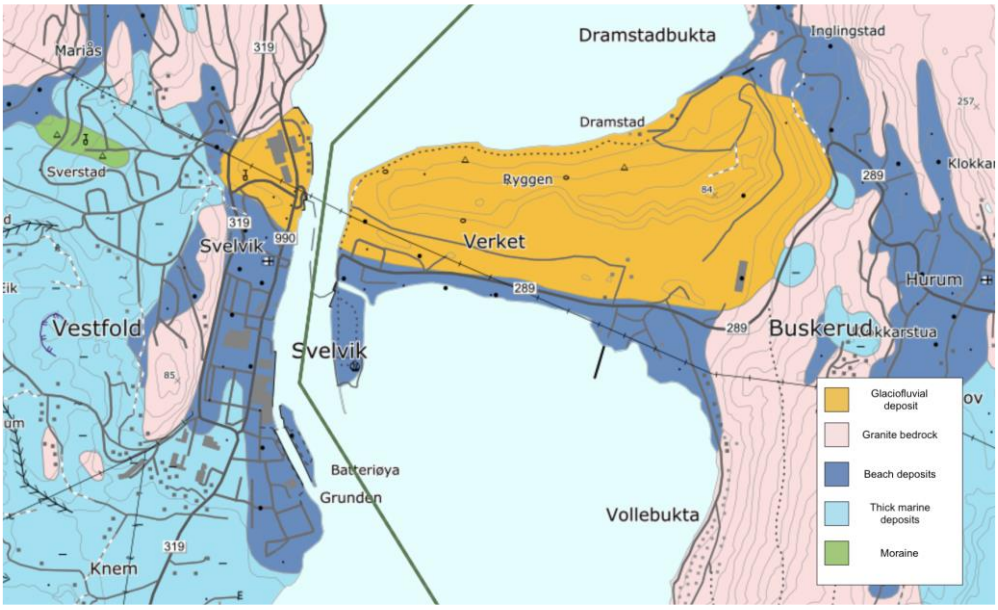

Figure 2.3: Geological map showing the Svelvik ridge, by The Geological Survey of Norway (NGU, 2018)

The Svelvik Ridge has been interpreted by Sorensen in 1981 (Sørensen, 1981) and 1990 (Sørensen, et al., 1990), and Melø in 2011 (Melø, 2011). The three main facies of the depositional systems of glaciomarine: Ice-contact submarine fans; Ice-contact deltas; and glaciofluvial deltas (Lønne, 1995). The Svelvik rigde is classified as ice-contact submarine fan with the common features shown in Figure 2.4. The ice-contact glaciomarine systems used to describe the Svelvik ridge in Melø's finding was based on Lønne (Lønne, 1995) models described that there was a moment where the glacier contacts with the ocean, resulting the deposit is characterized as ice-contact system (Melø, 2011). The ice-contact submarine fan deposit has a wedge of coarse-grained materials that has been deposited under water right in front of the glacier. It was formed by re-sedimentation of the poorly sorted glacial material together with ice rafted debris from the melting sea (Lønne, 1995).

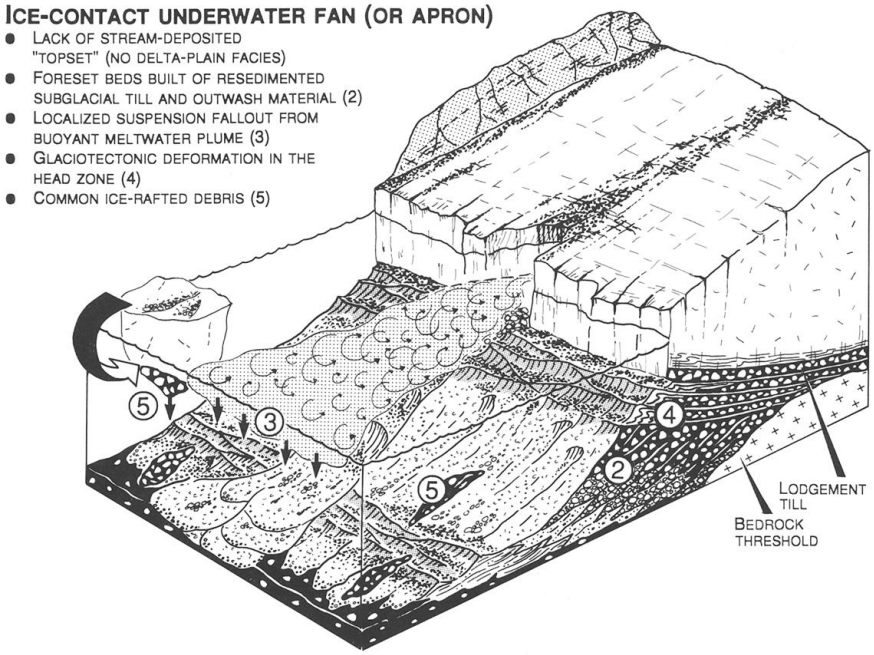

Figure 2.4: Principal characteristics of ice-contact submarine fan (Lønne, 1995)

Based on the Lønne's ideal conceptual model, the ice-contact submarine fan will generally consist of four allostratigraphic units: A, B, D and E shown in Figure 2.5..

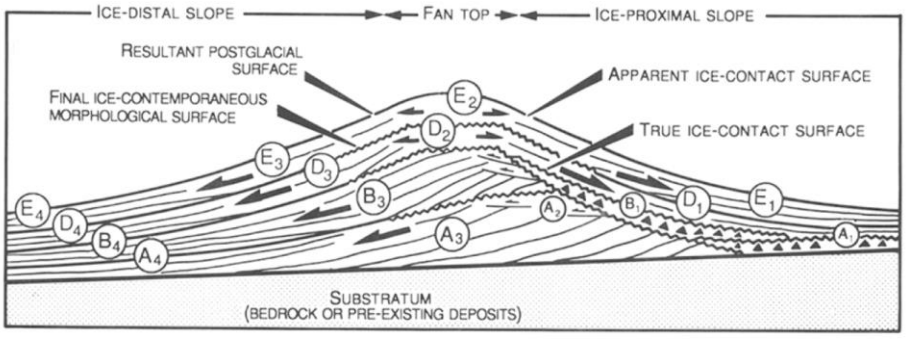

Figure 2.5: Cross-sectional conceptual model for the development of an ice-contact submarine fan (Lønne, 1995)

Unit A representing the ice-contact facies formed during glacier advance which shows the progradation of an ice-contact submarine fan contemporaneous with advance of the ice front. The subunit A_3 representing the coarse-grained foreset facies, passes downfan into

sub-horizontal bottomset facies that represents by subunit A_4. The subunit A_4 comprises of silty mud inserted with fine-grained turbiditic sand. The subunit A_1 and A_2 will be form if the glacier moves across the fan top and subject to subglacial processes including deposition of basal till and sorted debris, erosion and/or deformation. This means that the subunit A_1 and A_2 generally have a low preservation potential due to the requirement of both the vigorous meltwater outflow and the advancing glacier itself. (Lønne, 1995)

Unit B representing the formation of the ice-contact facies during glacier stillsand or retreat. This may also consist of facies similar to the unit A. The foreset of this type of facies generally dipping away from the glacier terminus, and the upper part may show syn-sedimentary glaciotectonic deformation. The unit B sediment are coarse grained and might have a high content of sub-glacial derived debris and ice-rafted debris. (Lønne, 1995)

Unit D represent the ice-distal facies during glacier retreat. The retreat of the glacier terminus shown when the sediment is being deposited majorly from the buoyant meltwater plume, drifting icebergs, and contemporaneous gravitational removed from the fan surface by itself. The unit D usually shows an upward fining, but the sedimentary are highly varied. Therefore, the unit D are highly heterogenous facies with common mud clasts and inverted textures. This is depending on the morphology and facies of the abandoned fan surface and the dynamics of the retreating glacier. (Lønne, 1995)

The retreat of a glacier will create an uplift of the submarine fan (post-glacial isostatic uplift) which resulting in another succession of ice-contact units. This is labelled as unit E in Figure 2.5, where it generally coarsens upwards and is formed by re-sedimentation and reworking of the fan deposits. The whole succession of ice-contact units can be repeated with the cyclical pattern A-B-D-A*d*-D-E based on the Figure 2.5 (Lønne, 1995)

Based on Sørensen (Sørensen, 1981) interpretation, for the glacier halt, a preexisting moraine or bedrock threshold should present. The Svelvik ridge in Figure 2.6, shows that the bedrock to the south is capable for a threshold to halt the glacier. There is also a moraine that is deposited under the glaciofluvial deposit and marine deposit which also serve as threshold for the advancing glacier and probably formed by the oscillating glacier front. Additionally, due to the isostatic rebound by deglaciation, the deposits were exposed to air around 7000 years ago. The exposure introduces erosional forces in several form (rivers, wave and tidal) (Sørensen, et al., 1990).

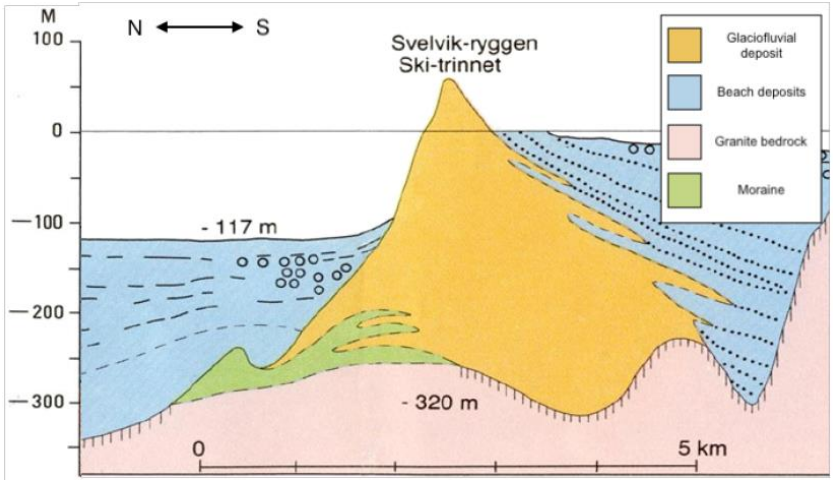

Figure 2.6: Cross-section north-south interpretation of Svelvik ridge by Sørensen (Lønne, 1995)

According to Melø, the Svelvik ridge consist of two types of aquifers, which is upper and lower. Aquifer is defined as a body of rock whose fluid saturation, porosity and permeability permit production of groundwater (Schlumberger, 2014). The upper aquifer limit is defined with the groundwater table and the lower aquifer limit is shown as below the confining layer (Melø, 2011). The understanding of the aquifer itself is useful to model the aquifer in the later section. In Melø thesis, the result of the aquifer is shown with parameters of transmissivity, storativity and anisotropic ratio (Melø, 2011).

2.1.3 Current Conceptual Model

Current conceptual model follows the interpretation from Ruden AS and Rendall, H. from the Svelvik#1 well with the summarization of the interpretation shown in Table 2.1.

Table 2.1: Summary of the sand interval and description

Intervals (m)	Sample (m)	Description
37.1 – 50.7	37 – 38	9% clay, 49% silt, and sand mainly coarse to very coarse.
61.2 – 71.2	64 – 65	Fine to very coarse sand and with about 10% coarser grains in the granule/pebble category 11% silt but clay is absent Coarser downward
	67 – 68	4% silt, medium to very coarse sand dominated
85 – 115	100 – 101	An upper sandy part from 85 to 95m A more clayey horizon at 95 – 96. Sample dominated by fine to very coarse sand (85%). In addition, 15% very fine sand and silt, almost no clay
	110 – 111	Well sorted sample dominated by very fine to fine sand (50%) 30% sand in the medium to very coarse 9% silt and 2% clay
122 – 130.8	126 – 127	Relatively poor sorted with 4% clay, 13% silt, and sand from very fine to very coarse
220 - 236	221 – 222	Sample has 4% clay and 16% silt Very fine to coarse sand
	229 – 230	Sample has 3% clay and 15% silt. Slightly better sorted than sample 221 -222. 80% sand in the range of fine to coarse.

The interpretation results from the Svelvik#1 well correspond with the interpretation result from Svelvik#2 well. Based on the interpretation of gamma and clay content logs, the sand layer can be identified are from 36.2 – 49.8 m and 60.4 – 70.9 m. These intervals very well correspond to the previous interpretation of sand layer in Svelvik#1 well which has the sand interval from 37.1 – 50.7 m and 61.2 – 71.7 m (Wiranda, 2021). The illustration of the current interpretation of the geological model is shown in Figure 2.7. The upper layer down to 35m consist of sand and gravel deposits close to the glacier front. After the 35m, alternating layers of sand, silt and clay deposition further away from the glacier front. (Eliasson, et al., 2017 - 2020)

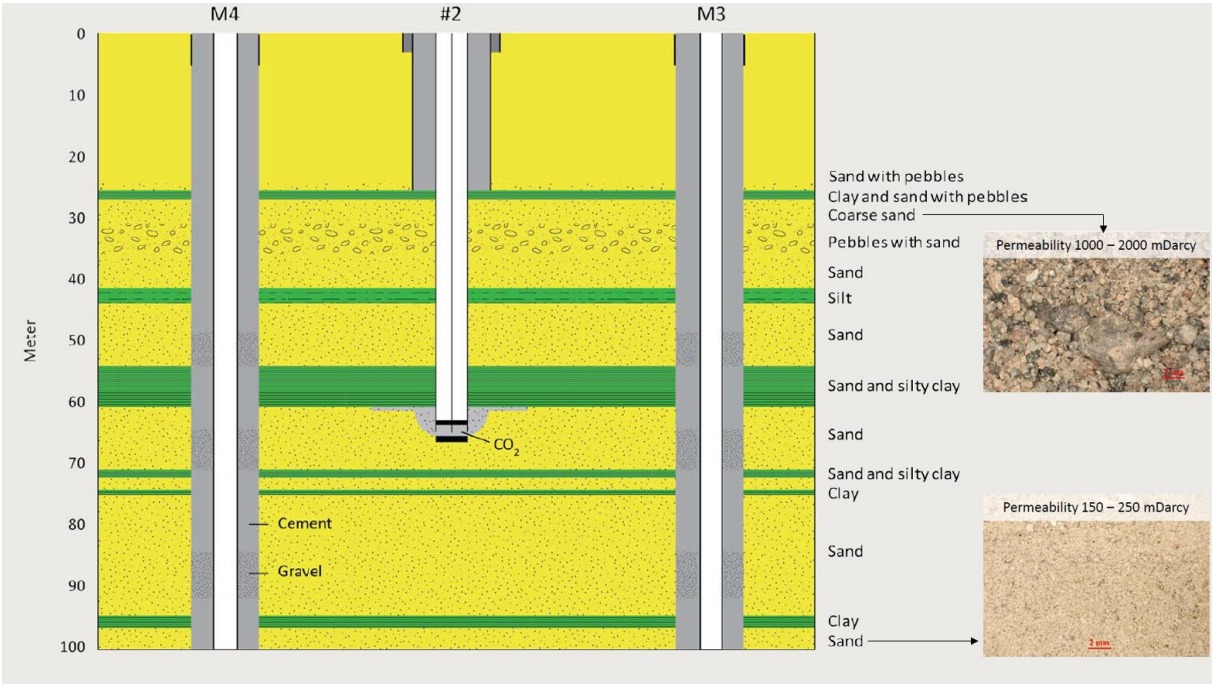

Figure 2.7: Illustration of the geological model N-S cross-section of Svelvik CO_2 Field Laboratory (Eliasson, 2020)

A suggested geo-model by Anja Sundal from UiO is shown in Figure 2.8, where the clinoform of the sand is represented as a dipping grid. The model that is newly updated by Anja is provided in the methodology section.

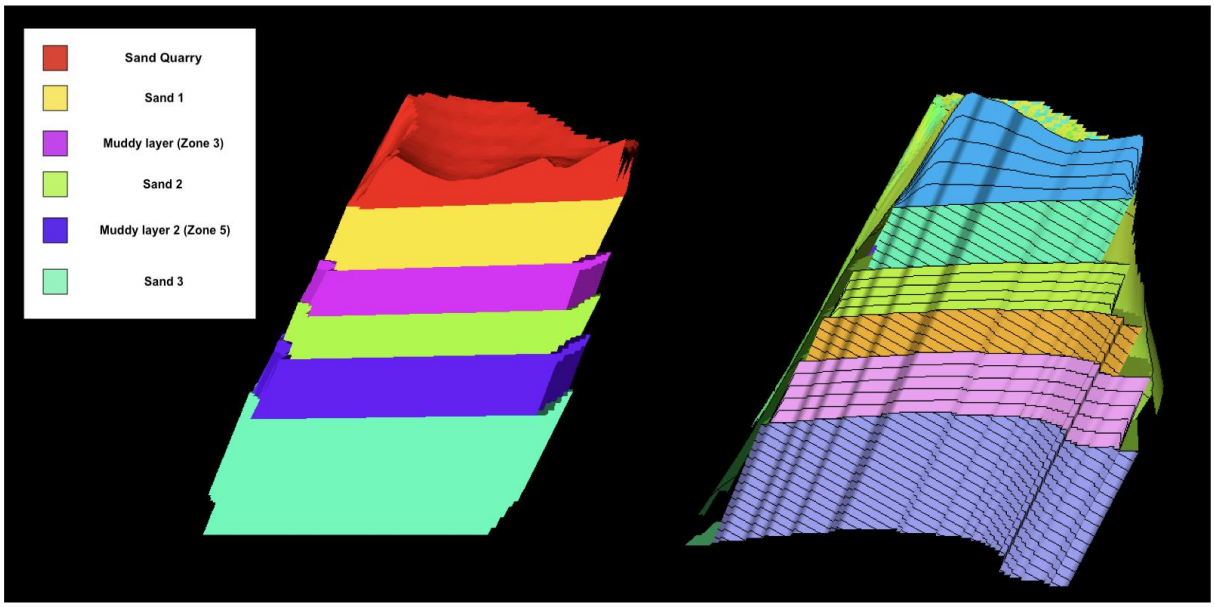

Figure 2.8: Suggested geo-model by Sundal (2017) with dipping sand layer modelling clinoform. Facies on the left and grid model on the right

2.1.4 Pre-ACT 2019 Injection Campaign

The Svelvik CO_2 Field Laboratory undergoes an injection of saline water and CO_2 with the period from September to November 2019. The initial studies shown that the CO_2 can be accurately localized by seismic and electrical methods (Eliasson, et al., 2017 - 2020). The valuable geophysical data and the tested method to measure the downhole pressure, is

used in this project as an input to update the understanding in Svelvik CO_2 Field Laboratory.

Figure 2.9a shows the water and CO_2 injection rate that was applied in the injection campaign. The water injection has the salinity being match with the salinity in the injection depth (0.5% wt.). The total water volume injected is 69m^3 and started in 27th of September 2019. The pressure gauge measured in the Figure 2.9b is relative to the atmospheric pressure. It is also shown that there is a strong tidal variation throughout the measured data from the pressure gauge (Jordan & Weinzierl, 2020). The pressure gauge is located slightly above the injection depth due to the pressure gauge located above the packer. A correction towards these effects will be explain in the next chapter.

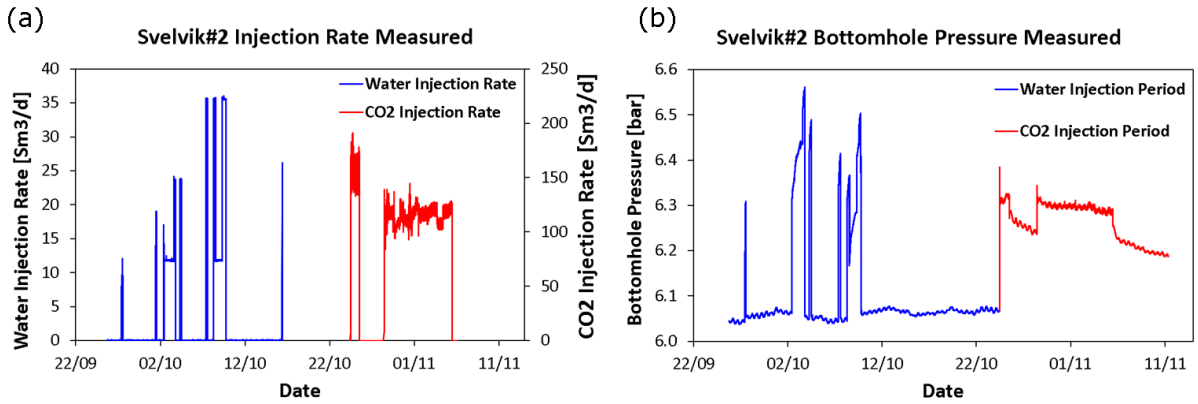

Figure 2.9: Water and CO_2 injection rate in Pre-ACT 2019 injection campaign.

After the water injection completed, on 24th of October 2019 the CO_2 injection started with high rate, stop the injection and continue with a lower rate. A total of ~1.8T CO_2 (~1000 Sm^3) was injected during this period with the initial rate up to 12 kg/hour (~150 Sm^3/d) and second injection with rate up to 8 kg/hour (~105 Sm^3/d). In order to determine the location of the CO_2 plume, a geoelectric array with 64 electrodes was installed. With this small amount of CO_2, the geoelectric survey was able to locate the CO_2 plume, but unexpectedly not located close to the well injection nor the initial illustration, but several meters above (Eliasson, et al., 2017 - 2020).

The result of the initial CO_2 monitoring is presented in Figure 2.10. Based on the P-wave inversion, it is compared between the baseline and when the CO_2 injection started. Based on the p-wave velocity difference, it shows that the highest difference from the baseline is on the depth of 38 – 40m. The highest difference from the baseline shows the location of the CO_2 plume. The mud zone that is interpreted based on the 1D velocity profile is only the mud zone in between the 30 – 40 m. The location was considered reliable, as consistent results were obtained with crosswell-based velocity tomography (Eliasson, et al., 2017 - 2020).

The location of the CO_2 plume and the measured data from the Pre-ACT injection is used in this study as input for the history matching and simulation.

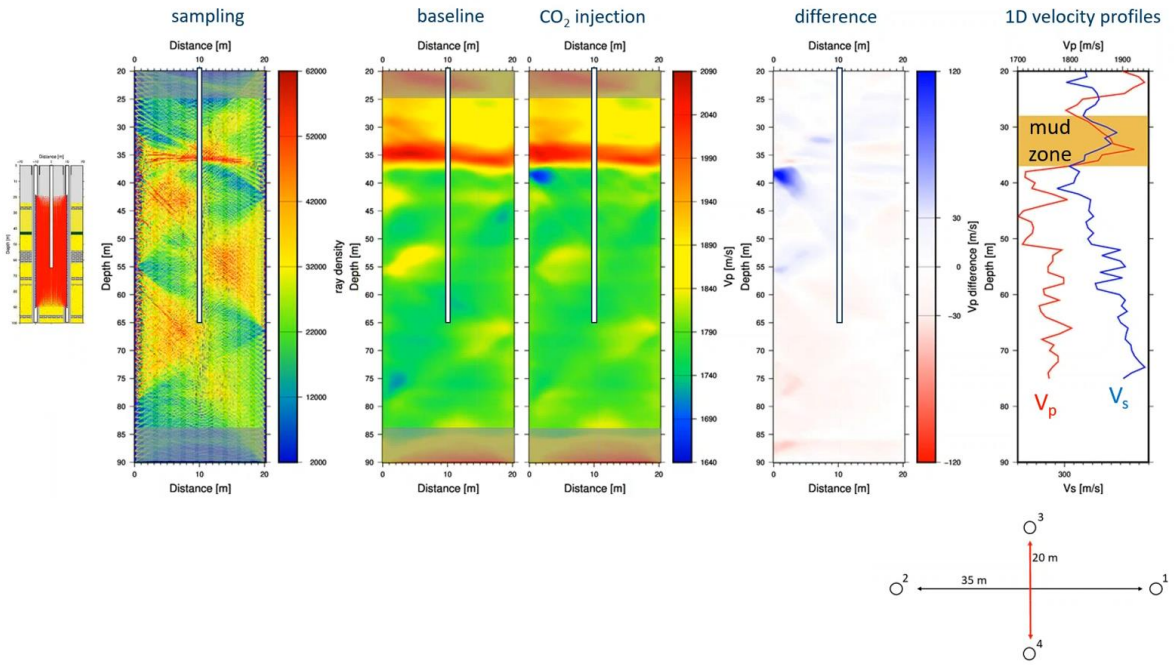

Figure 2.10: Initial CO_2 monitoring results based on P-wave inversion (Jordan & Weinzierl, 2020)

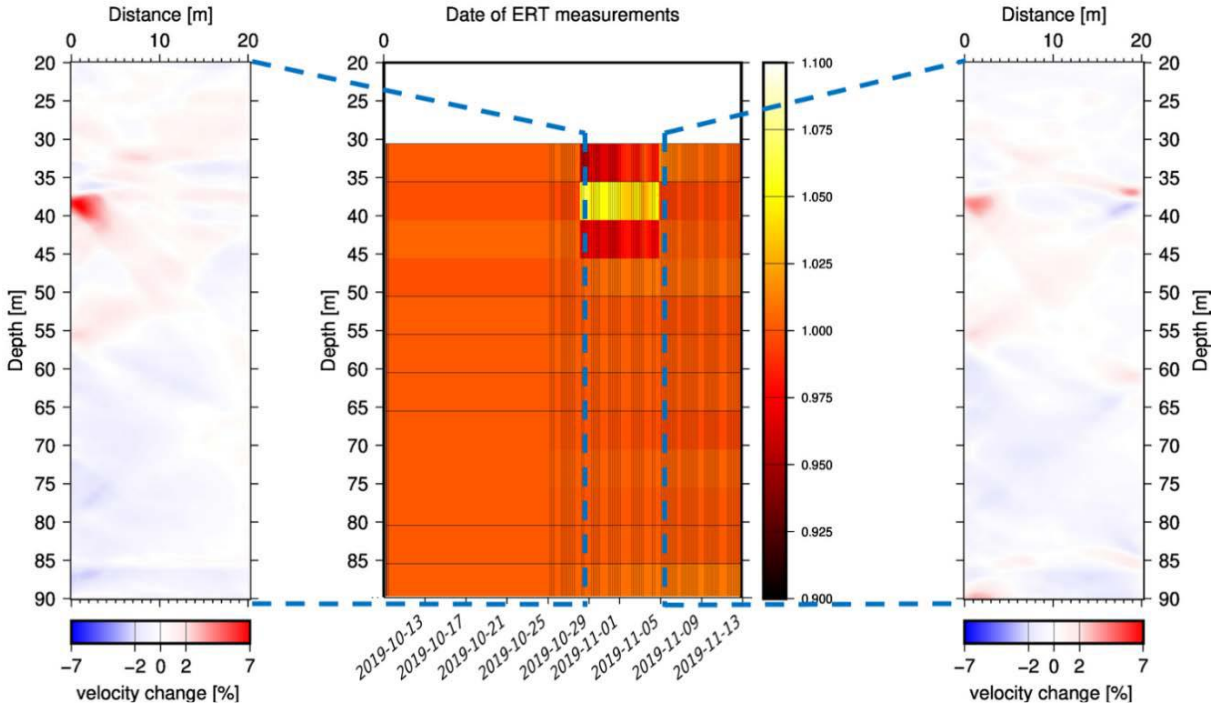

Figure 2.11: Velocity changes derived from the cross-well seismic tomography at two-time steps: Initial CO_2 injection (left) and Post CO_2 injection (right)。 The highest change of velocity shown in red color in the difference chart (Jordan & Weinzierl, 2020)

2.1.5 Data Availability

The data availability starting from initial site characterization until pre-ACT 2019 CO_2 injection campaign is shown in Table 2.2.

Table 2.2: Data Availability from Svelvik CO_2 Field Laboratory (Wiranda, 2021)

Well	Available Data	Details	Source:
Svelvik#1	Well Log Data	• Borehole: CALI • Formation: GR, U, Th, K, Temp • Resistivity: ILD, ILS, RLLD, RLLS	• D4-3-3B_Gamma&Grain-size-flow-line-samples-deep well-Svelvik_Rendall_Memo • Petrel Project: Svelvik 2021 - Student
	Core Analysis Report	• Petrophysical Analysis: Core at depth: 30m, 102m, 201m, and surface taken at 40m above sea level • Water Analysis	• D2-1-7_Core-analysis-report_characterization_core-flooding
	Grain Size Report	• Grain Distribution • Sand intervals	• D4-3-3B_Gamma&Grain-size-flow-line-samples-deep well-Svelvik_Rendall_Memo • D4-3-3C1_Svelvik-Geo-model-interpretation_June-2012_Ruden-Ltd
Svelvik#2	Well Log Data	• Borehole: CALI • Formation: GR, U, Th, K, DT, Temp • Resistivity: RLLD, RLLS	• D2-3-1A-2_Svelvik-well-logging-in-permeabiliy-test-well_jan-2013_Report • Petrel Project: Svelvik 2021 - Student
	Injection Rate Data	Water: September 25, 2019 (19:00) – October 16, 2019 (11:00) CO_2: October 24, 2019 (11:00) – November 5, 2019 (13:00)	• Pre-ACT injection rate data set
	Pressure & Temp Data	September 25, 2019 (19:00) – November 11, 2019 (08:00)	• Pre-ACT injection rate data set
M1	Bottomhole Pressure Data	September 17, 2019 (16:00) – November 7, 2019 (09:00)	• Pre-ACT pressure data reduced
M2	Bottomhole Pressure Data	September 17, 2019 (16:00) – November 7, 2019 (09:00)	• Pre-ACT pressure data reduced
M3	Bottomhole Pressure Data	September 17, 2019 (16:00) – November 7, 2019 (09:00)	• Pre-ACT pressure data reduced

The measurement of the pressure data of the M4 is not included due to the data only from capillaries. All of the data are summarized in the attachment section adapted from the specialization project report prepared by (Wiranda, 2021)

2.2 Numerical Reservoir Simulation

Numerical simulation or full physics simulation has been used to describe the reservoir behaviour and fluid flows in the reservoir. This consist of building geological model, petrophysical interpretations and field measurements, which resulting on having a very large grid cells to be evaluated in order to achieve a higher resolution (Jaber, et al., 2019). With these inputs, a numerical simulation was done by evaluating the partial differential equations for each grid cells to solve the diffusivity equations of fluid flow in porous media. With more advance simulation, the numerical simulation can incorporate with multi-physics simulation, which enable the evaluation in different temperature and compositional simulation (Jaber, et al., 2019). An integrated reservoir modelling from geo-modelling to simulation is shown in Figure 2.12.

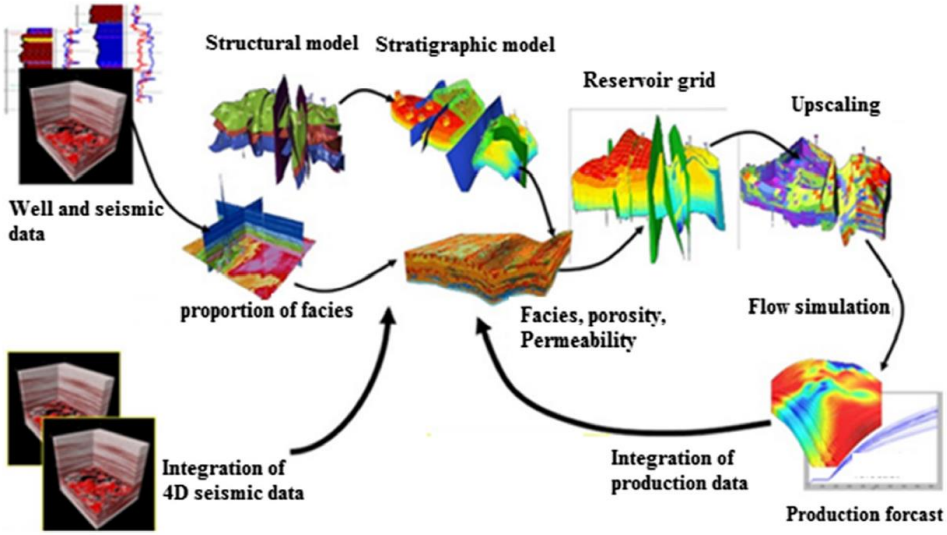

Figure 2.12: Integrated reservoir modelling to numerical simulation workflow (Jaber, et al., 2019)

There are a variety of numerical simulator that can be used to model CO_2 storage. The summary of simulators that can be used for CO_2 storage with the advantages and disadvantages is shown in Table 2.3.

Table 2.3: Reservoir simulation tools for CO_2 storage (Nazarian, 2021)

Simulator	Method	Advantages	Disadvantages
Eclipse 100	Two-phase gas/oil phase	Speed E100 functionalities	Deterministic dissolution Demanding PVT Preparation
Eclipse 300	Equation of State	E300 functionalities	Poor performance in large models Dissolution needs additional model
E300 + CO2STORE	Equation of State Spycher & Pruess solubility model	Easy to model E300 functionalities Dedicated storage output parameters	Limited to pure CO_2 injection Poor performance in large models

2.3 CO_2 Storage Trapping Mechanism

When injecting CO_2 towards a geological formation, several trapping mechanisms occur during the CO_2 injection until post-injection. The trapping mechanism can be group based on the physical and chemical factors (Ringrose, 2020).

1. Physical trapping related to the basin-scale consists of regional structure, basin history fluid flow and pressure distribution;
2. Physical trapping related to the form of structural and stratigraphic traps;
3. Physical trapping related to the residual trapping by the principal of capillary interfaces between fluids and rock properties retention CO_2 as residual phase;
4. Geochemical trapping mechanism with the principal of CO_2 dissolution in brine, precipitation as mineral phase and sorption/absorption on clay minerals.

shows the differences of mechanism over time and combining all of the mechanism, there will be increase of storage security during the injection and post-injection.

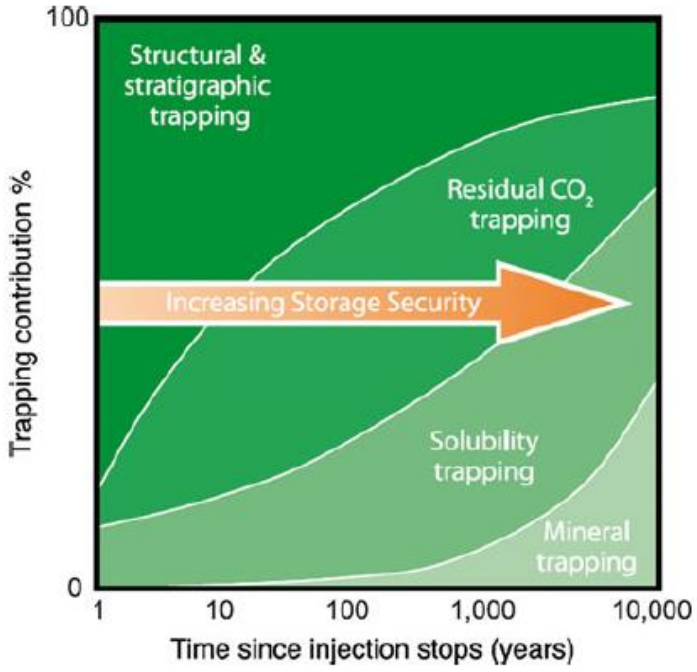

Figure 2.13: Storage efficiency factor as a function of viscous and gravity force (Benson & Cook, 2005)

The trapping mechanism of the structural and stratigraphic trapping depend on the physical process of capillary trapping due to the interfacial tension between fluids in a porous medium. The capillary trapping itself is a critical phenomenon to determine the size of the CO_2. In general, (Naylor, et al., 2011) have observed several effects where the capillary entry pressure for CO_2 water system is ~50% lower than gas/water systems while the buoyance effect is lower due to supercritical CO_2 has a higher density.

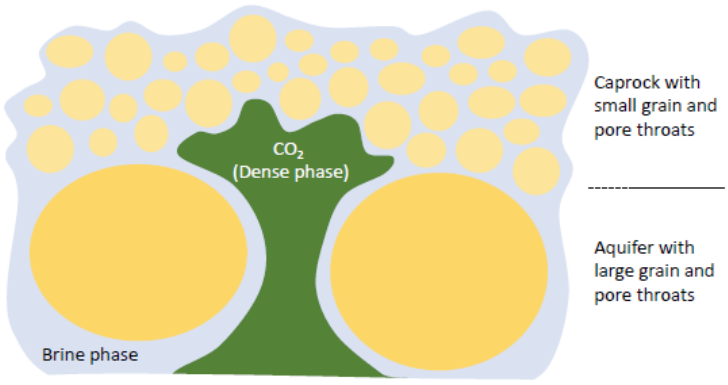

Figure 2.14: Simple sketch of capillary trapping of CO_2-water system (Ringrose, 2020)

Another trapping mechanism affected by the capillary is the residual trapping, where the term is summarized as residual CO_2 saturation. The residual CO_2 saturation is obtained from relative permeability as a function of saturation and other factors such as the grain size distribution. In the CO_2-water system in a sandstone reservoir, the CO_2 is considered the non-wetting phase, and water is the wetting phase. The residual CO_2 saturation occurs when the CO_2 as the non-wetting phase is no longer in contact with the surface and water rapidly fills the pore throat where the CO_2 will be snapped and effectively trapped the CO_2.

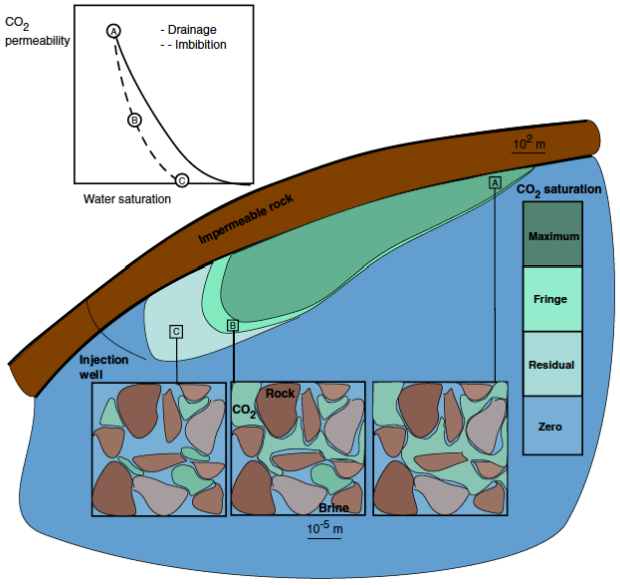

Figure 2.15: A sketch of capillary trapping post CO_2 injection at a storage site (Krevor, et al., 2015)

2.4 Proxy Modeling

To understand the phenomenon of CO_2 sequestration, quantifying, and predicting how much CO_2 can be stored in aquifer, a conventional full physics simulation is used to describe the CO_2 behaviour in the reservoir. The drawback of the full physics conventional simulation is the time to simulate a model is high and the resources required to run the simulation is very demanding (Schuetter, et al., 2014).

One of the approaches to tackle this challenge is to build a proxy model based on the understanding of the storage itself. The proxy model is a function that approximates the response of the full physics model for a given set of input values. The benefit of the proxy model is that it typically takes a fraction of the time to run as compared to the full physics model (Schuetter, et al., 2014). The application of proxy modelling has been widely used in petroleum industry with a broad range of functionality from sensitivity analysis, assisted history matching, field development planning, risk analysis, optimization and reservoir characterization (Jaber, et al., 2019).

Depending on the data availability and the objectives of the study, there are several types of proxy that can be develop from field basis, well basis, and grid basis. The summary of the input required for developing each type of proxy model is shown in Table 2.4.

Table 2.4: Input required for each type of proxy model (Matthew, 2021)

Data	Grid-based		Well-based		Field-based	
	Property	Domain	Property	Domain	Property	Domain
Static	Grid Type Location (i, j, k, Long, Lat) Thickness Porosity Permeability (x, y, z) Grid top Distance to boundary	Grid Grid/Tier Grid Grid Grid/Tier Grid/Tier Grid/Tier	Drainage Area Location (i, j, k, Long, Lat) Thickness Porosity Permeability (x, y, z) Grid top Distance to boundary	Well Well Tier Tier Tier Tier Well	No input required with the assumption constant geological/static condistion	
Dynamic	Time Pressure Saturation CO_2 Mole Fraction Wells BHP Wells Prod/Inj Rate Total Prod/Inj Rate	 Grid/Tier Grid/Tier Grid/Tier Well Well Field	Time Pressure Saturation CO_2 Mole Fraction Wells BHP Wells Prod/Inj Rate Total Prod/Inj Rate	 Tier Tier Tier Well Well Field	Time Total Prod/Inj Rate	 Field

The differences between the grid-based, well-based and field-based proxy are in the result and variables that can be predicted:

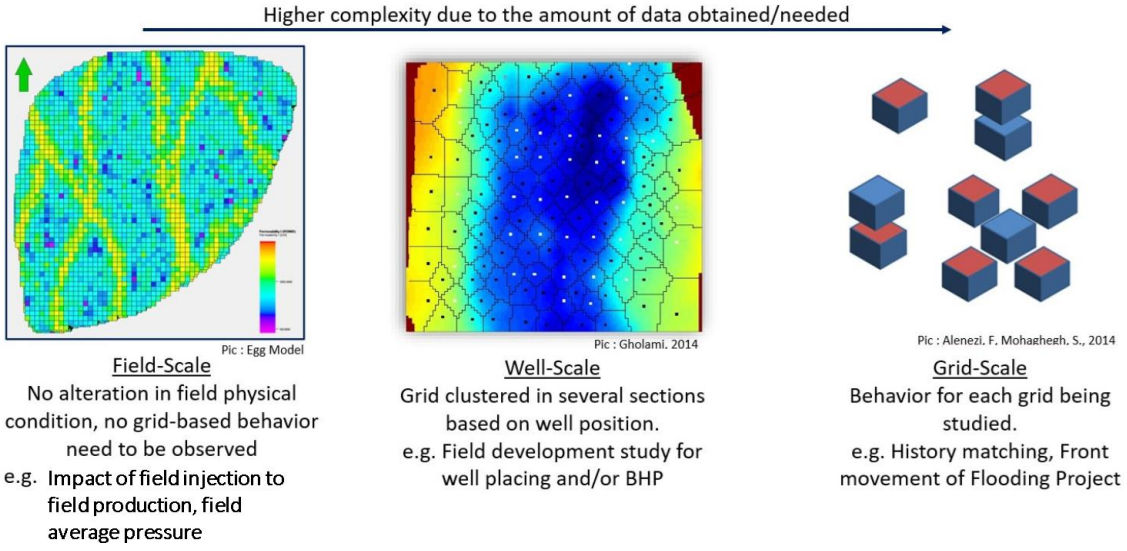

Figure 2.16: Difference of proxy models with increasing complexity and data required (Matthew, 2021)

There are two types of proxy modelling based on the background information used to build the proxy: proxy modelling based on virtual intelligence and proxy modelling based on statistical methods (Jaber, et al., 2019). Proxy modelling based on virtual intelligence

used a more sophisticated learning algorithm as artificial neural network, evolutionary programming, and fuzzy logic (Jaber, et al., 2019). Proxy modelling based on statistical methods mainly achieved by utilizing the design of experiments (DOEs) and the response of the results based on the experiments (Jaber, et al., 2019). Zubarev, et al.,2019 (Zubarev, 2009) shows workflow for proxy modelling (Figure 2.17) that is adapted in this study.

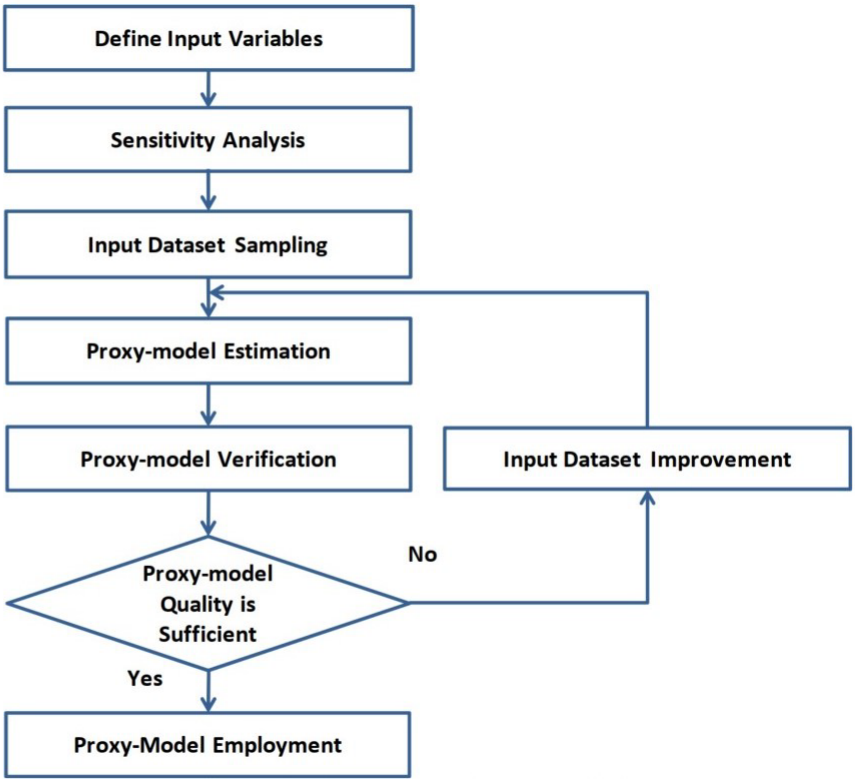

Figure 2.17: Proxy modelling workflow proposed by Zubarev, et al. (Zubarev, 2009)

There are several proxy models that has been studied. Several of the studies that is related to the CO_2 sequestration are shown in Table 2.5.

Table 2.5: Published literature about proxy models for CO_2 sequestration (Jaber, et al., 2019)

Authors	Work description
(Amini, et al., 2012)	Used artificial intelligence and data mining techniques to build SRM to predict pressure distribution at the grid block level during sequestration of CO_2 into a depleted gas reservoir
(Schuetter, et al., 2014)	Built a statistical proxy model for the CO2 geological sequestration in the caprock; they used Box-Behnken experimental design with a quadratic polynomial response surface and a space-filling maximum Latin hypercube sampling design with four different metamodeling techniques (quadratic polynomial, kriging, multivariate adaptive regression spline and additivity, and variance stabilization)

(Jaber, et al., 2017)	Developed a statistical proxy model for real heterogeneous clastic reservoir during the miscible CO2-WAG flooding. They utilize Box-Behnken design based on four parameters to develop a new statistical proxy model as a function of the most influential parameters of the miscible CO2-WAG flooding considering the flow compositional simulation model as the data generator for the proxy model
(Ahmadi, et al., 2018)	Proposed a proxy model to predict the ultimate oil recovery during miscible CO2 injection through coupling the least square and Box-Behnken design

In this study, the proxy modelling is limited to the statistical proxy modelling. Two types of statistical proxy model are investigated and being compared to represent the full physics simulation. The statistical proxy modelling that are investigated are: response surface proxy and universal kriging proxy.

2.4.1 Data Sampling

There are several types of sampling method for proxy modelling. In this study based on the objective with limited time, the detailed fractional factorial sampler is used for training dataset, while the evaluation is carried out with Latin hypercube sampler.

Fractional factorial sampler

A fractional factorial sampler is a deterministic sampling algorithm best suited for building linear proxy models with or without interactions (that is, bilinear terms) (Schlumberger, 2019). With the same sampling method, the universal kriging proxy model also carried out. The training and validation data in this study has the similarity with the fractional factorial sampler where it samples the minimum (-), central (0) and maximum (+) values and the combination as shown in Table 2.6.

Table 2.6: Illustration of fractional factorial sampler

Sample	Variable A	Variable B
1	0	0
2	-	-
3	+	-
4	-	+
5	+	+

Latin hypercube sampler (LHS)

Latin-hypercube is a sampling method that requires fewer model runs to approximate the desired variable distribution than a completely random sampling (Schlumberger, 2019). The evaluation uses a Latin Hypercube sampling where the sample is distributed over the entire range of the parameter. Figure 2.18. has the red dot that shows the outcome difference of seven samples from Monte-Carlo simulation and Latin-hypercube sampling.

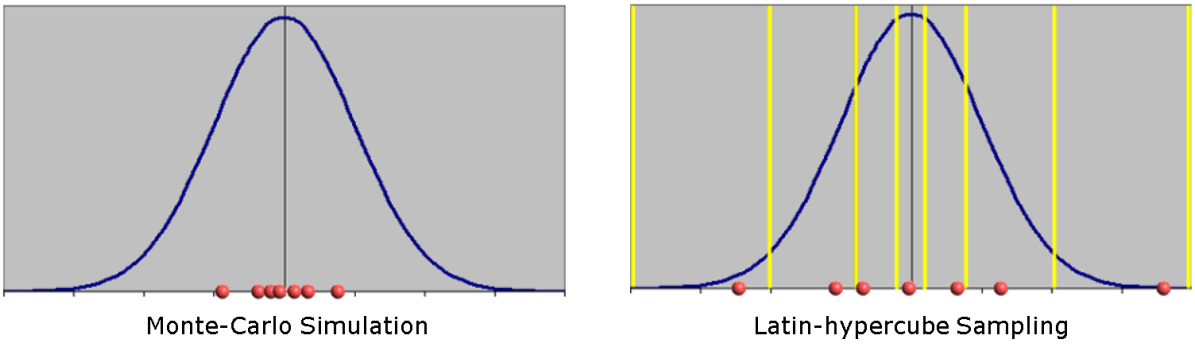

Figure 2.18: Difference of the outcome uses Latin-hypercube sampling method (Schlumberger, 2019)

LHS is usually performed in safety assessment, computer modelling, and petroleum industry, particularly in optimization schemes (Iman, 2008).

2.4.2 Response Surface Proxy

The response surface proxy is a polynomial model of first order (linear or bilinear) or second order (quadratic) that is fitted to the supplied training data and the coefficient of the proxy is determined by the least-square fit (Schlumberger, 2019).

The assumption of the response surface method is that the output response ($y(x)$) of the model can be approximated with a polynomial model. The general term of the polynomial proxy is shown in Equation ((1)).

$$y(x) = \beta_o + \sum_i \beta_i x_i + \sum_i \sum_j \beta_{ij} x_i x_j + \sum_i \beta_{ii} x_i^2 \quad (1)$$

Where x is a vector of N input variables, β_i is the unknown coefficient for the linear terms, β_{ij} is the unknown coefficient for the first-order interaction terms, and β_{ii} is the unknown coefficient for the quadratic terms.

The general term can be simplified depending on the usage such as the first two terms of the general term is linear equation. Adding the first-order interaction will yield into a bilinear equation, and the last term will result a full quadratic model. Adding the terms possibly increases the accuracy with the trade-off increasing the number of sufficient training model (Schlumberger, 2019).

The minimum required number of training data for different terms can be summarize as follows, where N is the number of the input variable:

- Linear model: N+1
- Bilinear model: N(N+1)/2+1
- Quadratic model: (N+1)(N+2)/2

2.4.3 Universal Kriging Proxy

The universal kriging proxy follows a Gaussian process where the correlation function and unknown of the variance determined by maximizing outcome likelihood (Schlumberger, 2019).

The general term of the universal kriging proxy is shown in Equation (2).

$$y(x) = \sum_i \beta_i B_i(x) + z(x) \tag{2}$$

where B_i is a linear basis over the experimental domain and $z(x)$ is a random error. The z(x) is a Gaussian process with zero mean, unknown variance and correlation function (r). The correlation function (r) implemented in the Universal kriging proxy has the general term shown by Equation (3).

$$r(\theta; s, t) = \exp\left(-\sum_i \sigma_i \theta |s_i - t_i|^p\right) \tag{3}$$

where θ is the smoothing parameter that inversely proportional to the correlation length of the model, σ_i is the variance, the term $|s_i - t_i|$ is the residue and p is the power-exponential selector.

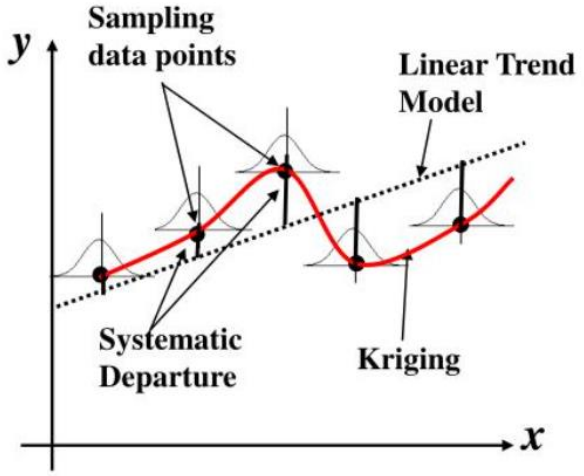

Figure 2.19: Illustration of universal kriging method vs linear trend model

3 Methodology

In this section, a thorough methodology that has been used to reach the objectives is being elaborated. This study can be categorized into two major parts, history matching and proxy modelling.

3.1 Study Workflow

The proposed study workflow in this research is shown in Figure 3.1. The current proposed workflow is limited to the designated uncertainties defined from the previous project in the history matching part. With increasing data availability, the uncertainty parameters can be refined. The proxy model workflow is inspired from "Pros and cons of applying proxy-models as a substitute for full reservoir simulations." (Zubarev, 2009).

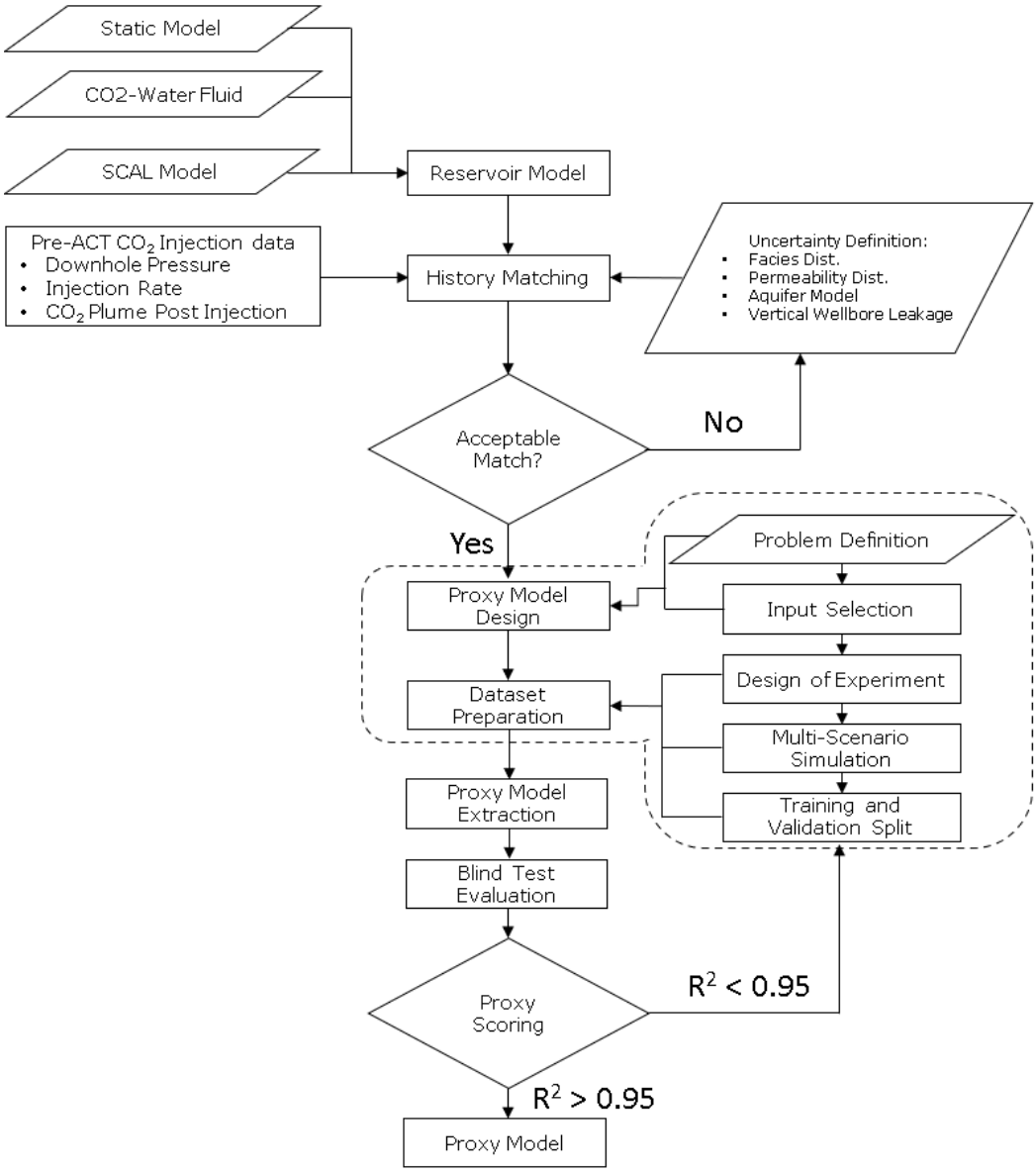

Figure 3.1: Study workflow

3.2 Software and Hardware Used

The software used for this study is Schlumberger Petrel 2019.3 for the reservoir modelling and visualization with Schlumberger Eclipse 2016.2 for simulation.

The hardware used is a PC with processor Intel(R) Xeon(R) CPU E5-1650 v3 @ 3.50GHz (6 cores/12 logical processors) operating in 64-bit with Windows 10 Education and 64.0 GB RAM.

3.3 Svelvik CO_2 Field Laboratory Reservoir Description

3.3.1 Fluid Model

The fluid model is based on CO2Thermodynamics VBA Excel from SINTEF. The VBA Excel generates a pVT table with the gas phase as CO_2 and oil as pseudo-phase of CO_2-Water based on the pressure and temperature. The temperature of the pVT table is generated at the temperature 10°C and pressure of 7 bar (Grimstad, et al., 2018). The water salinity is 0.5% wt and the solubility of CO_2 in 1000 kg water is about 14 kg at 7 bar and increases to 19 kg at 10 bar (Grimstad, et al., 2018). The resulting pVT table for CO_2 is shown in Figure 3.2. and pseudo-phase CO_2-Water in Figure 3.3.

A water phase is introduced to model the open boundary in the Svelvik ridge below the injection layer. The water phase is modelled by using the salinity to determine the water formation volume factor, compressibility, and viscosity. Correlation used in the water phase model is from "A correlation for water compressibility" and "Correlation for water viscosity" by (Meehan, 1980) as the default correlation in Petrel.

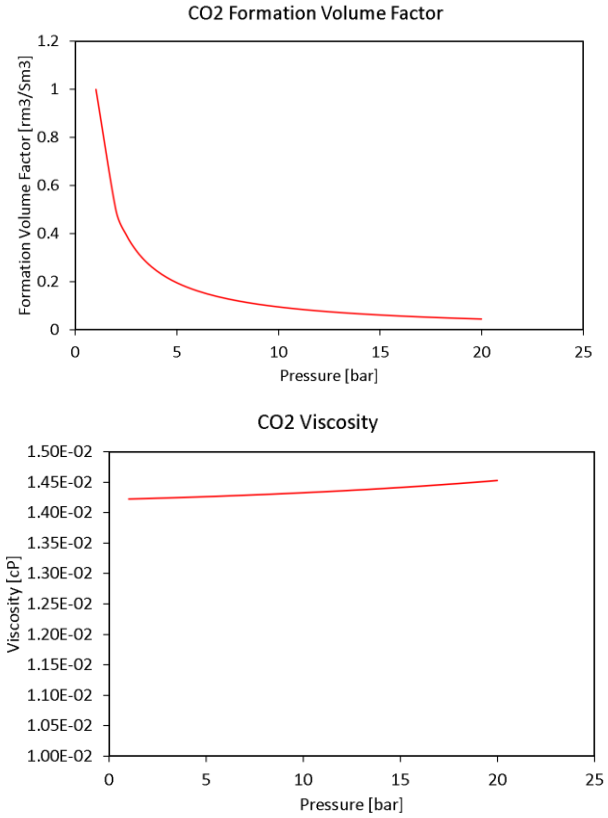

Figure 3.2: Black oil model – CO_2 properties vs pressure

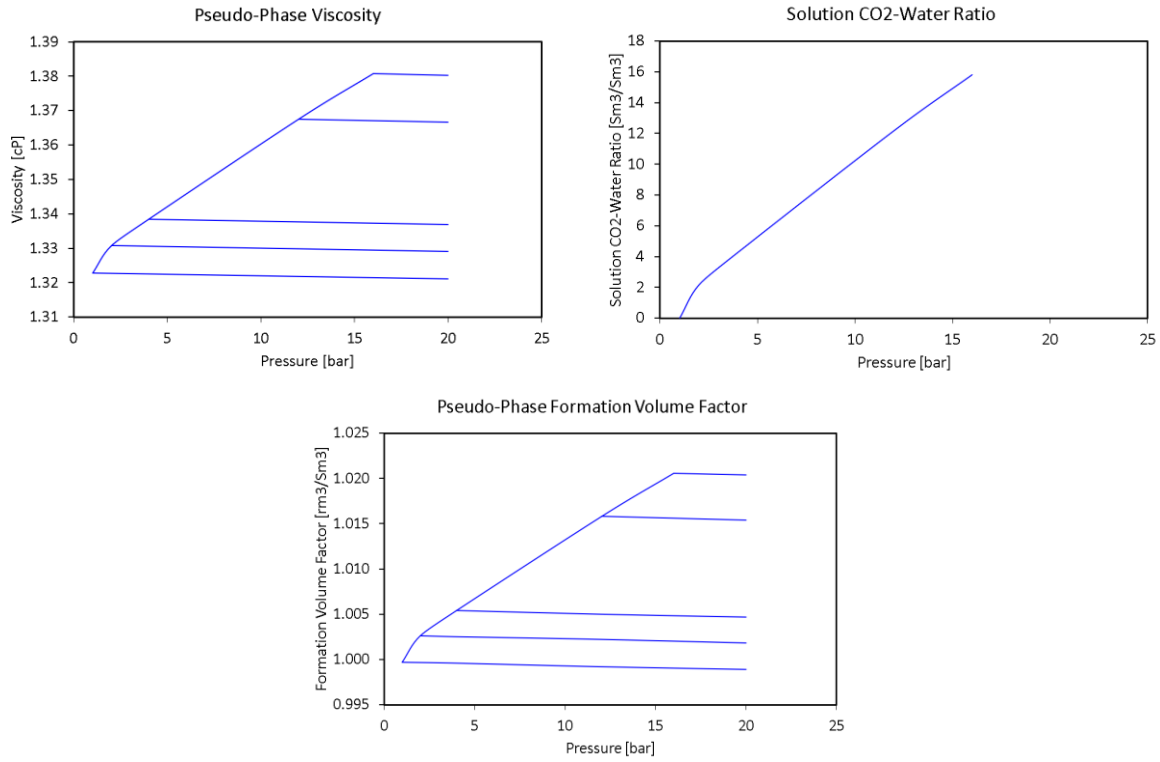

Figure 3.3: Black oil model – Pseudo-phase (CO_2-Water) properties vs pressure

3.3.2 Svelvik Ridge Geo-model

The geo-model of the Svelvik Ridge has improved understanding from the beginning of site characterization in 2012 and continued with the understanding from designing the Pre-ACT 2019 CO_2 injection campaign in 2018. The latest update of the geo-model was built in 2021 by Anja Sundal from UiO with two different scenarios based on the different geometry models to model the clinoform in the sand layer.

3.3.2.1 Dipping Grid Scenario (Scenario#1)

In this geo-model, the dipping is modelled by the grid geometry, as shown in Figure 3.4.

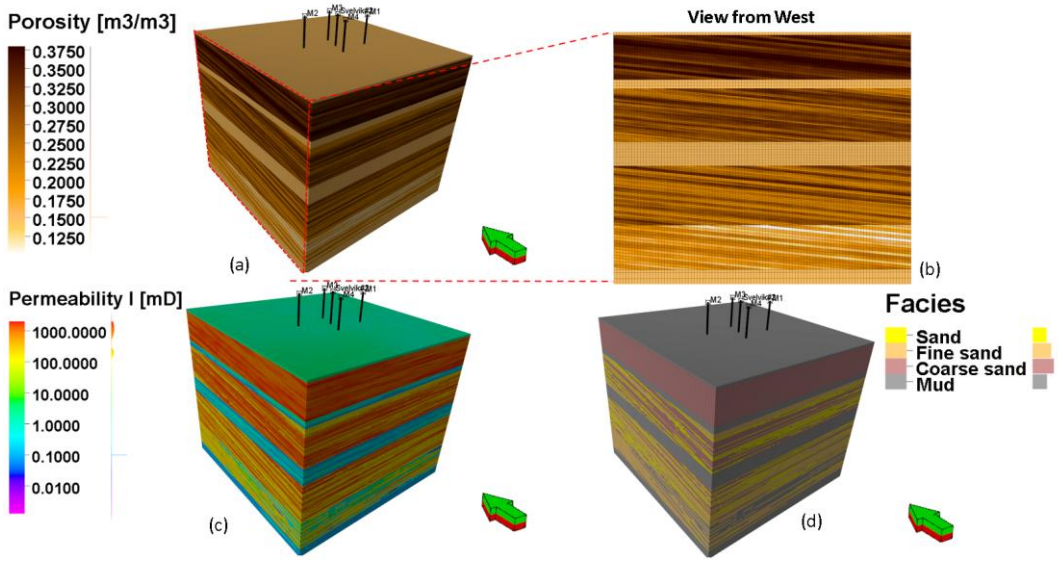

Figure 3.4: Dipping grid scenario (Scenario#1): (a) porosity distribution; (b) the dipping grid view from west; (c) permeability distribution; (d) facies distribution

The grid is 100m x 100m with a resolution of 1m x 1m per cell. Figure 3.4(b) presents the porosity distribution from the west side and the inclined grid in the sand layer. The mud layer act as a horizontal reference was made with a regular grid. The height per cell is different depending on the layer. The injected layer and the upper sand of the injected layer have a higher resolution with 0.5m height per cell, while the other has 1m height per cell (Figure 3.5).

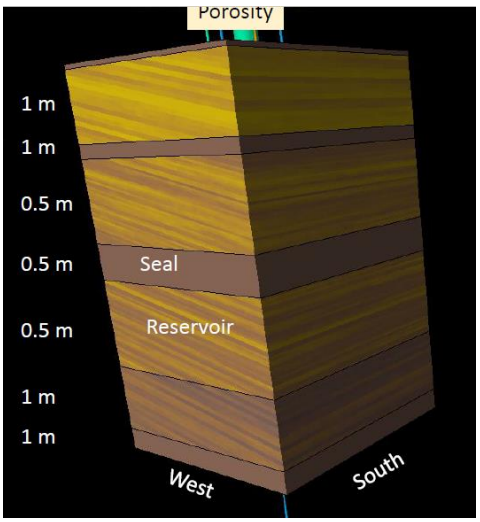

Figure 3.5: Cell height for different layering; reservoir and interest sand have cell height of 0.5m; the rest of the model has cell height of 1m

Facies distribution is based on the log interpretation from Chapter 2.1.3. The defined facies consist of coarse sand, sand, fine sand, and mud zone. The porosity distribution is based on the facies, where the coarse sand has an average porosity of 0.35, the sand has an average porosity of 0.25, fine sand has an average porosity of 0.2 and mud (seal) has an average porosity of 0.15. The permeability is also facies dependent on the porosity. The porosity and permeability distribution for this scenario is presented in Figure 3.6.

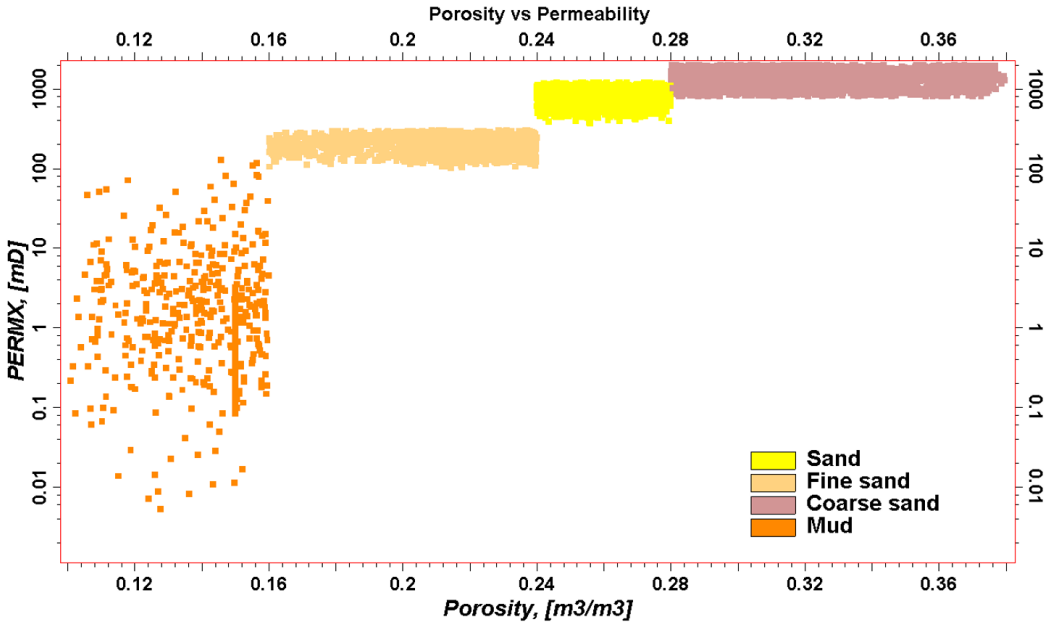

Figure 3.6: Porosity vs Permeability distribution with different facies for dipping grid scenario

The grid summary is shown in Table 3.1. and reservoir property distribution is presented in Table 3.2.

Table 3.1: Gridding in dipping grid scenario

Description	Value
Grid cells (nI x nJ x nK)	100 x 100 x 189
Total number of grids	1323816

Table 3.2: Summary of the reservoir properties in dipping grid scenario

Facies	Porosity [-]			Permeability [mD]		
	Mean	Min	Max	Mean	Min	Max
Coarse Sand	0.35	0.28	0.38	1500	800	2000
Sand	0.25	0.24	0.28	800	300	1200
Fine Sand	0.20	0.16	0.24	200	100	300
Mud (Silt)	0.15	0.10	0.16	10	0.1	100

3.3.2.2 Dipping Properties Scenario (Scenario#2)

I In this scenario, the grid on the model is regular gridding which does not consist of any inclined grid or irregular grid. The clinoform-like of the Svelvik ridge is modelled in the reservoir property distribution, as presented in Figure 3.7. Porosity is assigned by a distribution range, while permeability is a single value for each facies.

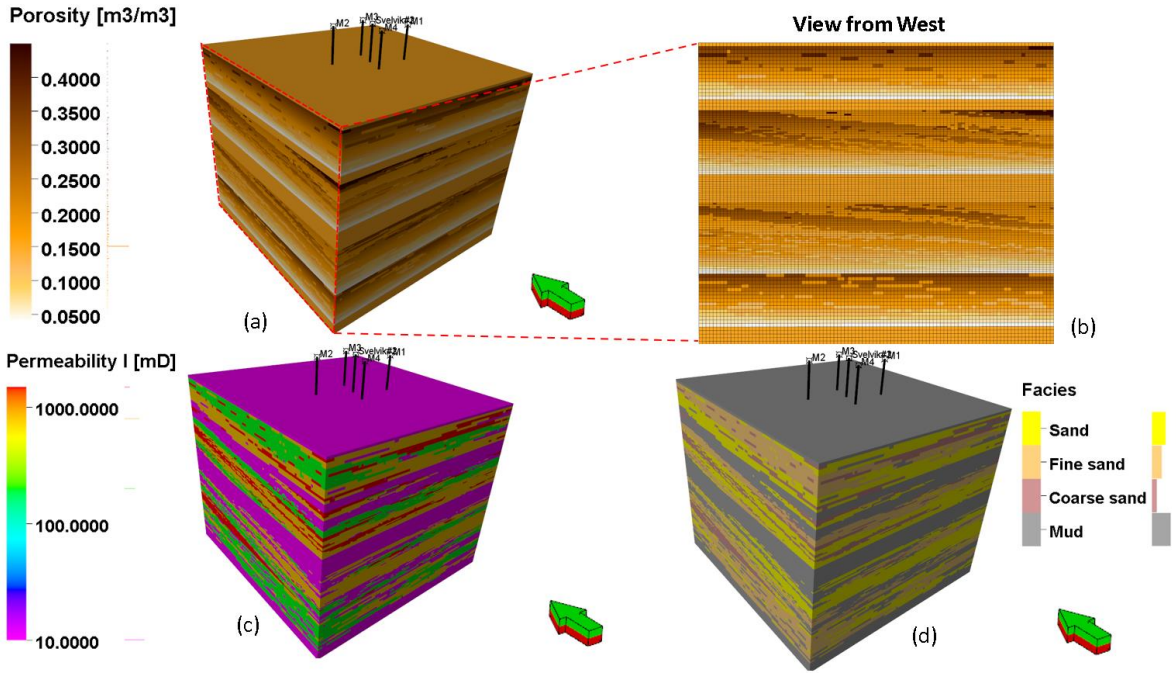

Figure 3.7: Dipping properties scenario (Scenario#2): (a) porosity distribution; (b) the dipping properties view from west; (c) permeability distribution; (d) facies distribution

The resolution of the grid is the same as in scenario 1, where each cell has the size of 1m x 1m. The cell height of the grid is similar to the first scenario, where the injected sand zone and upper layer of the sand zone have 0.5m cell height while the other has 1m cell height.

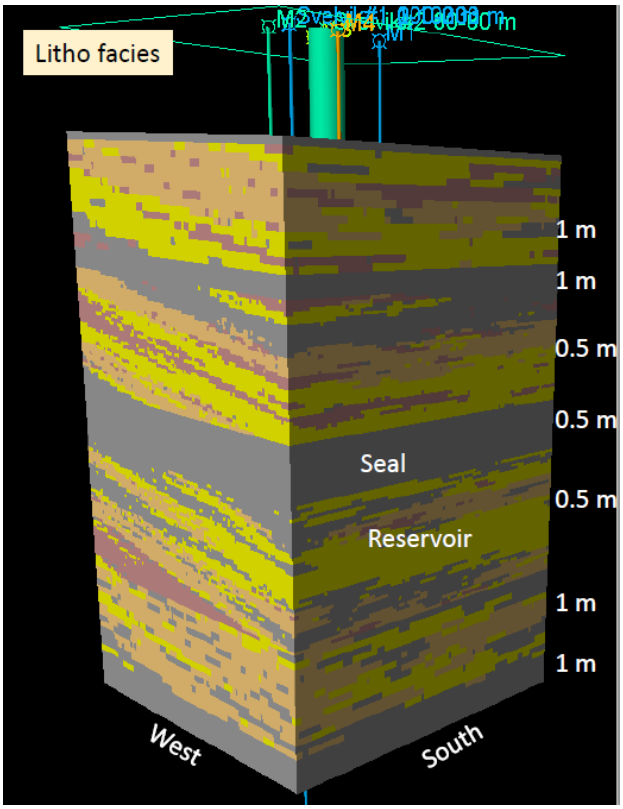

Figure 3.8: Cell height for different layering; reservoir and interest sand have cell height of 0.5m; the rest of the model has cell height of 1m

The porosity and permeability distribution with respect to the facies is presented in Figure 3.9.

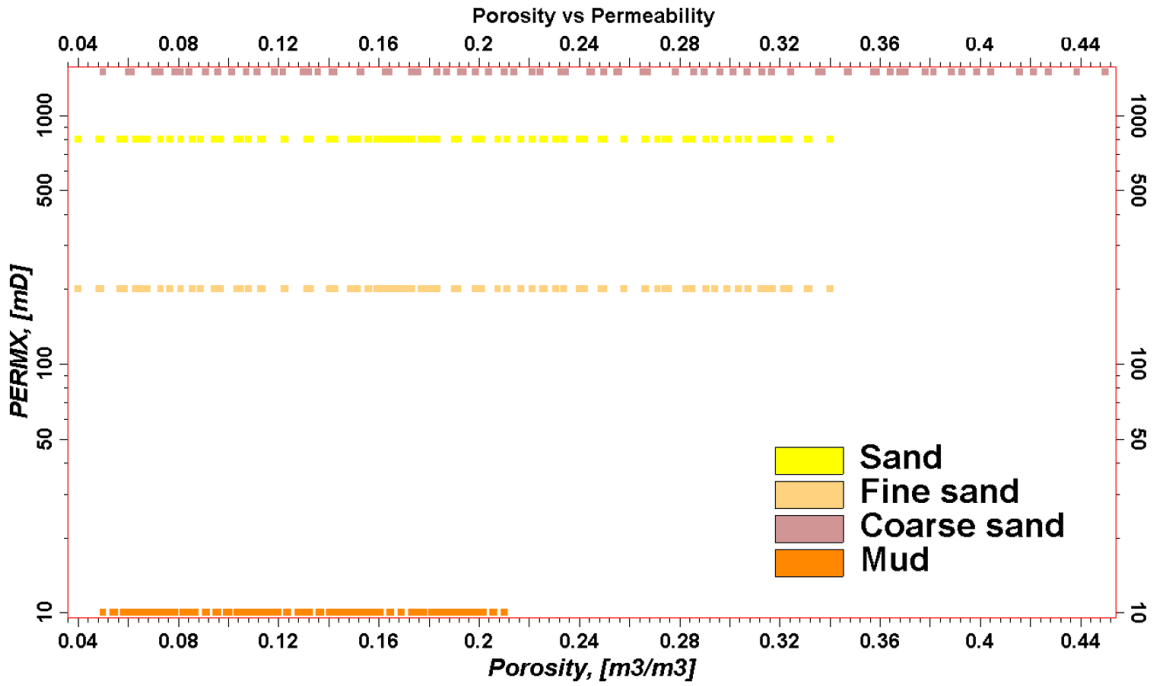

Figure 3.9: Porosity vs Permeability distribution with different facies for dipping properties scenario

The summary of the grid is shown in Table 3.3. and reservoir property distribution is shown in table Table 3.4.

Table 3.3: Gridding in dipping properties scenario

Description	Value
Grid cells (nI x nJ x nK)	100 x 100 x 131
Total number of grids	1310000

Table 3.4: Summary of the reservoir properties in dipping properties scenario

Facies	Porosity [-]			Permeability [mD]		
	Mean	Min	Max	Mean	Min	Max
Coarse Sand	0.35	0.05	0.45	1500	1500	1500
Sand	0.25	0.04	0.34	800	800	800
Fine Sand	0.20	0.04	0.34	200	200	200
Mud (Silt)	0.15	0.05	0.21	10	10	10

3.3.3 Relative Permeability and Capillary Pressure

The relative permeability model is based on a previous study for Svelvik modelling (Hagby, 2018), which explained that the identified lithofacies has their relative permeability curve.

(Corey & Brooks, 1964) stated that the relative permeability is a function of not only saturation but also grain size distribution. The equation relating the relative permeability with the relative permeability is shown in the equation:

$$k_{r,w} = \left(\frac{S_w - S_{wr}}{1 - S_{wr}}\right)^{\frac{2+3\lambda}{\lambda}} \tag{4}$$

$$k_{r,nw} = \left(\frac{1 - S_w}{1 - S_{wr}}\right)^2 \left[1 - \left(\frac{S_w - S_{wr}}{1 - S_{wr}}\right)^{\frac{2+\lambda}{\lambda}}\right] \tag{5}$$

where $k_{r,w}$ is the wetting phase relative permeability, $k_{r,nw}$ is the non-wetting phase relative permeability, S_w is the wetting phase saturation, S_{wr} is the wetting phase residual saturation, and λ is grain size distribution index.

Figure 3.10 depicts the original relative permeability curves used in simulation. The original permeability curve is based on Corey and Brook's equation. The CO_2 end point saturations are S_w 0.25 and 1.0 with the exponent of 2.5. The water end point saturations are S_w 0.1 and 1.0 with the exponent of 4. (Grimstad, 2013)

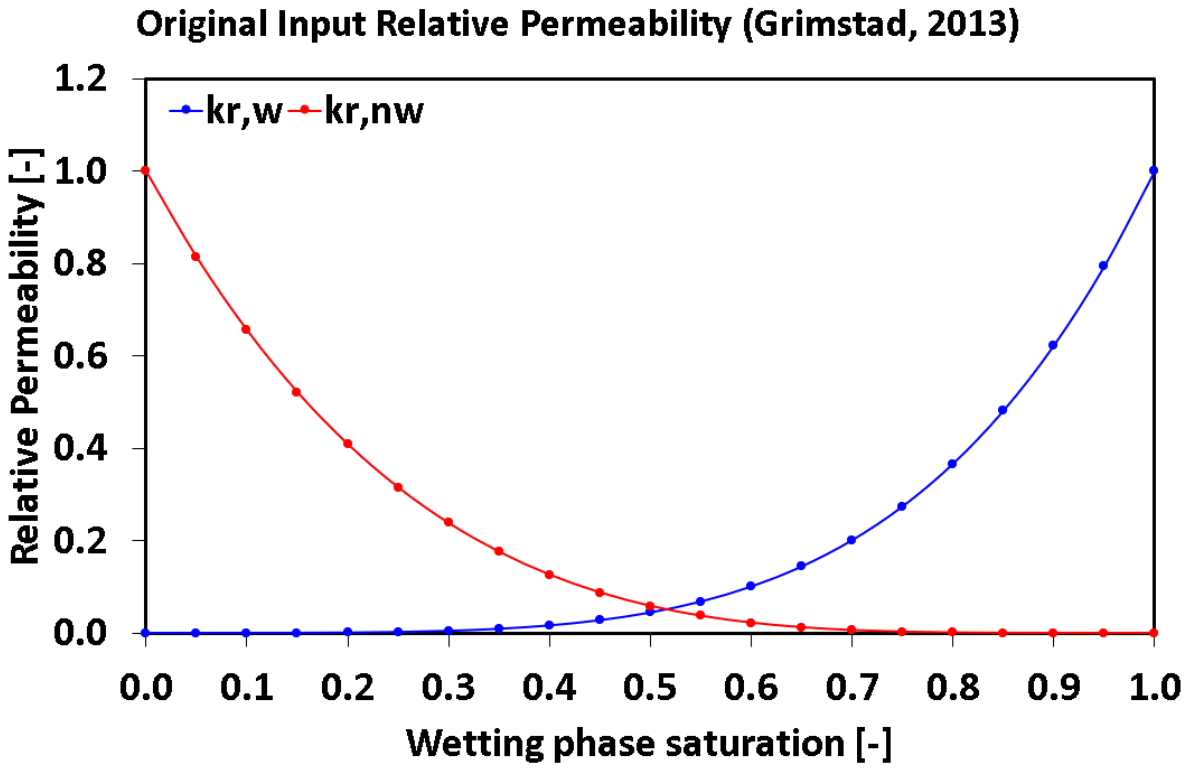

Figure 3.10: Relative permeability versus water saturation, as original input (Grimstad, 2013)

Based on the lithofacies and grain size distribution index in Table 3.5. Grain size distribution index, for different porous media (Assouline, 2005), the drainage relative permeability for each lithofacies is calculated using Equation (4).

Table 3.5: Grain size distribution index, for different porous media (Assouline, 2005)

Lithofacies	Grain size distribution index, λ
Unconsolidated Sand	3.70
Silt	1.82
Consolidated Sand	2.29

The imbibition relative permeability was calculated using the Carlson model, which assumes that the relative permeability of the wetting phase shows no hysteric behaviour (Hagby, 2018). Figure 3.11 shows the relative permeability used in the simulation based on the calculation and grouped for each lithofacies used in the simulation.

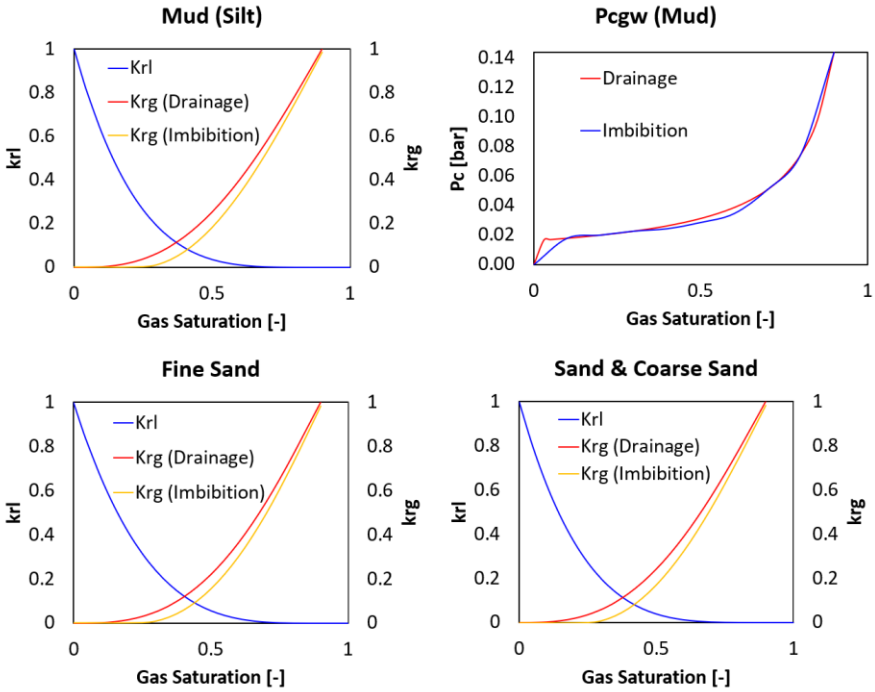

Figure 3.11: Relative permeability and capillary pressure curve for simulation

3.3.4 Initialization Properties

Based on the known datum pressure, the initialization of the model is built for the Eclipse E100. The E100 initialization properties are shown in Table 3.6. The pressure datum known as the pore pressure at a depth of 61m is 6.04 barg relative to the atmospheric pressure. Therefore, in the eclipse file, the pressure@61m is added 1 bar for the atmospheric pressure correction. The aquifer water depth represents where the open boundary is located and the aquifer attachment is placed.

Table 3.6 Initialization Properties

Property	Value
Pressure@datum	7.04 bar
Datum depth	-61.0 m
Gas-Water-contact	0.0 m
Water-gas Pc	0.0 bar
Aquifer water depth	-70.0 m
Pc at aquifer water	0.0 bar

3.3.5 Aquifer Model (Open Boundary)

The aquifer model is used to model the open boundary in the Svelvik ridge. It can be seen through the Pre-ACT injection Svelvik#2 bottomhole pressure response in injection and shut-in. The aquifer is attached at the bottom and side of the model to a depth of 70m (Figure 3.12). The aquifer calculation uses the Carter-Tracy method. This model approximates a fully transient model that avoids the requirement for superposition calculation.

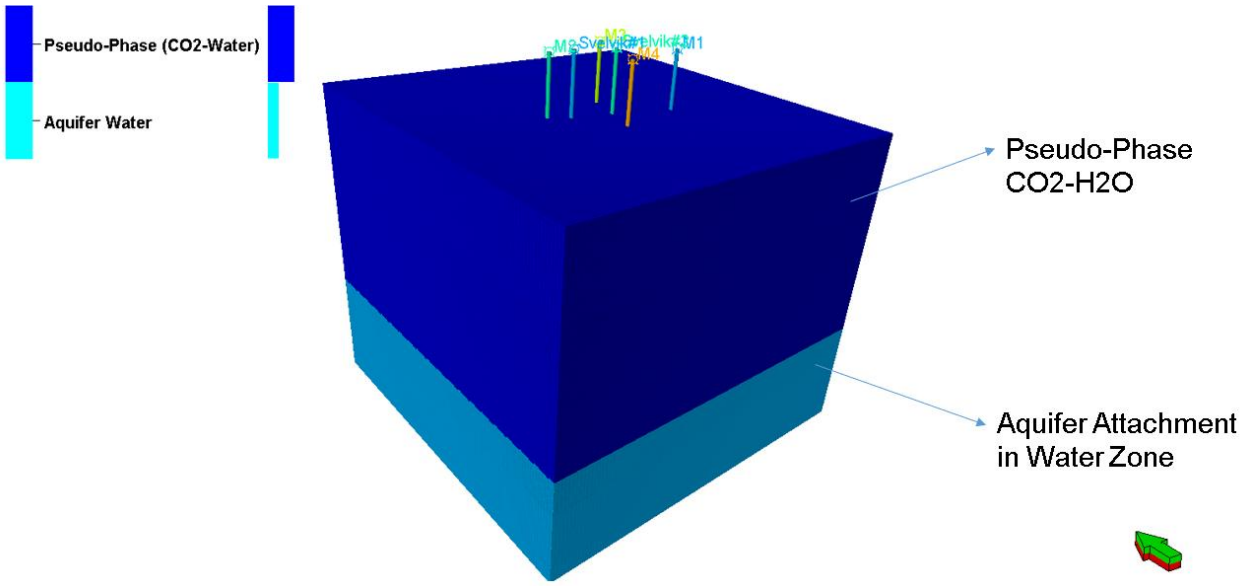

Figure 3.12: Aquifer and open boundary model

The Carter-Tracy aquifer model uses a table to supply a constant terminal rate influence function given by van Everdingen and Hurst. The parameters used to define the Carter-Tracy aquifer model are shown in Table 3.7. The table is used later as one of the matching parameters in history matching. The parameter is defined to have a large extent and infinite boundary.

Table 3.7 Aquifer model properties

Aquifer model	Carter-Tracy
Pressure initialization	Equilibrium
Permeability	300000 mD
Porosity	0.25
Total compressibility	0.00014504 1/bar
External radius	2000 m
Thickness	15.24 m
Angle of influence	360^0

3.3.6 Pre-ACT 2019 Injection Campaign Data

The data used in this study is the Svelvik#2 bottomhole pressure and rate data for the history matching input. Initial data measured is prepared as in Figure 2.9. The pressure data undergoes correction to the ambient pressure, tide effect, and below packer volume. The shifting of the measured pressure data with the corrected is shown in Figure 3.13. The rest of the data is upscaled in hourly basis to reduce the time step for simulation.

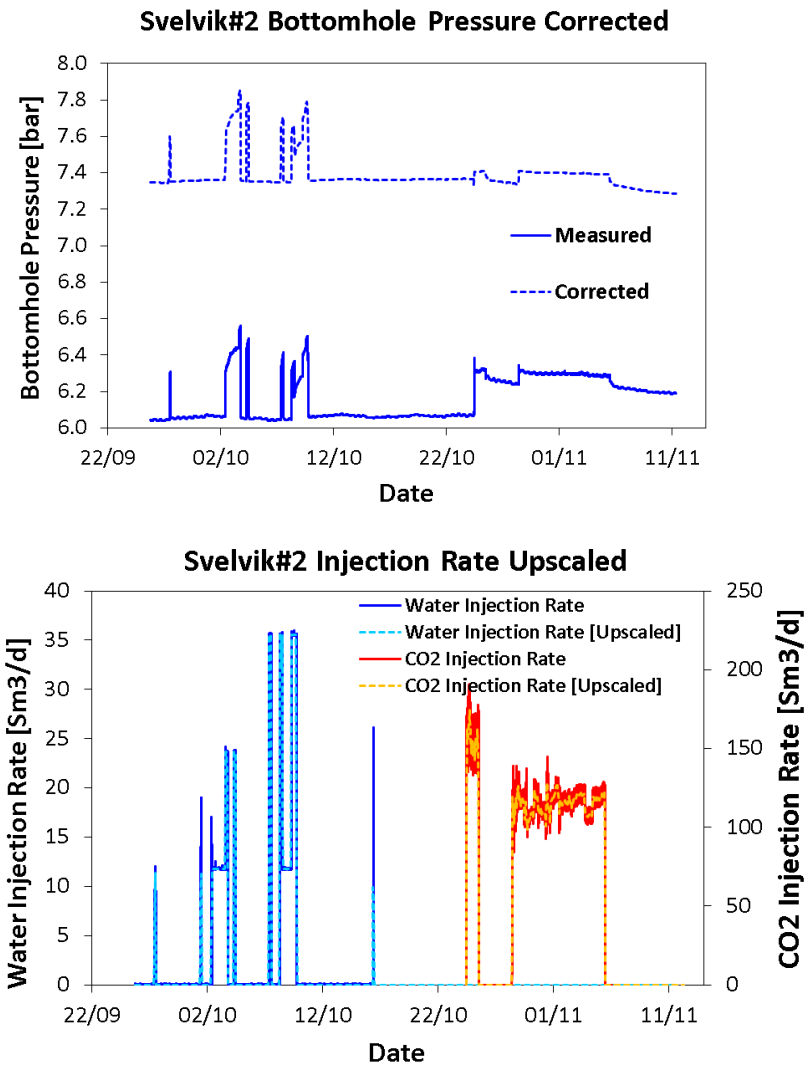

Figure 3.13: Svelvik#2 corrected and upscaled data

The correction applied to the pressure data are:

- The relative difference with atmospheric pressure (additional 1 bar),
- increase in air pressure from the surface to packer depth (around 7mbar), and
- the hydrostatic pressure difference between transmitter depth and screened interval (around 3m, or 300mbar).

The upscaled data is used as the input for history matching, where the model is adjusted to match the behaviour from this data.

3.4 Reservoir Model & Schedule Upscaling

3.4.1 Reservoir Model Upscaling

The initial run of the model took 22435.52 s (7.11hr) per history matching case. With this amount of time required for one simulation case, upscaling is recommended to decrease the amount of time required.

The upscale process is shown in Figure 3.14. Both geo-model scenarios undergo upscaling to decrease the simulation time required. The workflow of upscaling is as follows:

1. Define an area of interest in which the grid size will be preserved.
2. Define the amount of coarsening in I and J direction for the grid outside of the area of interest
3. Define the method of properties coarsening in the coarsened area.
4. Check the distribution of the properties and the simulation results to prove that upscaling will not change the simulation results.

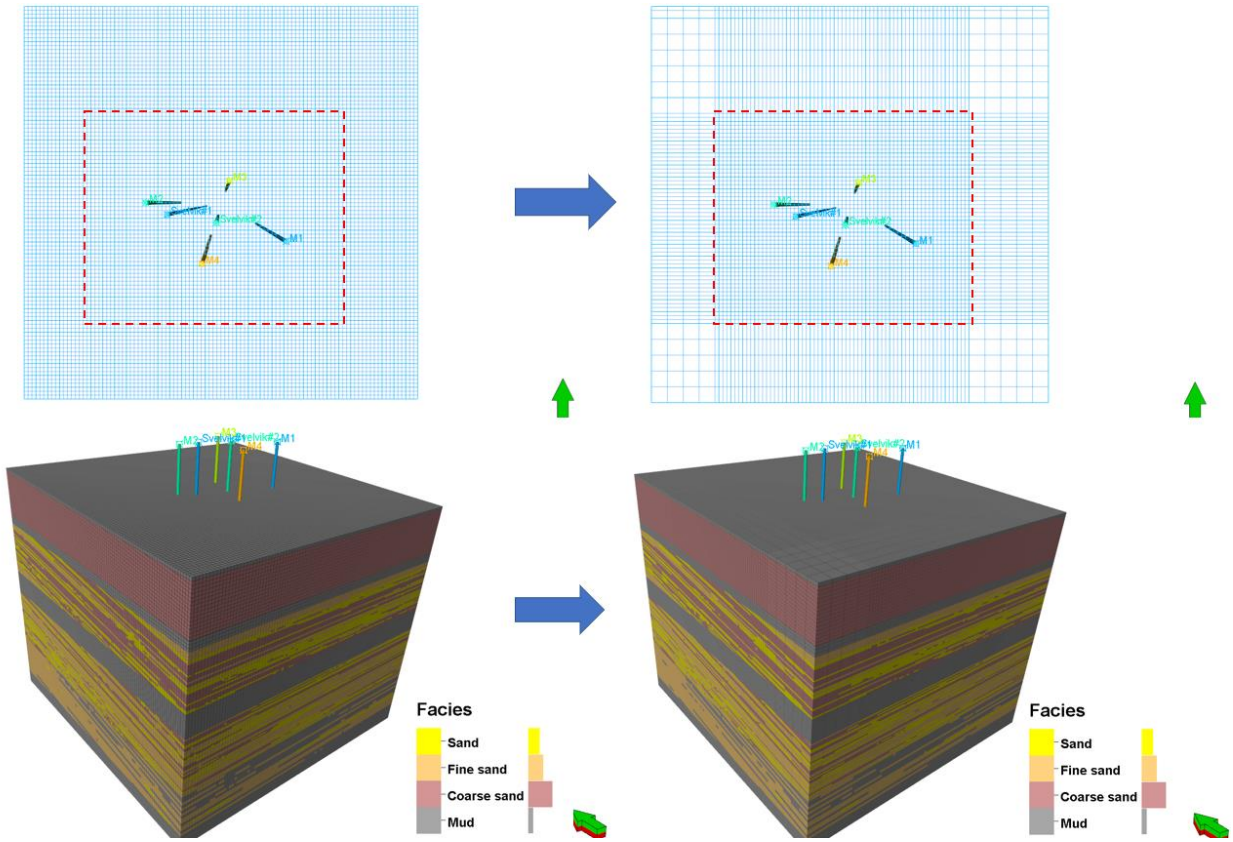

Figure 3.14: Upscale process: Original (left) and Upscaled (right)

Depending on the properties, the upscaled properties follow the method as below:

- Porosity: Arithmetic averaging, volume-weighted
- Facies: Most of averaging, volume-weighted
- Permeability: Arithmetic averaging, volume-weighted

The comparison of the original model and upscaled is shown in Figure 3.15. Based on the Svelvik#2 bottomhole pressure, the average field pressure, and the CO_2 Plume from the initial history matching case, it can be inferred that the original and upscaled model is

identical in terms of the interest area.

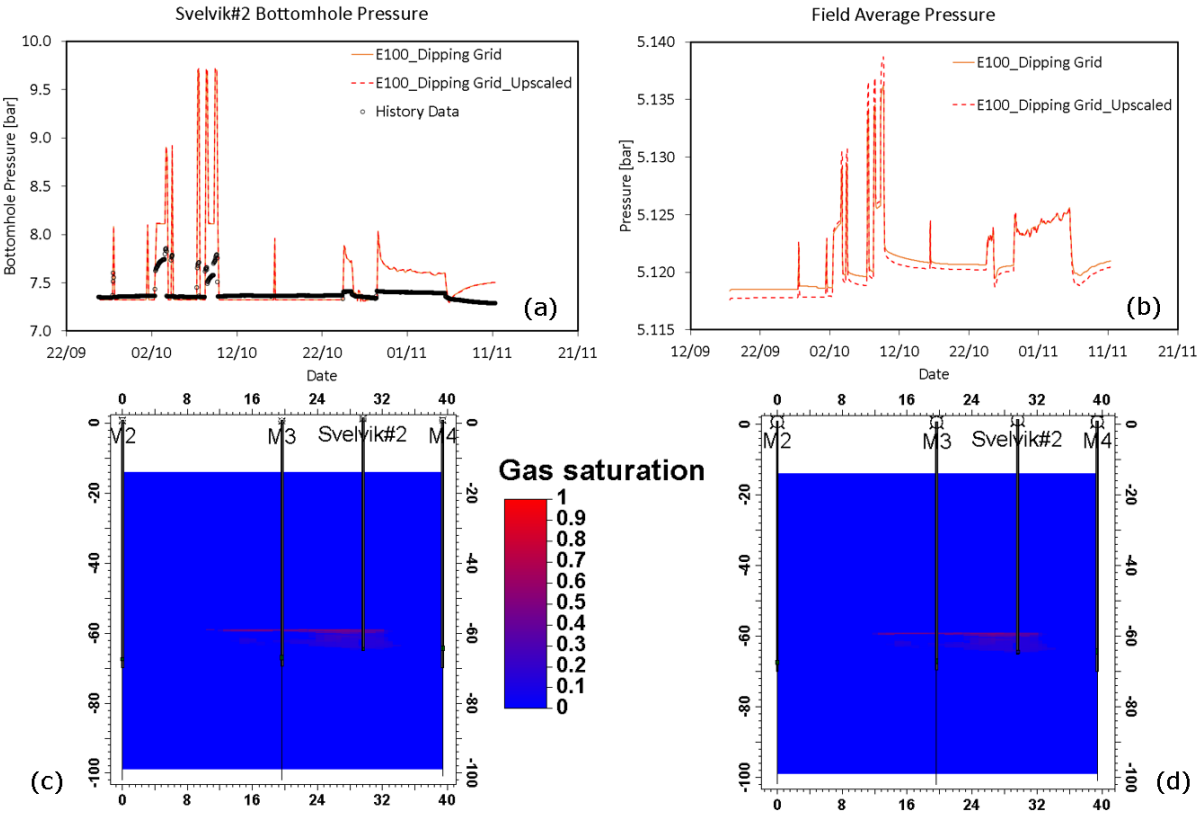

Figure 3.15: Dipping grid scenario original and upscaled comparison: (a) Svelvik#2 bottomhole pressure; (b) Average field pressure; (c) Original CO_2 plume cross-section; (d) Upscaled CO_2 plume cross-section

The summarization of the time reduction from this upscaling is shown in Table 3.8.

Table 3.8 Comparison of original and upscaled CPU time (Scenario#1)

Properties	Original Model	Upscaled Model
Total Active Grids	1323816	648633
CPU Time	22435.52s (6.23 hr)	11372.48s (3.15 hr)
Time steps	3941 steps (2019-09-17 16:00 to 2019-11-11 09:00)	3941 steps (2019-09-17 16:00 to 2019-11-11 09:00)

3.4.2 Schedule Upscaling

The timestep required for the whole history matching is 3941 timesteps which started from 17th September 2019 at 16:00 to 11th November 2019 at 09:00, with a 1-hour difference for each timestep.

The new schedule is introduced to reduce the number of the timestep.

Table 3.9 Reduced timestep definition

Date	Timestep
17-09-2019 16:00 to 27-09-2019 08:00	1 month
27-09-2019 08:00 to 27-09-2019 14:00	1 hour
27-09-2019 14:00 to 02-10-2019 07:00	1 month
02-10-2019 07:00 to 04-10-2019 22:00	1 hour
04-10-2019 22:00 to 07-10-2019 08:00	1 month
07-10-2019 08:00 to 09-10-2019 19:00	1 hour
09-10-2019 19:00 to 24-10-2019 10:00	1 month
24-10-2019 10:00 to 06-11-2019 12:00	1 hour
06-11-2019 12:00 to 11-11-2019 09:00	1 day

This timestep focuses more on the event where the injection happens. With the upscaled schedule, the number of timesteps is lowered significantly from 3941 timesteps to 1710 timesteps. This also reduces the simulation time and memory usage to do history matching.

Table 3.10 Upscaled schedule comparison

Properties	Original Schedule	Upscaled Schedule
Timesteps	3941 steps (2019-09-17 16:00 to 2019-11-11 09:00)	1710 steps (2019-09-17 16:00 to 2019-11-11 09:00)
CPU Time	11372.48s (3.15 hr)	8329.14 (2.31 hr)

3.5 Defining Uncertainties

The selected uncertainties are based on unknown parameters. The initial CO_2 monitoring proves that the CO2 migrated to the depth of 38m, and the mud zone is interpreted at a depth of 29 – 38m without any sign of a lower mud zone (50.7 – 61.2 m). The lower mud zone probably discontinues across the zone, which allows the migration of the CO_2 from 65m (injection depth) to 38m (Figure 2.10). The 50.7 – 61.2 m depth is modified to be the lithofacies most connected to this mud layer to model this. In this case, scenario#1 is defined as coarse sand, and scenario#2 is defined as sandstone, as depicted in Figure 3.16.

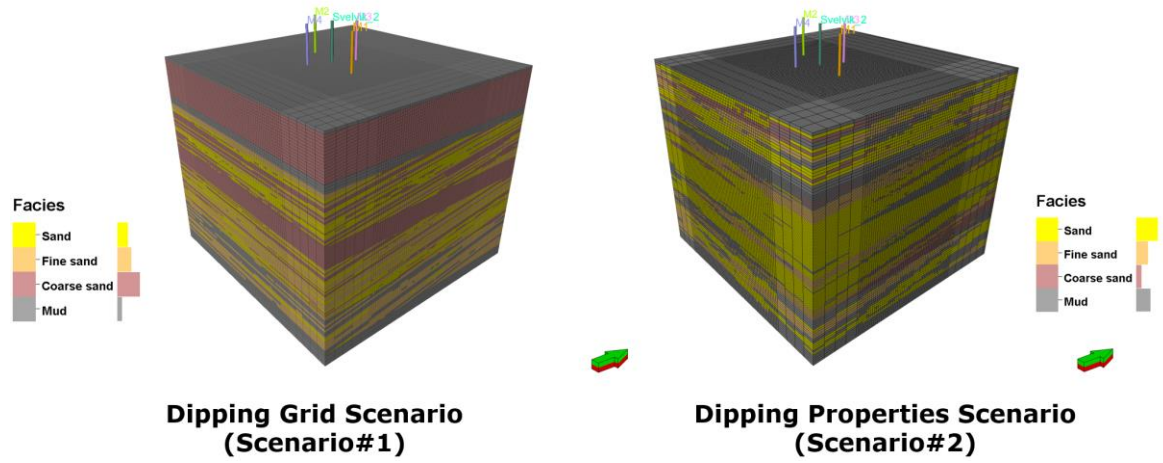

Figure 3.16: Modification of lithofacies for uncertainty

The design of the injection well and the possibilities of the CO_2 leakage from the annulus between the injection casing and open hole formation that is sealed using bentonite slurry is also uncertain. In the recent observation, the bubble is observable until the surface of the Svelvik#2 well. It is modelled by allowing a higher vertical permeability along with the well's grid cells until the mud layer region, assuming that the vertical permeability modelled the connection between the well and formation only (Figure 3.17).

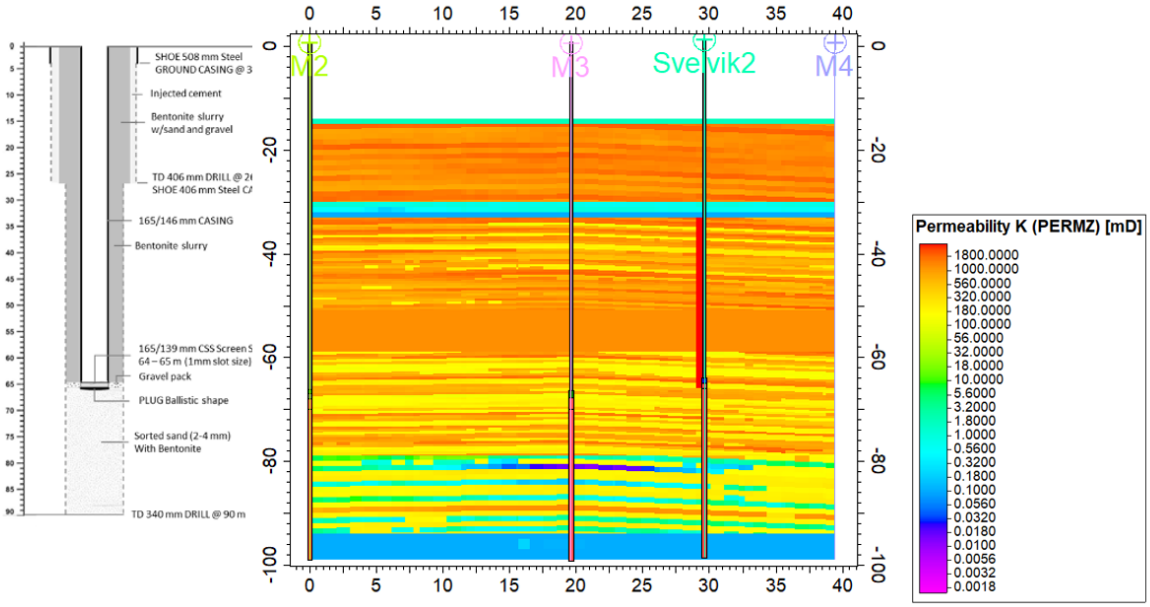

Figure 3.17: Vertical leakage permeability definition

The vertical leakage is not modelled to the top of the model due to the requirement to model the open boundaries at the top (since the CO_2 is observable until the surface).

Other uncertainties being studied come from global permeability distribution, permeability anisotropy, and aquifer properties. Along with the studies, it is observed that other uncertainties come from the water salinity injected at the beginning of the Pre-ACT injection, water table affecting the pressure measurement, below packer volume, and the requirement to model the tubing performance relationship for the injection well.

3.6 History Matching

Two methods are used to match the Pre-ACT 2019 injection data: Uncertainty-based history matching and conventional history matching based on the sensitivity results.

3.6.1 Uncertainty Based History Matching

The uncertainty-based history matching consists of the uncertainties defined in the uncertainty table and sampled by Latin Hypercube Method. Several samples are defined for history matching. This method's weakness is that the uncertainty should be studied thoroughly and defined within a specific range. This method works best with optimization algorithms but is not included in this study due to the time required to run many cases with too many uncertainty variables.

The main parameters being investigated at the beginning are the aquifer properties, permeability anisotropy, global permeability multiplier, and rock compressibility.

The summary of uncertainties that are studied initially is shown in Table 3.11.

Table 3.11: Uncertainty Parameters

Properties	Distribution	Minimum Value	Maximum Value
Global permeability multiplier [-]	Uniform	1	5
Permeability anisotropy [-]	Uniform	0.1	2
Vertical leakage permeability [mD]	Uniform	1000	10000
Rock compressibility [1/bar]	Uniform	1E-07	0.1
Aquifer rock compressibility [1/bar]	Uniform	1E-07	0.1
Aquifer permeability [mD]	Uniform	10	3000
Aquifer radius [m]	Uniform	200	100000
Aquifer thickness [m]	Uniform	1.524	1524

3.6.2 Conventional History Matching

In parallel with the uncertainty-based history matching, conventional history matching was being studied to adjust the uncertainty parameters. In this method, the most uncertain parameters affecting the history matching were being studied. In the previous studies, the parameter that affects the most is the global permeability multiplier. Therefore, a sensitivity study to this parameter was done. The other parameters are set to a more realistic value as follows:

1. Aquifer (Open Boundary setting)

Table 3.12: Aquifer mode properties

Aquifer model	Carter-Tracy
Pressure initialization	Equilibrium
Permeability	750 mD
Porosity	0.25
Total compressibility	0.00014504 1/bar
External radius	5000 m
Thickness	15.24 m
Angle of influence	360^0

2. Mud layer on 50.7m – 60m
   The mud layer is changed to coarse sand with 1200mD and porosity of 0.36 for the dipping grid scenario (scenario#1) and sand with 800mD and porosity of 0.15 for the dipping grid scenario (scenario#2). The facies are selected with respect to the lithofacies connected to this mud layer.

3. Rock compressibility
   The rock compressibility is the same as in previous studies (Hagby, 2018), in which the simulation file states that the rock compressibility was 1.0E-4 1/bar at 5 bar pressure.

4. Near wellbore vertical permeability
   The near-wellbore vertical permeability is set to 3000 mD, higher than the vertical permeability of the formation. The near-wellbore vertical permeability is modelled at the possible contact between bentonite slurry and formation that allows the CO_2 to migrate through, as shown in Figure 3.17.

   The limitation of this model is that the current simulation cannot create an open boundary on the top of the model to model the CO_2 released into the atmosphere from the bentonite slurry.

5. Permeability anisotropy (k_v/k_h)
   The permeability anisotropy that has been studied is presented in the attachment section. It is shown that permeability anisotropy plays a role in the migration of CO_2.
   With permeability anisotropy of 2, the CO_2 can naturally migrate upward until the depth of 31m. However, it will not spread enough to the north (M3 well). In contrast, permeability anisotropy of 0.1 results in the CO_2 spreading horizontally to the north way further than it should be. Therefore, a permeability anisotropy of 0.5 in combination with the near-wellbore vertical permeability is used in the history matching.

The history matching is applied to the dipping grid scenario and the dipping properties scenario follows.

3.7 Proxy Model Design

The proxy model design is started after the history matching is done. The history-matched model is simulated in constant conditions for up to three years to see the behaviour of CO_2 dissolving in the pseudo-phase (CO_2-Water). The objective of the proxy model is to simulate the CO_2 injection with different injection rates in two cycles of injection. The CO_2 is injected for one week and stopped for another week for each cycle. Thus, the proxy model will require the input of two injection rates, which are the first cycle injection rate and the second cycle injection rate.

3.7.1 Training Dataset

The training data uses the detailed fractional factorial design presented in Table 3.13. The minimum injection rate is 21.4 Sm3/d and the maximum injection rate is 192.9 Sm3/d, with the cumulative CO_2 injected being 1500 Sm3/d for samples 1 to 9. With this sample, the resulting proxy will work only in 1500 Sm3/d cumulative CO_2 injected. The

additional training data from 10 to 18 allows the proxy to work with the cumulative CO_2 injected ranging from 580 Sm3/d to 2700 Sm3/d.

Table 3.13: Training dataset for proxy model

Training Sample	1st Injection Cycle [Sm3/d]	2nd Injection Cycle [Sm3/d]
1	21.42857	192.8571
2	42.85714	171.4286
3	64.28571	150.0000
4	85.71429	128.5714
5	107.1429	107.1429
6	128.5714	85.71429
7	150.0000	64.28571
8	171.4286	42.85714
9	192.8571	21.42857
10	21.42857	21.42857
11	42.85714	42.85714
12	64.28571	64.28571
13	85.71429	85.71429
14	107.1429	107.1429
15	128.5714	128.5714
16	150.0000	150.0000
17	171.4286	171.4286
18	192.8571	192.8571

3.7.2 Validation Dataset

The validation dataset is the data that is used to check the usability of the proxy. These data should be different from the training dataset to ensure that the validation will not be biased. In this case, the validation data used is shown in Table 3.14.

Table 3.14: Validation dataset for proxy model

Validation Sample	1st Injection Cycle [Sm3/d]	2nd Injection Cycle [Sm3/d]
1	31.1428	182.1428
2	53.5714	160.7142
3	75.0000	139.2857
4	96.4285	117.8571
5	117.8571	96.4285
6	139.2857	75.0000
7	160.7142	53.5714
8	182.1428	31.1428

The validation dataset is mainly the data in between the training dataset. For example, between the 1st and 2nd training samples has the data which the 1st injection cycle will be 32.1428 Sm3/d and the 2nd injection cycle will be 182.1428 Sm3/d.

3.7.3 Evaluation Dataset

The evaluation data is generated using the Latin hypercube sampling (LHS) method, where the distribution, minimum and maximum values are determined for the first and second injection cycles. It means the evaluation data does not follow the training and validation rule, which ensures the proxy is usable in every case within the range.

The evaluation dataset is generated for both geological scenarios separately. Therefore, the evaluation for the dipping grid and properties scenario will differ.

Table 3.15: Evaluation dataset for dipping grid scenario (Scenario#1)

Evaluation Sample	1st Injection Cycle [Sm3/d]	2nd Injection Cycle [Sm3/d]
1_1	31.1428	182.1428
2_1	53.5714	160.7142
3_1	75.0000	139.2857
4_1	96.4285	117.8571
5_1	117.8571	96.4285

Table 3.16: Evaluation dataset for dipping properties scenario (Scenario#2)

Evaluation Sample	1st Injection Cycle [Sm3/d]	2nd Injection Cycle [Sm3/d]
1_2	40.4125	178.3760
2_2	139.709	93.3423
3_3	162.657	169.509
4_4	181.095	114.866
5_5	27.4022	164.649

3.7.4 Proxy Model Algorithm

This study used a statistical proxy model to complement the conventional numerical simulation model for the CO_2 injection prediction. The independent variables for the proxy model are the first injection cycle and the second injection cycle of the CO_2 injection rate. Several dependent variables are evaluated, from the Svelvik#2 bottomhole pressure, average field pressure, dissolved CO_2 in Water, and Free CO_2 volume per layer defined in Figure 3.18. The layering definition follows the different lithofacies as defined in the geo-model section.

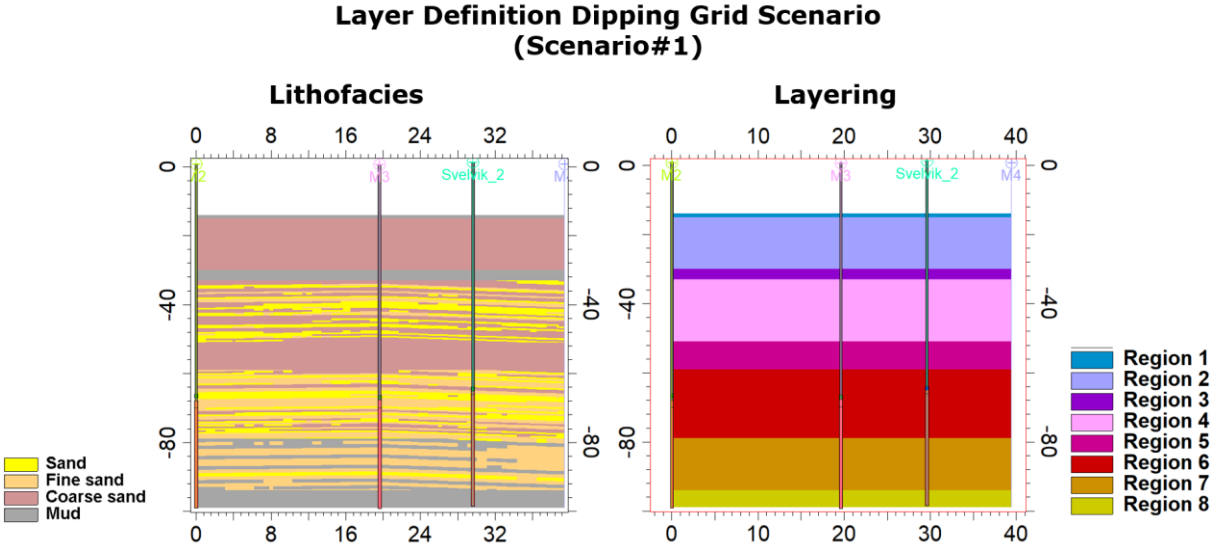

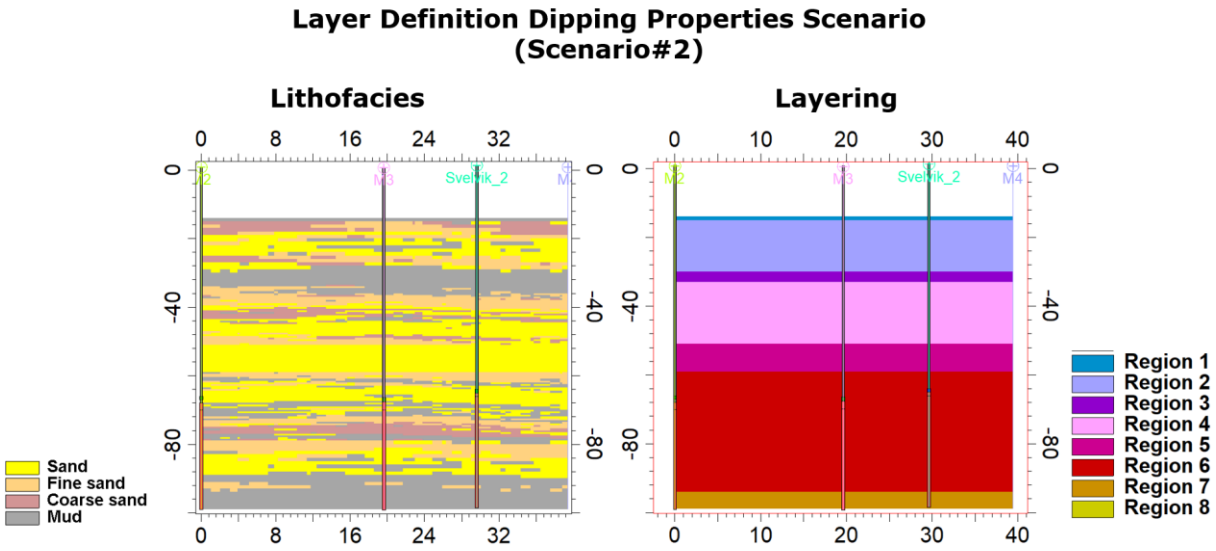

Figure 3.18: Layering definition: Dipping grid scenario (above) and dipping properties scenario (below)

Two types of statistical proxy models were used in this study, and a comparison between the proxy models can be made.

The first statistical proxy is the response surface proxy, where the predicted value will be based on a formula that has been fitted with the training data. This proxy model assumes that the predicted value follows a polynomial function with respect to the independent variable. There are several types of response surfaces, as explained in chapter 2.4.2. Based on the limited number of samples for the training and validation dataset, the proxy model built was linear model and bilinear model.

Based on the limited number of samples for the training and validation dataset, the proxy model built was the linear and bilinear model.

The second statistical proxy is the universal kriging proxy, where the proxy uses the Gaussian process to determine the random error with zero mean, unknown variance, and correlation function. This proxy model is built assuming that the model follows the gaussian process. Therefore, this proxy can model a more complex response with the training and validation dataset.

3.7.5 Proxy Model Scoring

The proxy model scoring used in this study is the R-squared method (Equation (6)) for evaluating the observed and predicted responses.

$$R^2 = \left[\frac{n\left(\sum P_{sim} P_{proxy}\right) - \left(\sum P_{sim}\right)\left(\sum P_{proxy}\right)}{\sqrt{\left[n\left(\sum P_{sim}^2\right) - \left(\sum P_{sim}\right)^2\right]\left[n\left(\sum P_{proxy}^2\right) - \left(\sum P_{proxy}\right)^2\right]}} \right]^2 \quad (6)$$

Each of the timesteps will also be evaluated by percent error (Equation (7)) to see the error cause in different timesteps.

$$Percent\ Error = \frac{\left|P_{simulation} - P_{proxy}\right|}{P_{simulation}} \times 100\% \quad (7)$$

This will ensure that the proxy model is evaluated thoroughly in the validation and evaluation case with the possibility of detecting the error and which situation the proxy model will not be able to follow the simulation model.

3.8 Assumptions and Limitations

The assumptions used and the limitations in this study are:

1. There is no leakage to the surface. In reality, there is leakage through the annulus to the surface, and the volume is still being investigated. To model the atmospheric situation in the reservoir model is complex due to the open boundary should exist at the top of the reservoir model.
2. The high vertical permeability is used to model the bentonite slurry that only contacts the formation, which assumes that the bentonite slurry creates a possibility of a CO2 migration pathway to the upper formation.
3. The aquifer model exists below the injection point (70m) since the requirement to model the pseudo phase at the top of the model cannot be attached by the aquifer model. The simulation uses the E100 simulation model that the aquifer attachment is not able to be attached at the pseudo-phase (CO_2-Water).
4. The proxy models use a statistical method where responses surface proxy assumes that the model follows a polynomial function. The universal kriging proxy assumes that the true model follows Gaussian processes in finding the random error.
5. The new CO2 injection started on the 22nd of April 2022, with the final state based on the history matching.

4 Results and Discussion

4.1 History Matching

In this section, the history matching results are discussed thoroughly.

4.1.1 Initial History Matching Results

The initial history matching result is the base result of the history matching without any modification to the model. The upscaled model of the dipping grid scenario and the dipping properties scenario are history matches. In Figure 4.1 depicts the Svelvik#2 bottomhole pressure with the history match result.

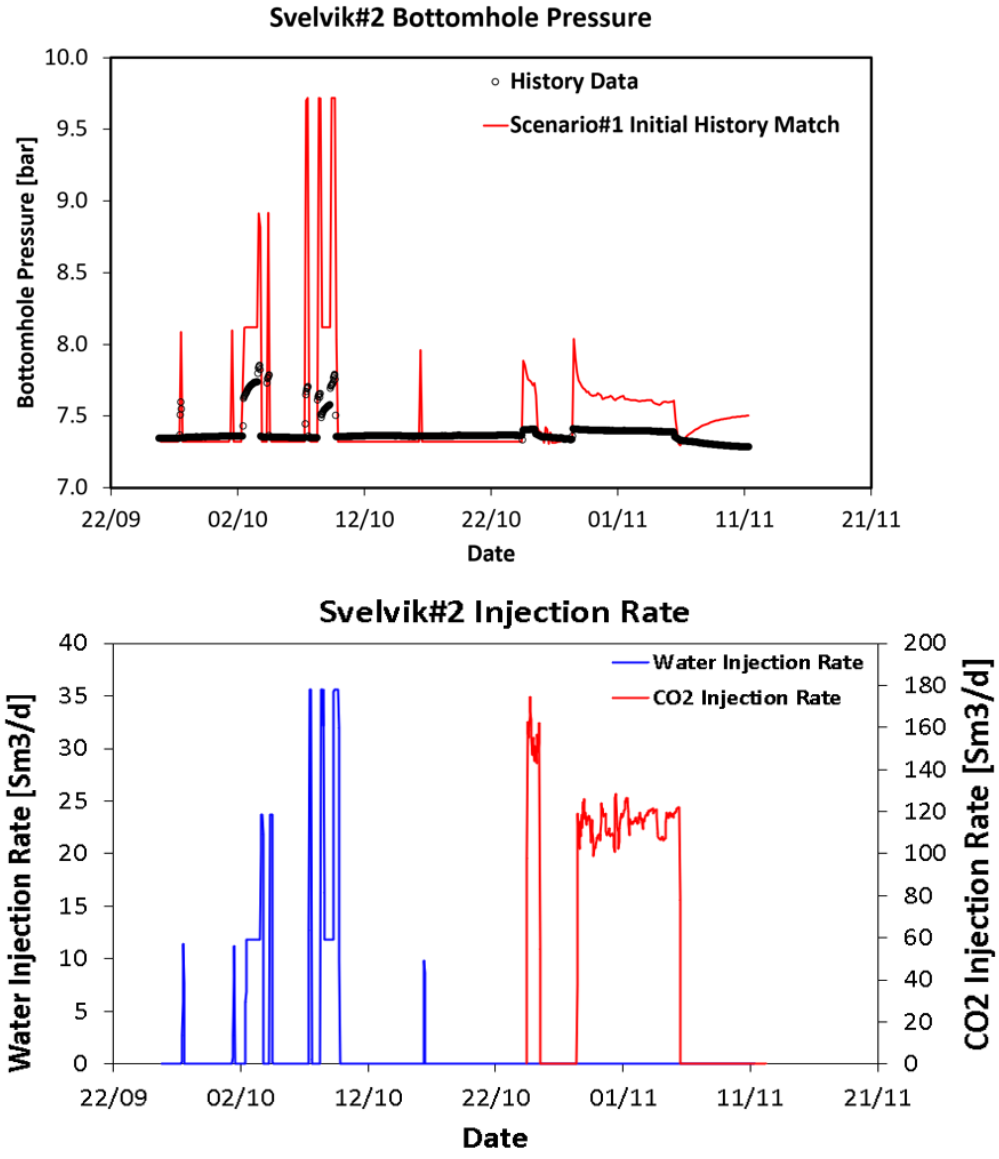

Figure 4.1: Initial history matching result

The initial history matching result points out several interesting findings. At the water injection phase, the bottomhole pressure simulated is much higher than the pressure increment recorded to inject the defined water injection rate. It is also shown at the initial CO2 injection period where the bottomhole pressure required to inject the CO_2 is higher than the historical data.

In the historical data, some water injected were measured, but the bottomhole pressure did not respond (Figure 4.2). This is where the water injection pump is being tested and the water is not injected into the formation. Therefore, this data is cleaned on the later history matching.

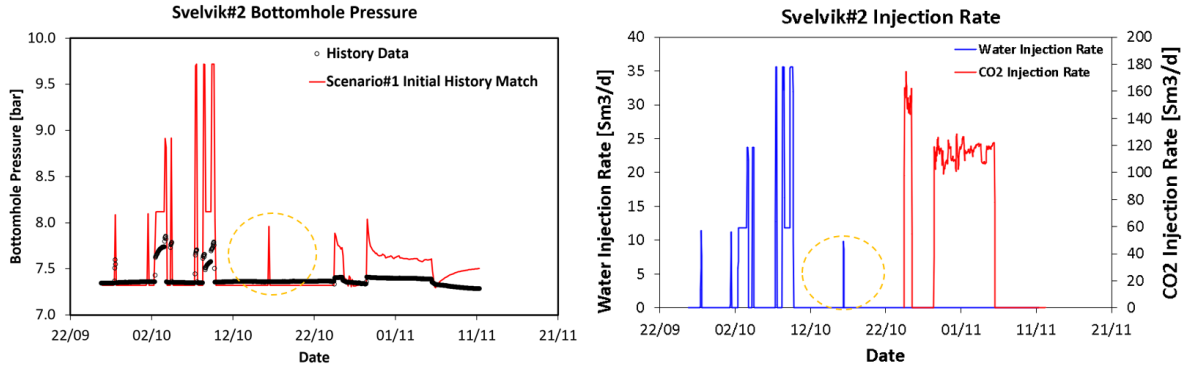

Figure 4.2: Water pump testing false data

Another interesting result in the water injection period is that the bottomhole pressure measured and the water injection rate is not very predictable. The simulation shows that the bottomhole pressure required should be higher to inject more water. However, the measured data does not have a conclusive trend, as presented in the comparison in Figure 4.3.

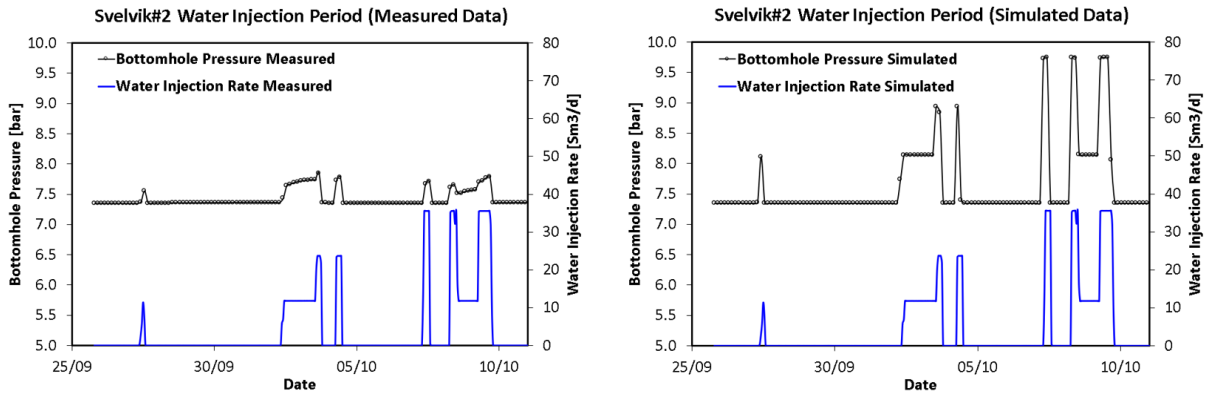

Figure 4.3: Comparison between measured data (left) and simulated result (right)

Several possibilities to explain this phenomenon:

1. Salinity differences from different water tanks at the injection site. With lower salinity on the second water injection, the bottomhole pressure required is less and similar to the first water injection, where water with higher salinity is injected. Unfortunately, the injected salinity is not measured.
2. Increasing formation injectivity. With a higher rate and unconsolidated sand, there is a possibility that the sand near the wellbore is washed-out by the high-water rate and increases the injectivity.

3. Skin effect from the well that is not able to be quantified.

With these results, the water injection period has given several valuable outputs to this study. Based on the history matching result, where the Svelvik#2 bottomhole pressure is significantly higher than the history data, it can be inferred that the absolute permeability for the Svelvik ridge might be higher than in the geo-model. Therefore, the sensitivity of the global permeability distribution will be carried out as an uncertainty parameter. With high uncertainty and the results of the water injection period being very inconsistent with the ideal performance, the history matching will continue only with the main CO_2 injection period.

The result of the dipping grid and dipping properties scenario for the CO_2 injection period are shown in Figure 4.4.

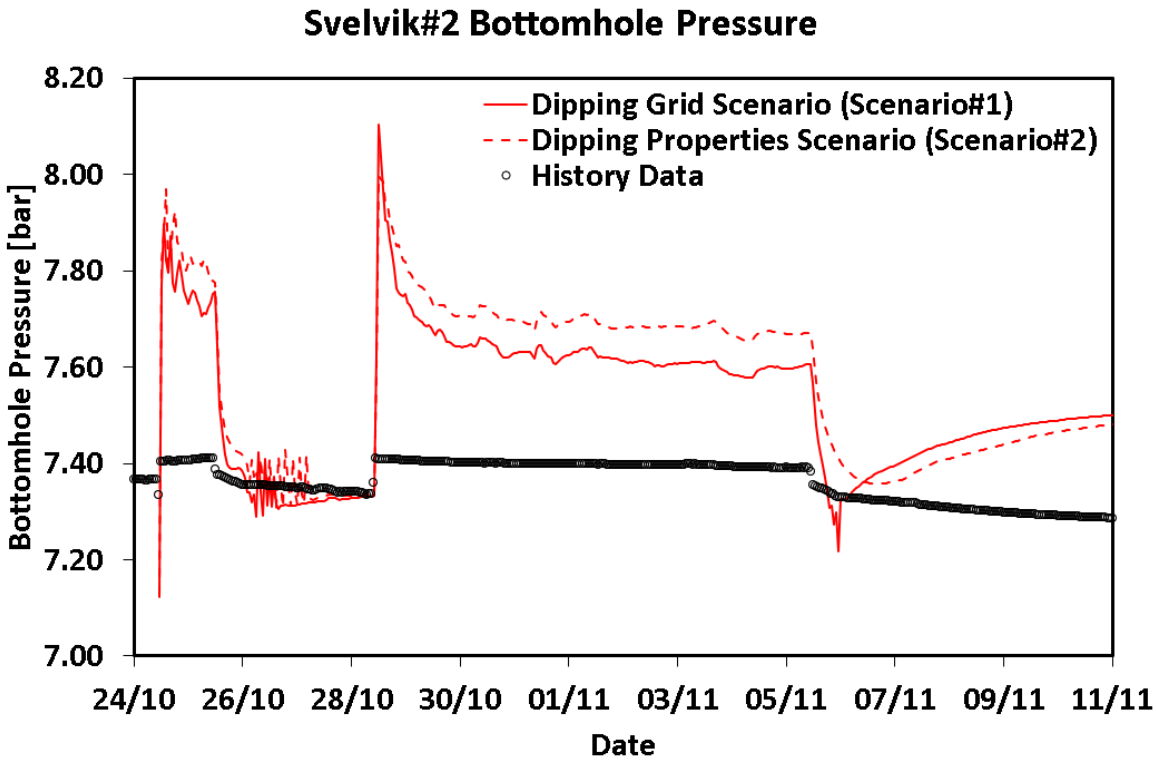

Figure 4.4: CO_2 injection period bottomhole pressure with simulation history matching

During the CO_2 injection period, it is shown that the bottomhole pressure when injecting the CO_2 is higher than the historical data. When the CO_2 injection was stopped, history shows a trend where the bottomhole pressure declined slowly to a pressure similar to the initial pressure. The initial shut-in in simulation shows a trend where it reaches the same pressure as the history, but on the second, it differs due to stabilization with the initial pressure. Based on the bottomhole pressure data, it shows that the dipping grid scenario and dipping properties scenario has similar trend and results.

Figure 4.5 and Figure 4.6 shows the CO_2 plume distribution at the end of the injection and 6 days post-injection from both geological scenarios. Several differences between both geological scenarios can be spotted with the CO_2 plume migration.

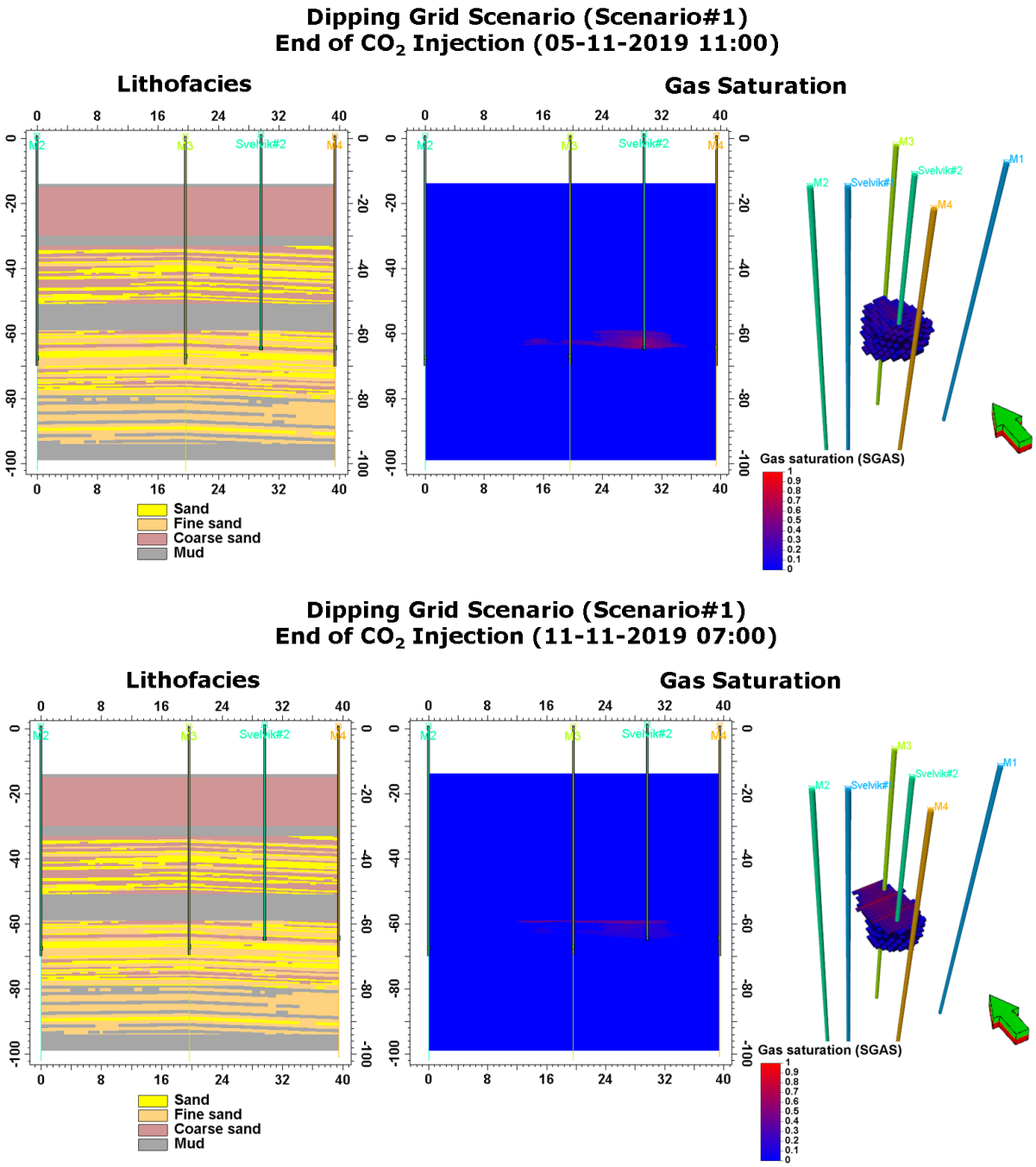

Figure 4.5: Dipping grid scenario CO_2 plume: Stop injection (above) and 6 days post injection (below)

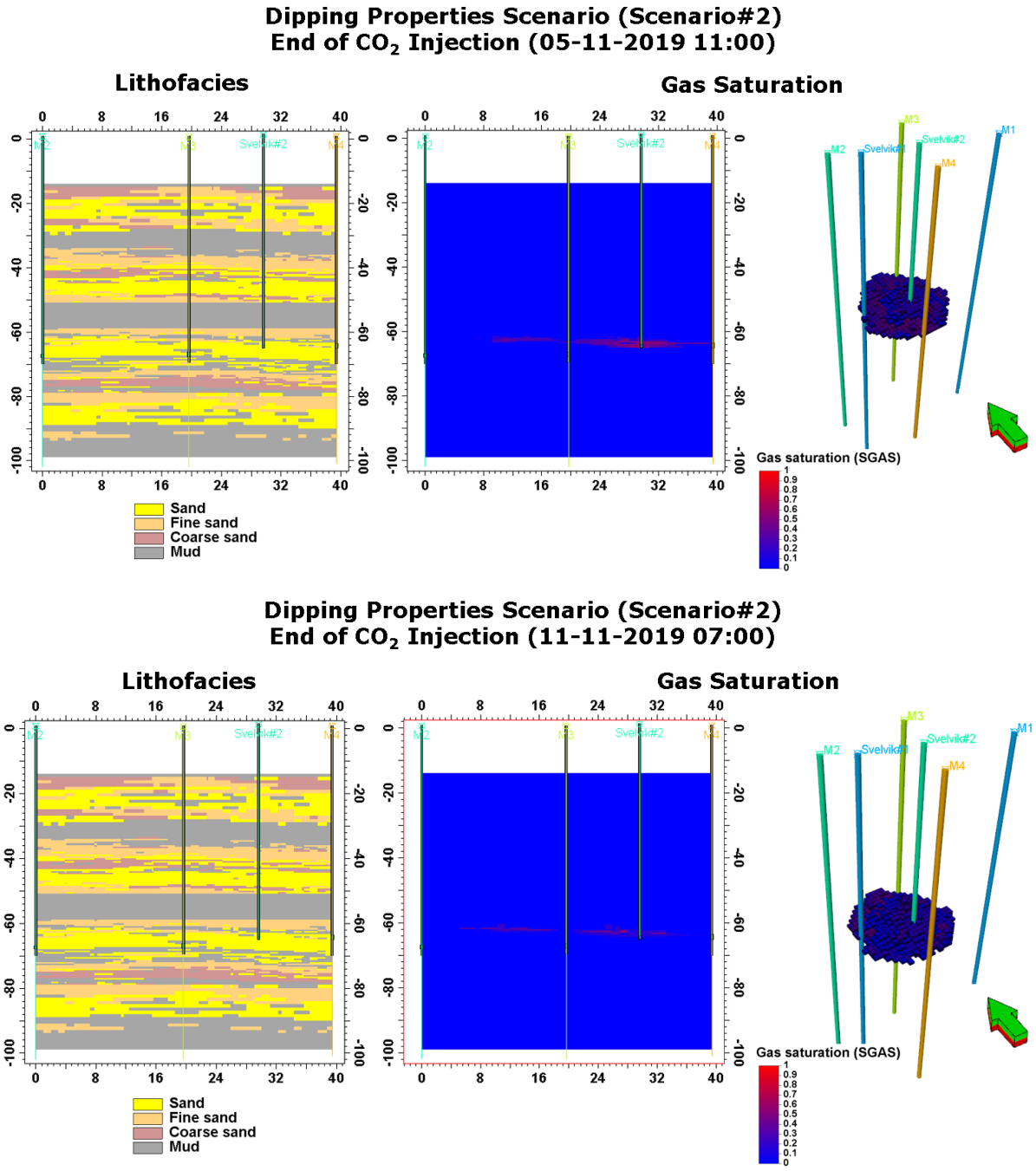

Figure 4.6: Dipping properties scenario CO_2 plume: Stop injection (above) and 6 days post injection (below)

The simulation result shows that the CO_2 migration will only spread horizontally and the vertical migration is only possible up to the 60m depth. In contrast, the result from P-wave inversion (Figure 2.10) shows that the CO_2 migrated to the depth of 38m and towards the north (M3 well).

In this case, several explanations that discuss the possibility for the CO_2 to move vertically up to the 38m are:

1. The mud layer at a depth of 50.7m to 60m is discontinuous by sand lobes. This is modelled as an uncertainty where the mud layer lithofacies is modified to coarse sand in the dipping grid scenario and sand in the dipping properties scenario.

2. The bentonite slurry in the annulus between the formation and the PVC tubing enables vertical communication to the formation.
3. The permeability anisotropy of the Svelvik ridge is uncertain.

With the result from the CO_2 injection period, the uncertainty included for the study in the history matching is the near-wellbore vertical communication, changing the lithofacies from 50.7 – 60m.

4.1.2 Uncertainty-Based History Matching Results

The uncertainty-based history matching uses the defined uncertainty provided in Table 3.11. With the modified 50.7m to 60m mud to sand layer, a total of seventeen different parameter combinations are sampled through the Latin hypercube method, where the sampled combinations are shown in Table 4.1.

Table 4.1: Uncertainty sampled by LHS method

Cases	Wellbore	Rock Data	Permeability Uncertainty		Carter-Tracy Aquifer Uncertainty			
	Near-Wellbore Vertical Permeability [mD]	Rock Compressibility @1bar [1/bar]	Global Permeability Multiplier [-]	Permeability Anisotropy [-]	Aquifer Thickness [m]	Aquifer Radius [m]	Aquifer Permeability [mD]	Aquifer Compressibility [1/bar]
Scenario1_1	4474.46	0.0098	3.33	0.70	1184.94	9742.07	760.74	0.0139
Scenario1_2	7093.44	0.0588	4.41	1.03	727.27	93395.93	1259.72	0.0744
Scenario1_3	1263.36	0.0571	2.28	1.07	1004.74	65175.31	2420.25	0.0551
Scenario1_4	3846.46	0.0480	4.07	0.13	374.91	50500.01	2020.33	0.0811
Scenario1_5	1860.90	0.0196	1.50	0.56	536.86	22784.60	1987.77	0.0621
Scenario1_6	9336.90	0.0825	3.78	1.93	631.92	72716.83	2612.04	0.0646
Scenario1_7	5606.63	0.0502	2.96	0.40	641.87	75513.72	1631.58	0.0434
Scenario1_8	2499.73	0.0644	2.43	1.66	495.87	55523.84	2141.38	0.0526
Scenario1_9	6389.71	0.0244	3.41	1.23	211.57	82115.50	2747.64	0.0755
Scenario1_10	6171.18	0.0676	4.79	0.42	1273.55	1364.87	1838.89	0.0268
Scenario1_11	5182.23	0.0876	3.84	0.61	130.10	40476.07	377.96	0.0870
Scenario1_12	8890.86	0.0073	4.98	1.47	303.12	34252.85	701.36	0.1000
Scenario1_13	6802.48	0.0952	1.51	1.53	1231.22	31480.97	2906.68	0.0299
Scenario1_14	8603.64	0.0417	2.50	1.34	905.35	6357.74	1002.29	0.0400
Scenario1_15	7709.18	0.0731	2.11	1.73	402.30	69897.74	384.63	0.0220
Scenario1_16	3452.02	0.0346	4.21	1.20	1452.05	49528.41	621.47	0.0697
Scenario1_17	2848.25	0.0843	4.58	1.78	1348.89	87561.68	244.63	0.0483

The result of the Svelvik#2 bottomhole pressure history matching results are shown in Figure 4.7.

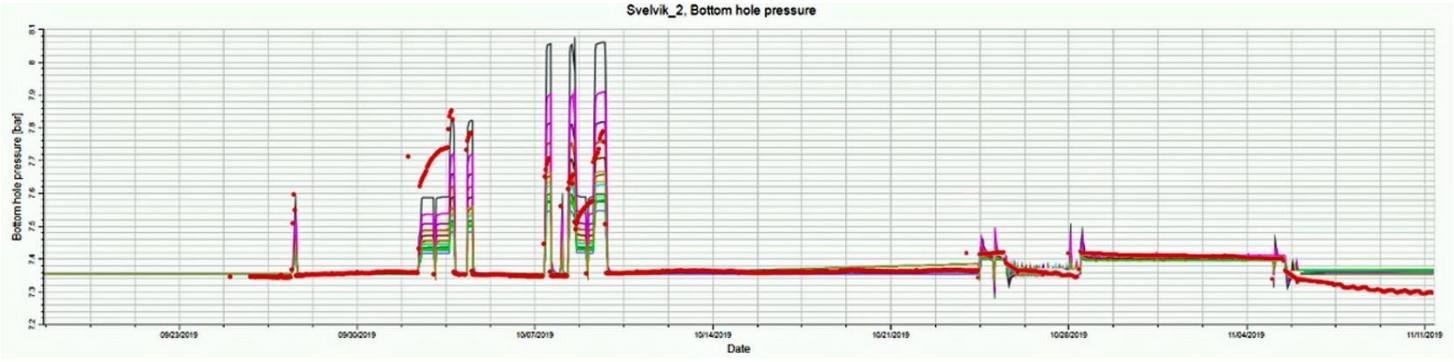

Figure 4.7: Result of seventeen realization of uncertainty history matching (bottomhole pressure)

Based on the result, it is shown that none of the combinations of these parameters could match the measured data. Several explanations regarding the result are:

1. The water injection period has uncertainty explained in the initial history matching result, where it differs from the physical expression. This phenomenon could come

from the different salinity of the water tank, increasing formation injectivity or skin.

2. The increasing and decreasing pressure trend in the water injection is not captured in the simulation model, wherein the simulation follows the same trend as the water injection rate.
3. The CO2 injection period has a good match during the injection but has a deviation when the injection is stopped. This deviation is due to the simulation result being stabilized to the initial pressure, while the measured data shows that pressure dropped slightly lower than the initial pressure.

4.1.3 Conventional History Matching Results

The result of the sensitivity of the absolute permeability is presented in Figure 4.8.

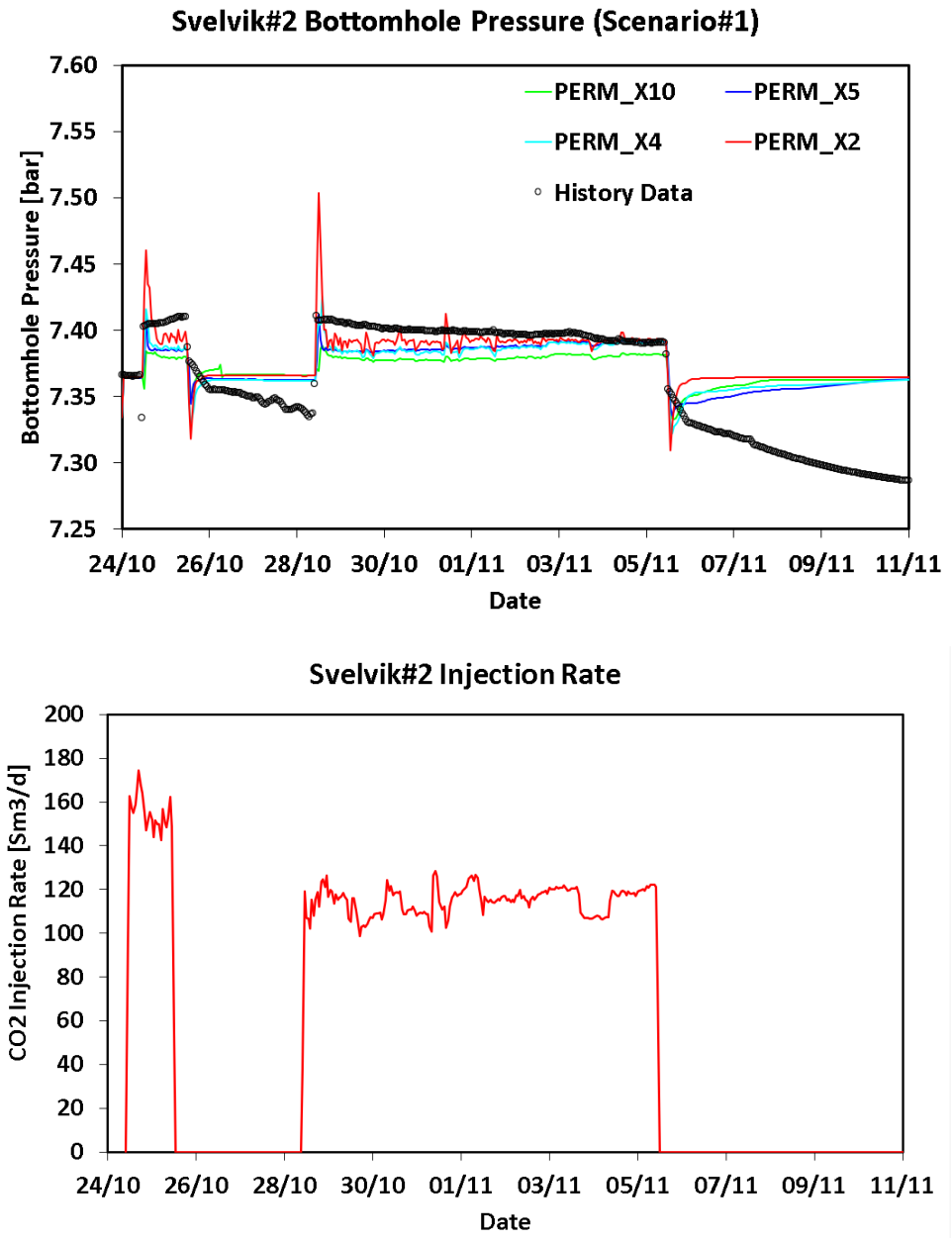

Figure 4.8: Svelvik#2 bottomhole pressure absolute permeability sensitivity

It can be seen that the effect of the increasing and decreasing pressure for the CO_2 injection is diminishing with higher permeability. For example, permeability multiplied by 2 shows a sharp increase in bottomhole pressure when the CO_2 is injected and a sharp

decrease of bottomhole pressure when the CO_2 injection is stopped, while permeability multiplied by 10 has a smoother increase and decrease of bottomhole pressure.

The fitness of the history matching is scored by several methods, as shown in Table 4.2.

Table 4.2: History matching error summary

Cases	Absolute Error [bar]		Percent Error [%]		RMSE [bar]	R^2 [-]
	Maximum	Average	Maximum	Average		
Perm_x10	0.074	0.023	1.018	0.305	0.0258	0.653
Perm_x5	0.074	0.016	1.014	0.219	0.0203	0.806
Perm_x4	0.073	0.017	1.004	0.235	0.0219	0.702
Perm_x2	0.096	0.017	1.297	0.236	0.0245	0.560

The breakdown of the percent error is presented in Figure 4.9. The error increases for all cases on the 7th of November due to the simulation stabilizing the initial pressure while the measured pressure keeps decreasing. An interesting finding is shown at each beginning of the CO_2 injection. The case where permeability is multiplied by 2 has the highest error and diminishes over time, while the other case has a lower error during this period. This effect is due to the sharp increase of the bottomhole pressure as in the simulation result.

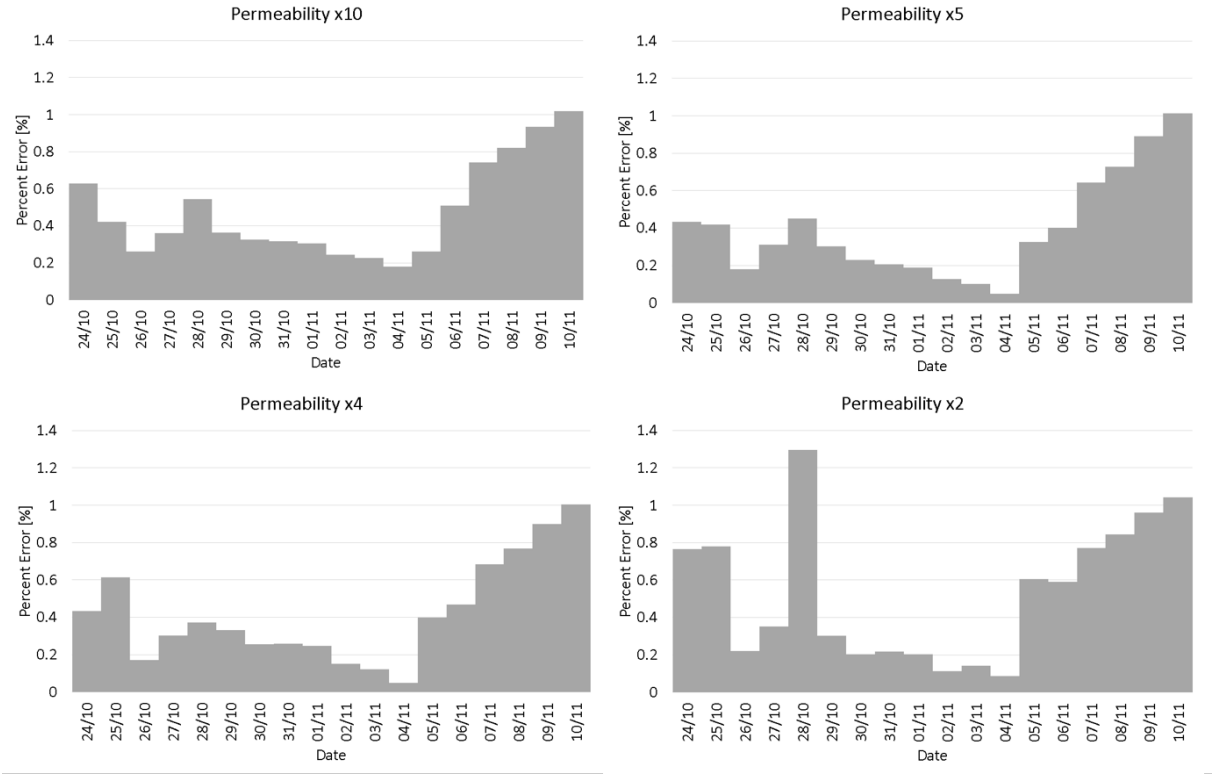

Figure 4.9: Percent error vs time for different absolute permeability

With this result, it is agreeable that a higher permeability as multiplication up to 5 times favours the given geo-model. A new distribution of the permeability is presented in Table 4.3.

Table 4.3: After history matching permeability distribution

Facies	Permeability [mD]		
	Mean	**Min**	**Max**
Coarse Sand	6000	4000	10000
Sand	4000	1500	6000
Fine Sand	1000	500	1500
Mud (Silt)	50	0.5	500

The permeability improvement required to match the Svelvik#2 bottomhole pressure data with the given CO_2 injection rate is too high. This value is not very realistic with the available data and contradicts the pumping test from the previous study. The possibilities that explain the differences in the results can come from:

1. The correction of the pressure data that require a further study
2. The pumping test results were not a pure unconsolidated sand result where it might be contaminated by mud that lower the pumping test permeability result.

4.1.4 Results Summarization

With several considerations taken into account from uncertainty definition and lots of history matching cases, none of these efforts that have been done could match with the behaviour of the Svelvik Pre-ACT injection campaign. A further study on the pressure data measured and CO2 plume migration is very recommended.

Based on the history matching results, it can be concluded that:

1. No simulation result can match precisely with the measured data. This can come from various uncertainty explained in each step of the history matching.
2. A higher permeability value than the current geo-model is expected. This is seen through the Svelvik#2 bottomhole pressure is always higher when injecting into the reservoir than the measured data.
3. The mud layer from 50.7 – 61.2 m, which is expected based on the well log analysis in the Svelvik#1 and Svelvik#2 wells, might not be continuous and have a connection to the upper layers through sand lobes.
4. The well annulus where the bentonite slurry was used as the sealing element between the injection PVC pipe and the formation shows that the CO2 can migrate through it.

In order to continue for proxy models, since no model w able to match with the pressure data, a model with a more realistic value is selected with a trade-off to the history matching accuracy. The permeability multiplied by 2 is continued to the proxy modelling part. The result of the CO_2 plume where the permeability is multiplied by 2, with near wellbore vertical permeability and permeability anisotropy of 0.5, is shown in Figure 4.10 for 1st geological scenario and Figure 4.11 for 2nd geological scenario.

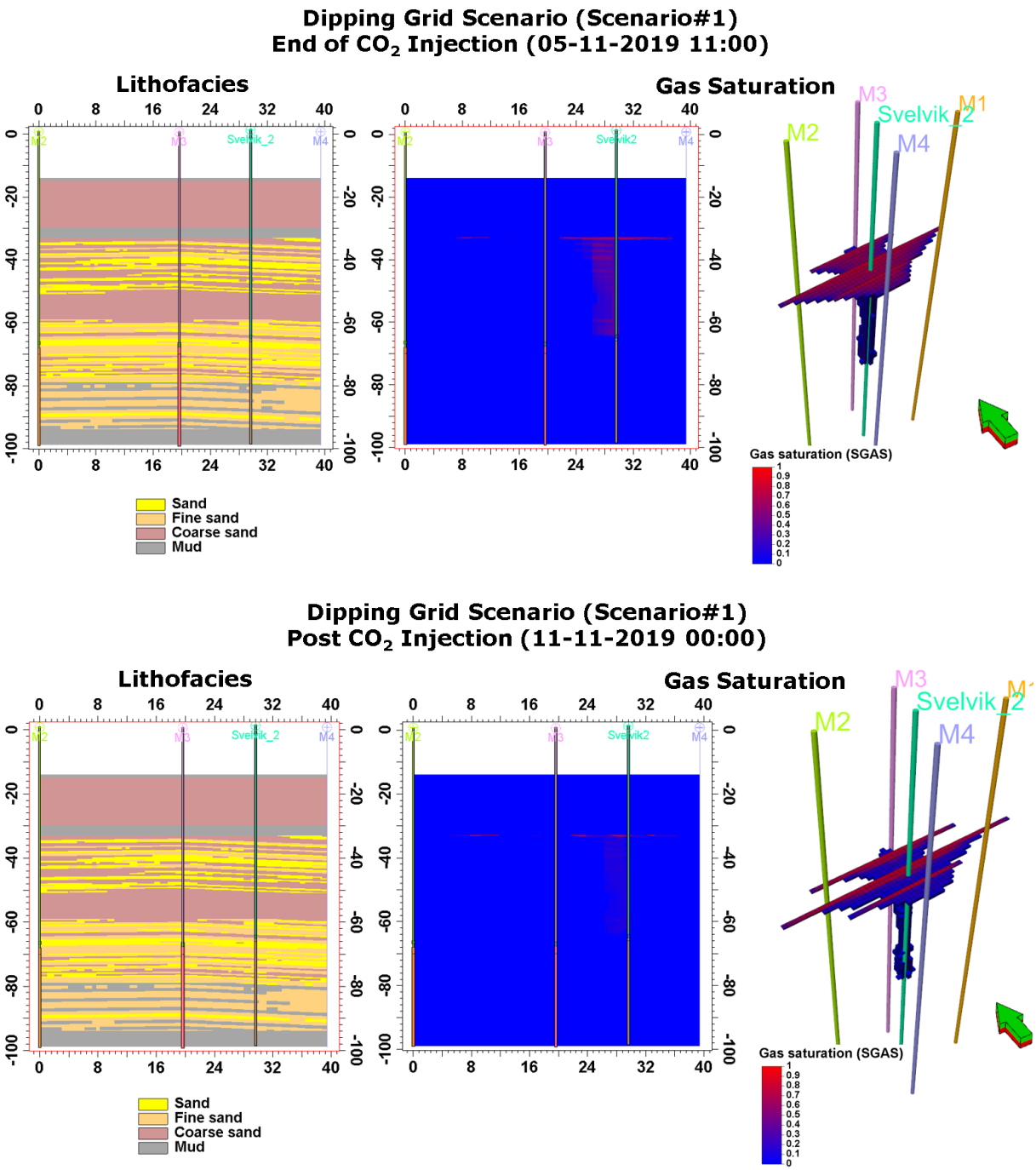

Figure 4.10: History matched dipping grid scenario CO_2 plume: Stop injection (above) and 6 days post injection (below)

The dipping grid realization shows that the CO_2 spreads across east-west (M1-M2) and slightly toward the north (M3). It is also shown that the top view has some part of cross-over between CO_2-water due to the grid definition.

The dipping properties realization depicts that the CO_2 plume tends to centralize in Svelvik#2 with the tendency to spread to the north (M3).

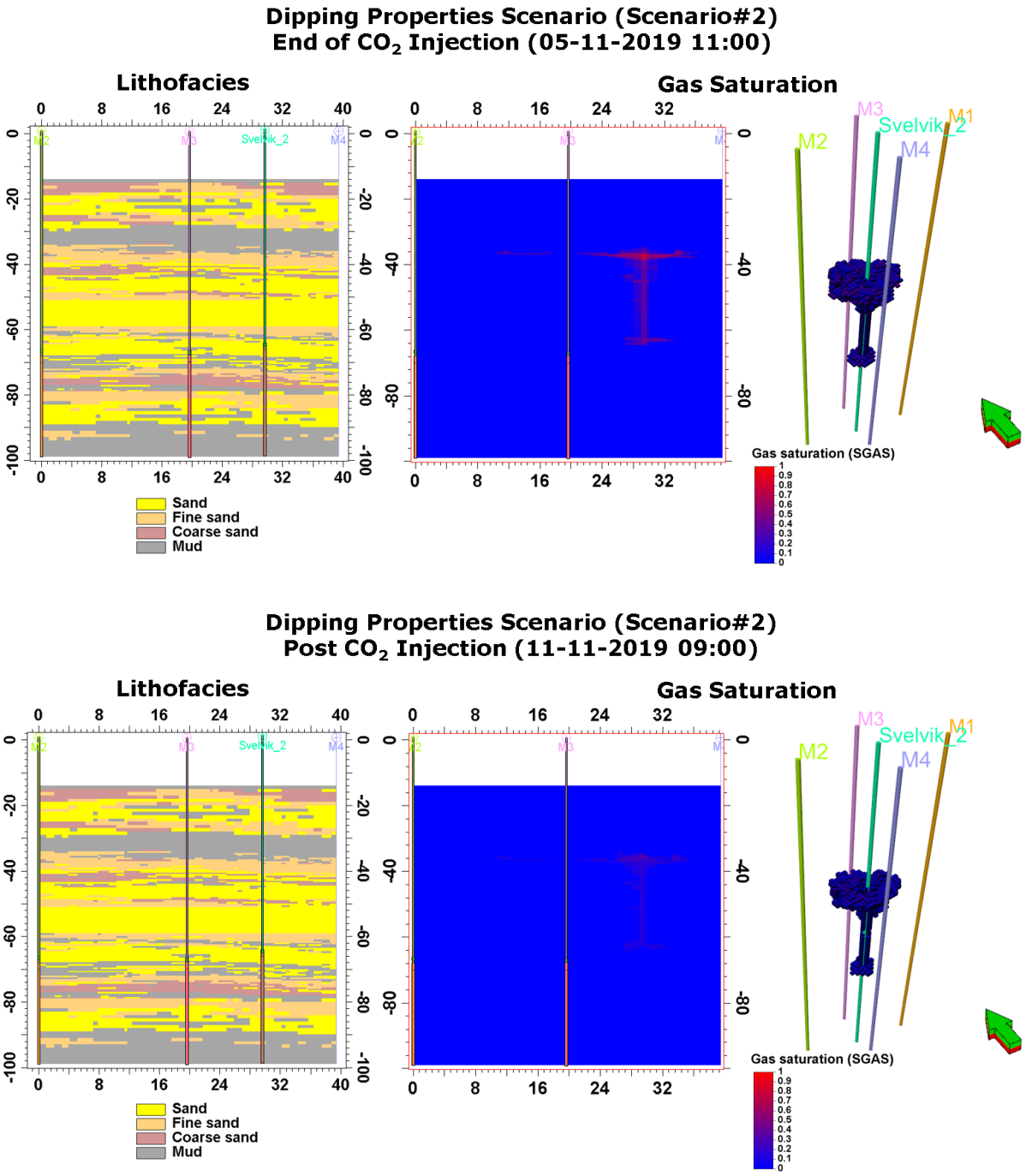

Figure 4.11: History matched dipping properties scenario CO_2 plume: Stop injection (above) and 6 days post injection (below)

The Svelvik#2 bottomhole pressure results in the simulation are similar to the two realizations shown in Figure 4.12.

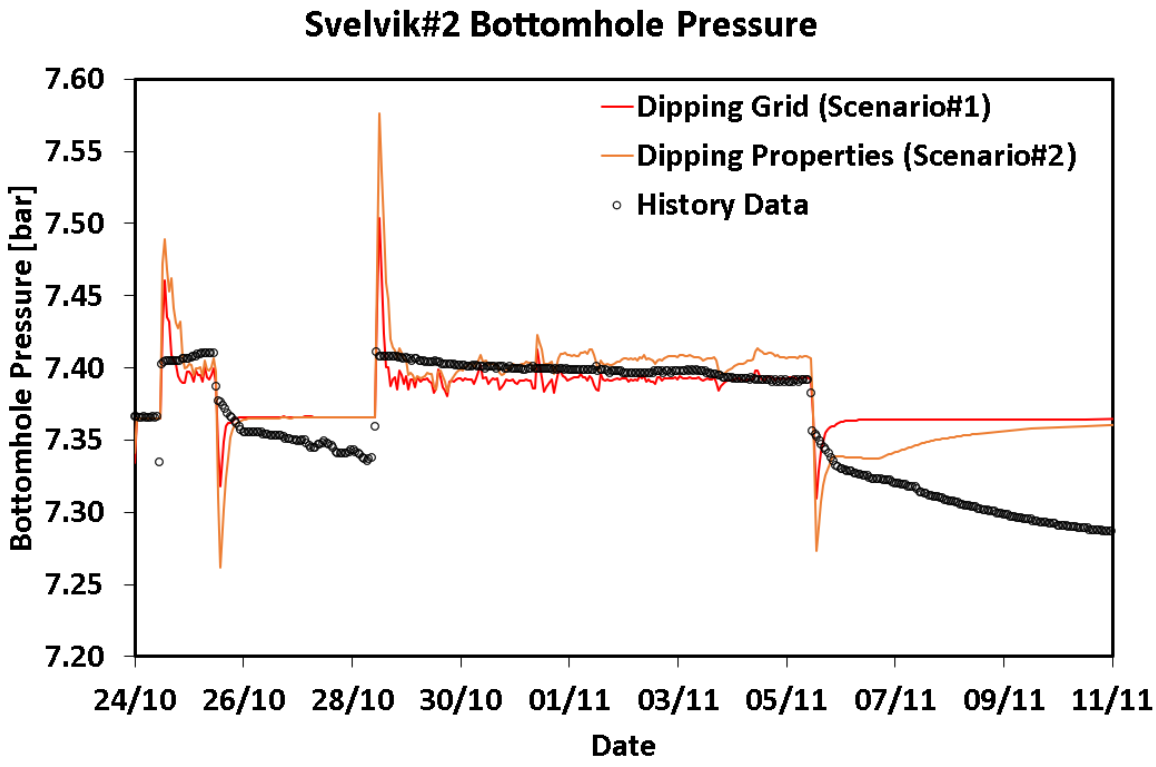

Figure 4.12: History matched Svelvik#2 bottomhole pressure

The error for the selected case between both geological realizations is presented in Table 4.4.

Table 4.4: Svelvik#2 bottomhole pressure history matching error

Cases		Scenario 1	Scenario 2
Absolute Error [bar]	Maximum	0.096	0.169
	Average	0.017	0.017
Percent Error [%]	Maximum	1.297	2.276
	Average	0.236	0.233
RMSE [bar]		0.024	0.025
R^2 [-]		0.560	0.604

4.2 Proxy Models

The proxy models are used to create a prediction for further injection. The history match model is predicted until the 22nd of April 2022 without any injection to see the migration and change of the CO_2 saturation when it is undisturbed for 3 years. After the prediction, the model is used as a starting point for the proxy model.

After three years, it is shown that the CO_2 in the gas phase has majorly dissolved in the water after three years. The starting point for the proxy modelling is shown in Figure 4.14 for the dipping grid scenario and Figure 4.14 for the dipping property scenario.

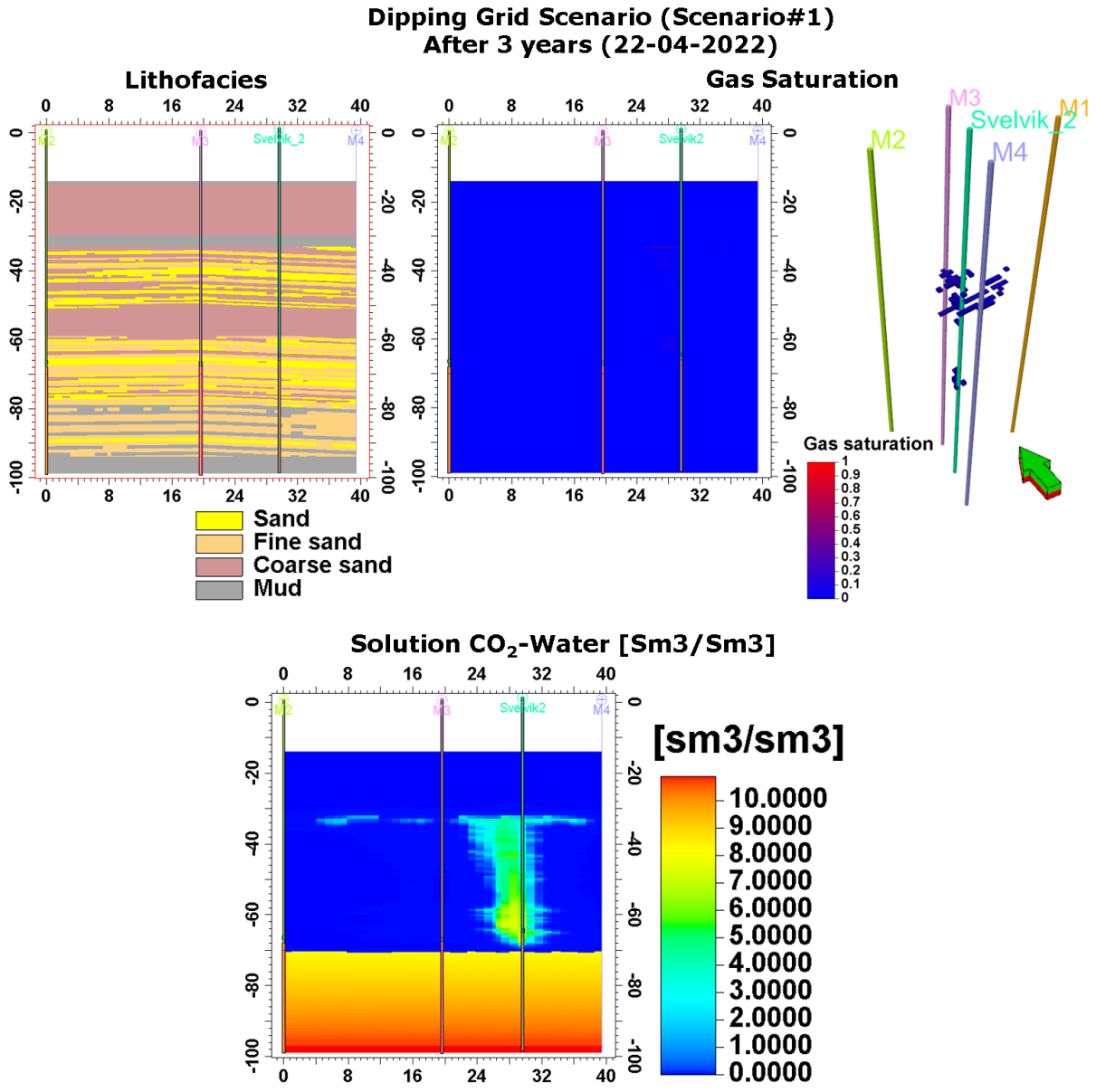

Figure 4.13: Three years post CO_2 injection: Dipping grid scenario

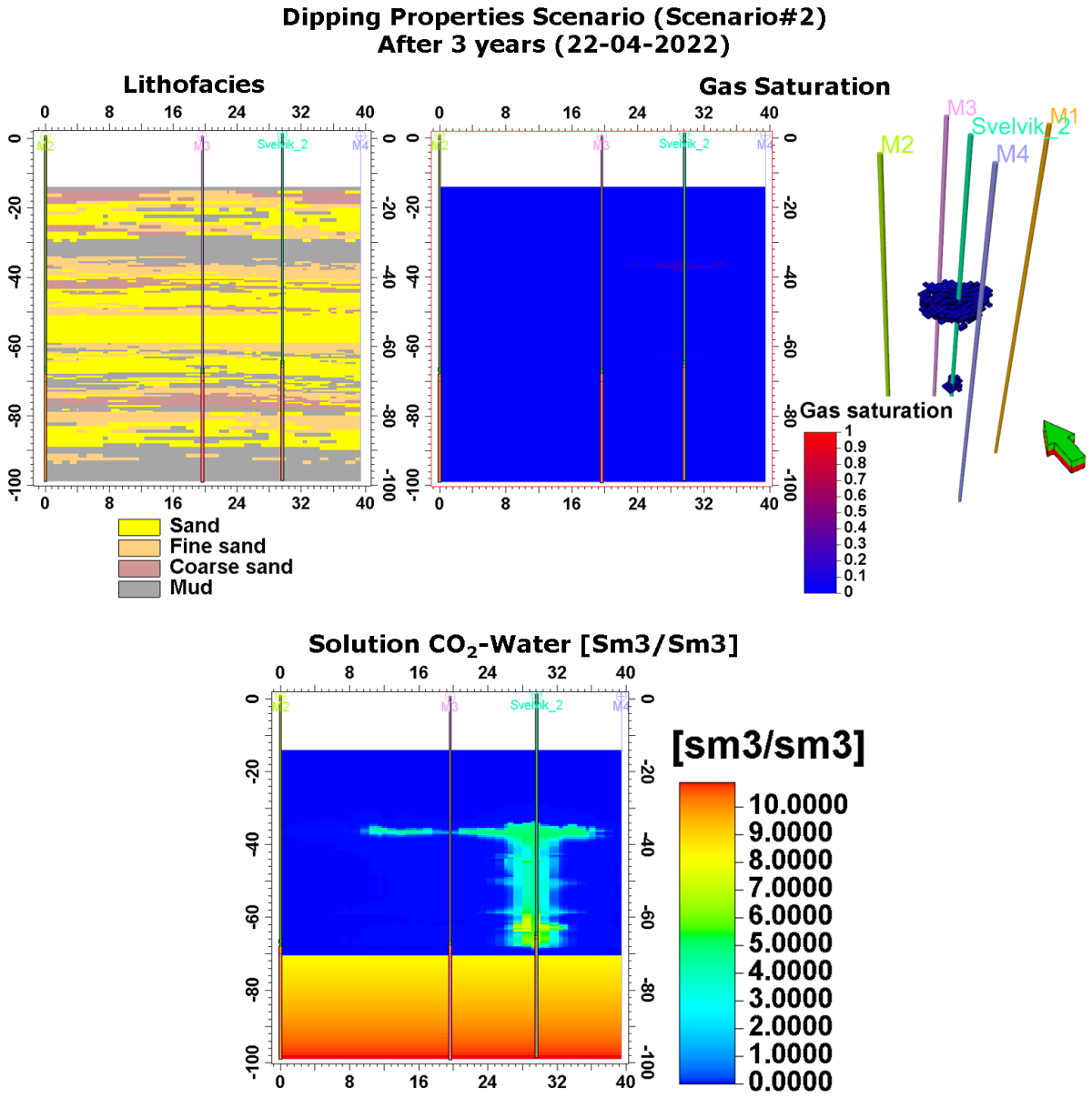

Figure 4.14: Three years post CO_2 injection: Dipping properties scenario

Using the training, validation, and evaluation dataset design in chapters 3.7.1 and 3.7.2, the proxy models were trained and tried to mimic the behaviour of CO_2 injection in the Svelvik Field Laboratory. Using the input of CO_2 injection rate, the Svelvik#2 bottomhole pressure, dissolved CO_2 in water, and CO_2 in gas phase are predicted. The illustration based on the dataset in Table 3.13 for the training dataset and Table 3.13 for the validation dataset is shown in Figure 4.15.

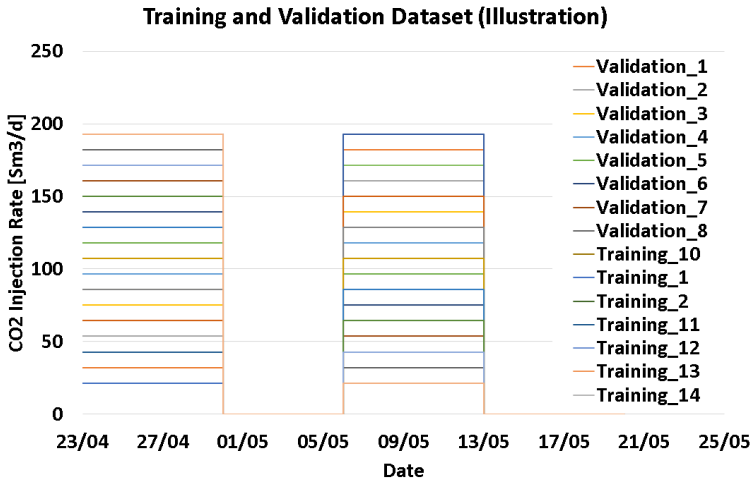

Figure 4.15: Training and validation dataset illustration

Since the proxy used to simulate the behaviour of the CO_2 injection is a statistical proxy, the probability of the predicted value is also shown as the proxy result as one of the validation methods, where the result predicted by the proxy should be in the range of the simulated value.

4.2.1 Response Surface Proxy

This study built two types of response surface proxy: linear and bilinear proxy.

4.2.1.1 Dipping Grid Scenario Proxy Model

The resulting probability for each predicted value is shown in Figure 4.16 for linear response surface proxy and Figure 4.17 for bilinear response surface proxy.

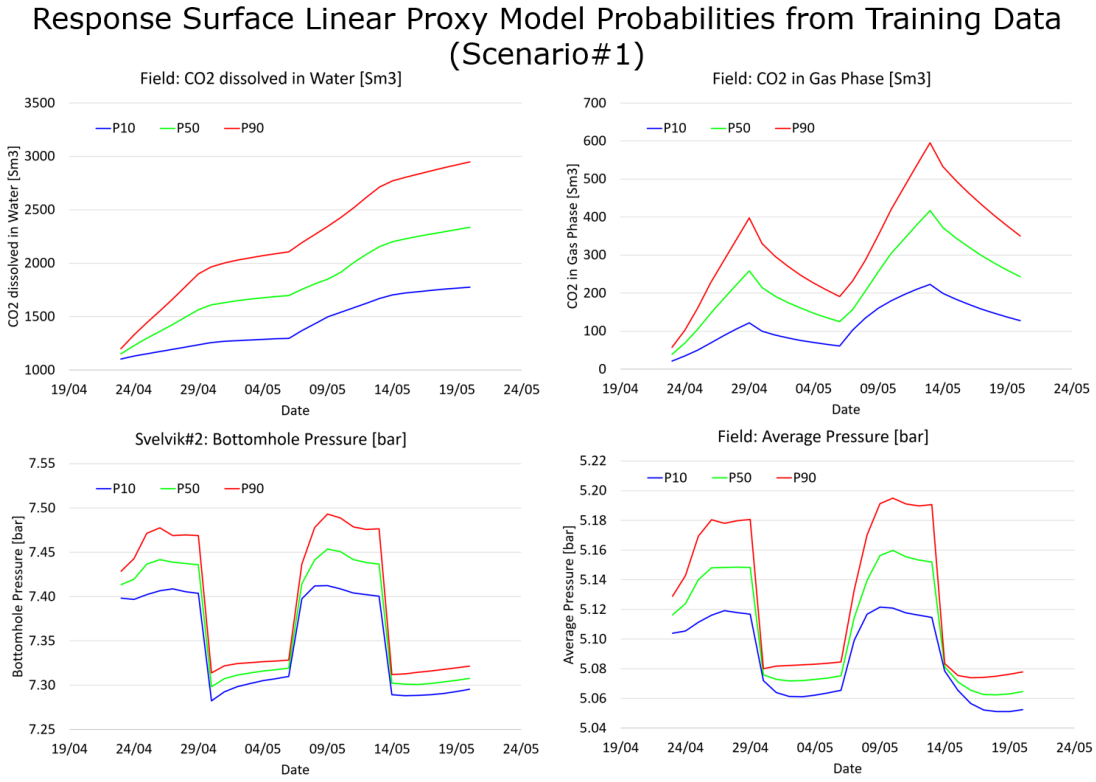

Figure 4.16: Linear response surface probabilities from training data (scenario#1)

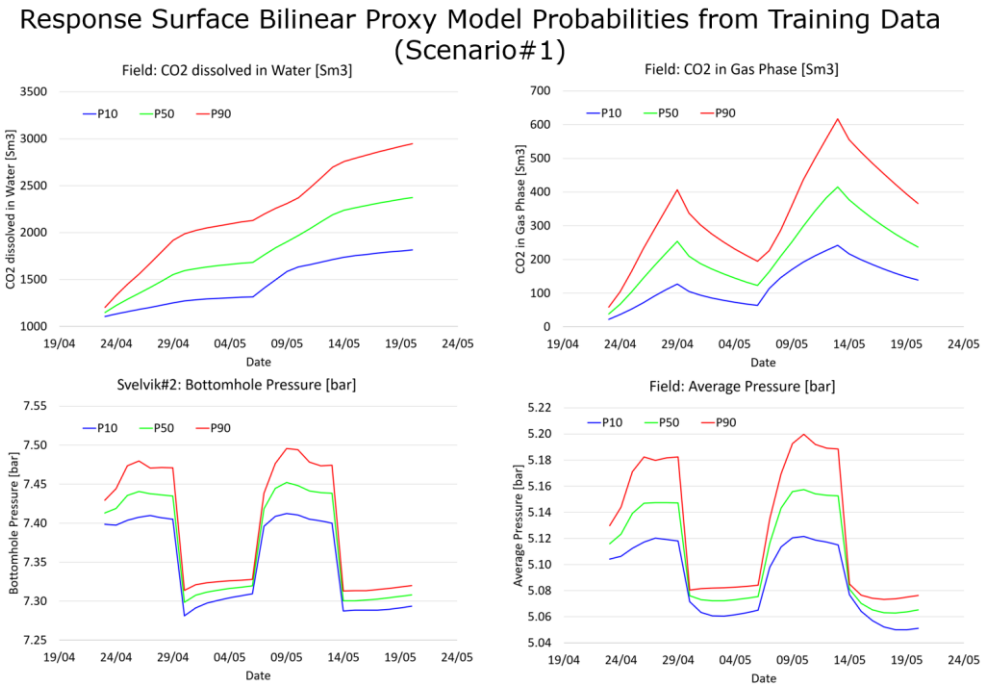

Figure 4.17: Bilinear response surface probabilities from training data (scenario#1)

The result of the proxy probabilities from the training dataset can simulate the trends from the injection and shut-in periods. The 1st result of the validation is presented in Figure 4.18.

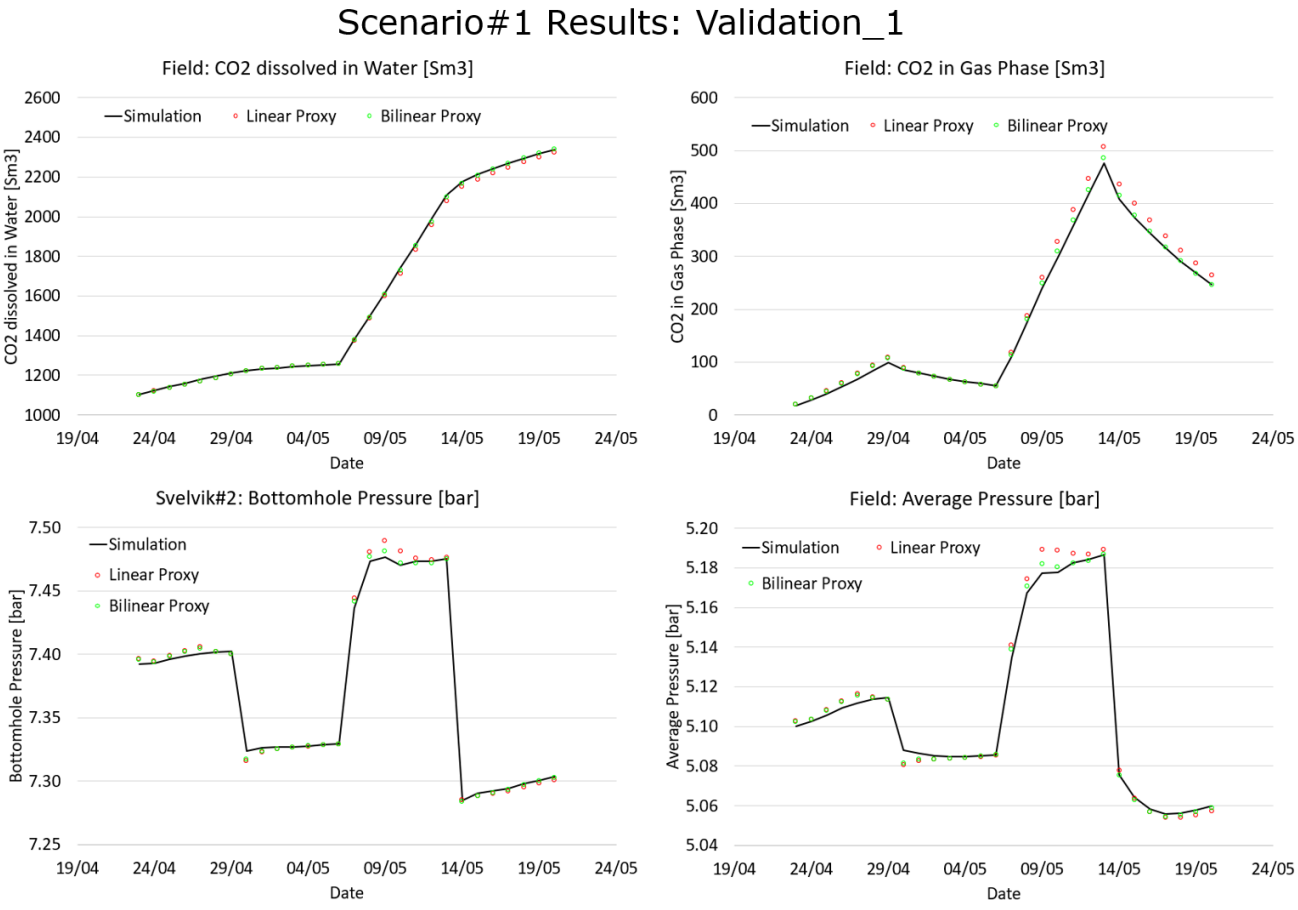

Figure 4.18: Validation_1 result for linear and bilinear proxy model (scenario#1)

The validation case 1 result demonstrates that the bilinear proxy is slightly better than the linear proxy. This is due to the additional interaction terms offered by the bilinear proxy that give a better approximation than the linear proxy. The detail of the percent error is illustrated in Figure 4.19. The validation result matches CO_2 dissolved in water, Svelvik#2 bottomhole pressure, and the average field pressure. Significant error is found in CO_2 in gas phase, where both of the response surface proxies have difficulty in the 1st injection, but the bilinear shows a better fit on the 2nd injection.

A summary of the error for every validation case is presented in Table 4.5 for the linear proxy model and Table 4.6 for the bilinear proxy model. In some cases, the linear proxy can perform better than the bilinear proxy. The R^2 for all cases is good (more than 0.99), which means that the trend and value are close between the response surface proxy and the simulation result. In terms of error, the CO_2 in gas phase has a relatively higher error than the other variables. The proxy captures the trend of the CO_2 in gas phase. However, the predicted value by proxy is not as exact as the simulation result, with the maximum error reaching about 13-15% and the average error about 4-7%. This error could come from the limitation of the response surface proxy model where it assumes the approximate variable following the response surface polynomial expression.

The other parameters, such as Field CO2 dissolved in water, Svelvik#2 bottomhole pressure, and average field pressure predicted by the linear and bilinear proxy model, have less than 1% error in all validation cases.

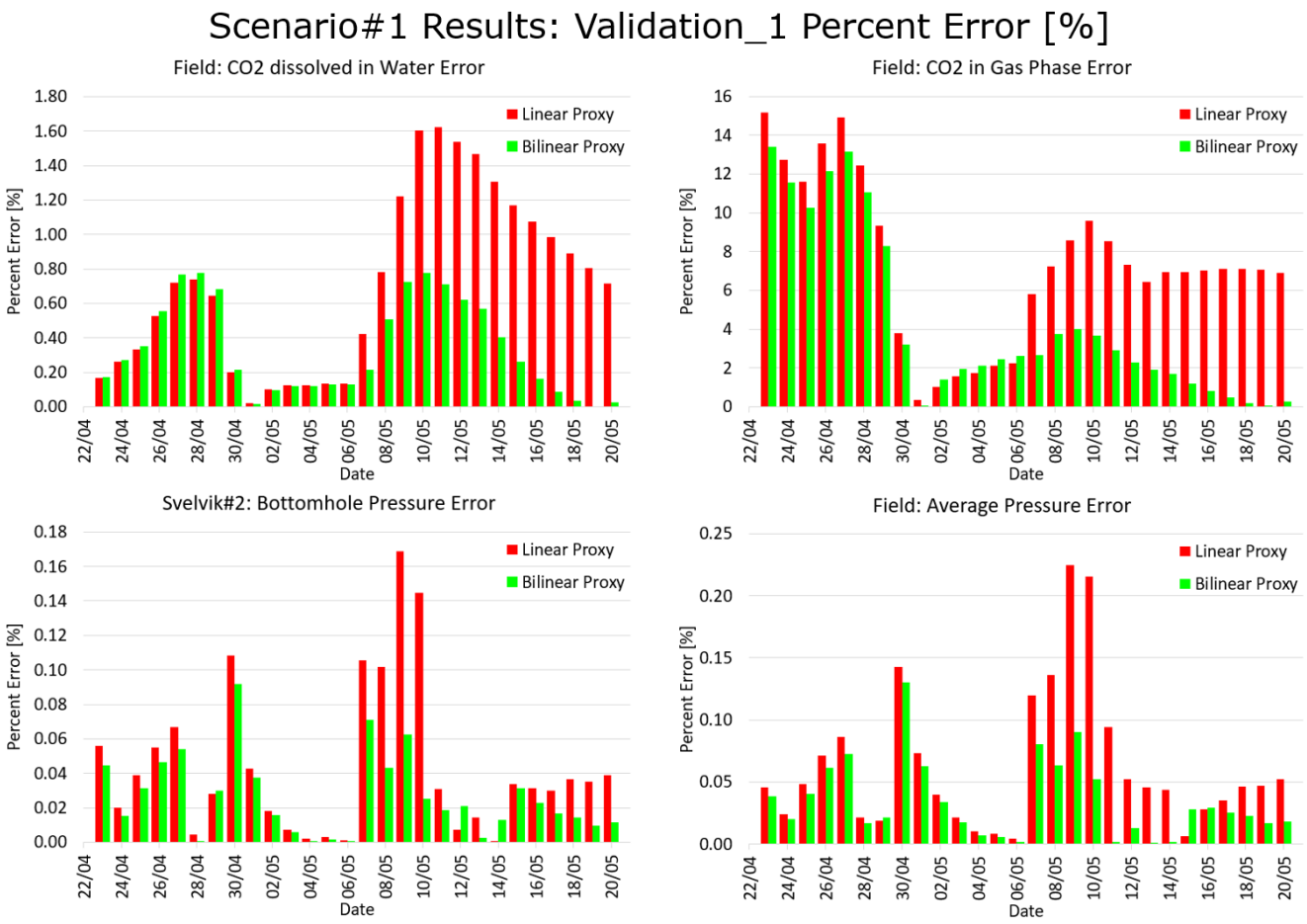

Figure 4.19: Validation_1 percent error for linear and bilinear proxy model (scenario#1)

Table 4.5: Linear proxy model validation cases error summary (scenario#1)

Linear	Svelvik#2 Bottomhole Pressure			Field: CO2 Dissolved in Water			Field: CO2 in Gas Phase			Field: Average Pressure		
	Max Percent Error [%]	Avg Percent Error [%]	R2 [-]	Max Percent Error [%]	Avg Percent Error [%]	R2 [-]	Max Percent Error [%]	Avg Percent Error [%]	R2 [-]	Max Percent Error [%]	Avg Percent Error [%]	R2 [-]
Sample_1	0.17	0.04	0.9982	1.62	0.71	0.9998	15.16	7.33	0.9994	0.22	0.06	0.9964
Sample_2	0.15	0.02	0.9982	0.72	0.39	0.9999	5.87	3.55	0.9993	0.19	0.03	0.9969
Sample_3	0.09	0.03	0.9983	0.78	0.22	0.9999	6.94	2.23	0.9988	0.10	0.04	0.9968
Sample_4	0.10	0.04	0.9986	0.70	0.27	0.9999	6.09	2.20	0.9985	0.12	0.04	0.9973
Sample_5	0.11	0.04	0.9988	0.88	0.32	0.9998	4.93	2.34	0.9984	0.15	0.05	0.9976
Sample_6	0.10	0.03	0.9993	0.74	0.25	0.9998	4.42	2.10	0.9986	0.12	0.03	0.9986
Sample_7	0.07	0.02	0.9991	0.29	0.07	1.0000	2.22	0.42	0.9995	0.11	0.02	0.9980
Sample_8	0.22	0.05	0.9944	1.59	0.68	0.9989	13.54	6.22	0.9623	0.32	0.07	0.9859

Table 4.6: Bilinear proxy model validation cases error summary (scenario#1)

Bilinear	Svelvik#2 Bottomhole Pressure			Field: CO2 Dissolved in Water			Field: CO2 in Gas Phase			Field: Average Pressure		
	Max Percent Error [%]	Avg Percent Error [%]	R2 [-]	Max Percent Error [%]	Avg Percent Error [%]	R2 [-]	Max Percent Error [%]	Avg Percent Error [%]	R2 [-]	Max Percent Error [%]	Avg Percent Error [%]	R2 [-]
Sample_1	0.09	0.03	0.9990	0.78	0.34	0.9999	13.41	4.27	0.9993	0.13	0.03	0.9978
Sample_2	0.09	0.02	0.9990	0.45	0.22	1.0000	5.99	2.62	0.9997	0.11	0.02	0.9983
Sample_3	0.09	0.03	0.9984	0.77	0.21	0.9999	7.11	2.21	0.9991	0.11	0.04	0.9971
Sample_4	0.10	0.04	0.9986	0.69	0.27	0.9999	6.11	2.23	0.9985	0.12	0.05	0.9973
Sample_5	0.12	0.04	0.9987	0.89	0.32	0.9998	5.11	2.44	0.9984	0.16	0.05	0.9975
Sample_6	0.11	0.03	0.9991	0.90	0.31	0.9998	5.58	2.70	0.9973	0.14	0.04	0.9980
Sample_7	0.07	0.02	0.9992	0.53	0.19	0.9999	4.45	1.58	0.9957	0.08	0.02	0.9985
Sample_8	0.12	0.03	0.9982	0.77	0.35	0.9998	5.59	2.40	0.9956	0.13	0.04	0.9961

4.2.1.2 Dipping Properties Scenario Proxy Model

With the same training and validation case based on Table 3.13 and Table 3.14, another linear and bilinear proxy model is created for the dipping properties scenario. The resulting probabilities are shown in Figure 4.20 for the linear proxy model and Figure 4.21 for the bilinear proxy model.

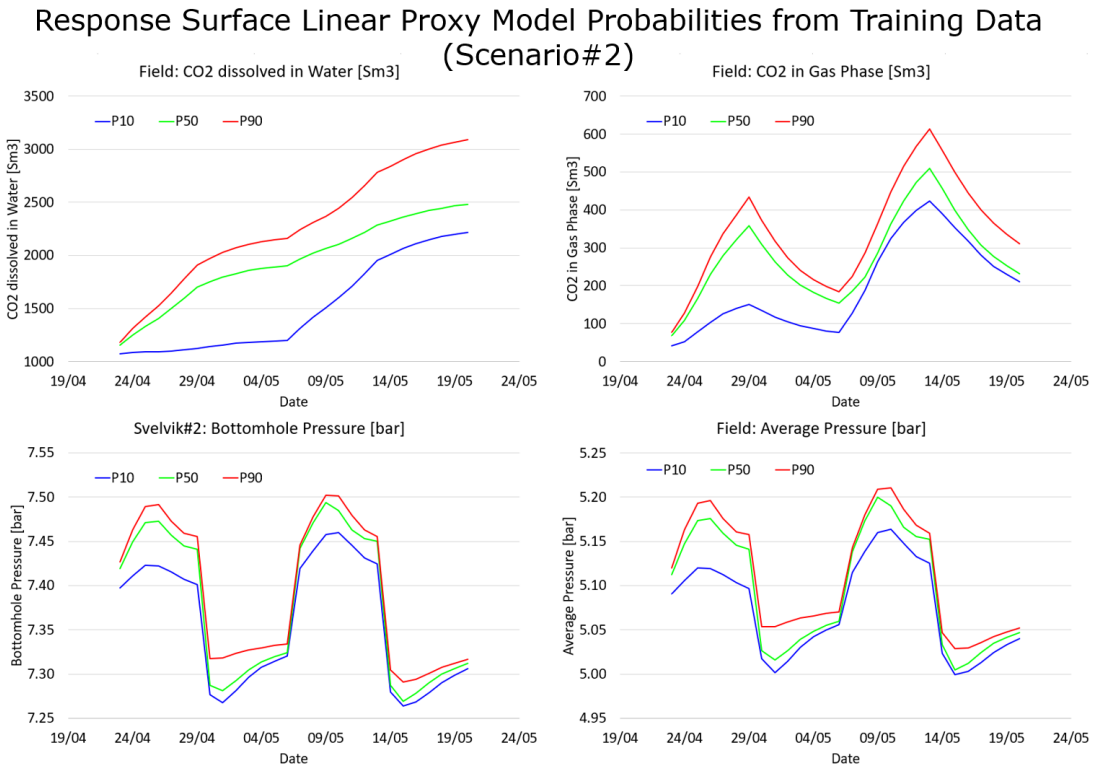

Figure 4.20: Linear response surface probabilities from training data (scenario#2)

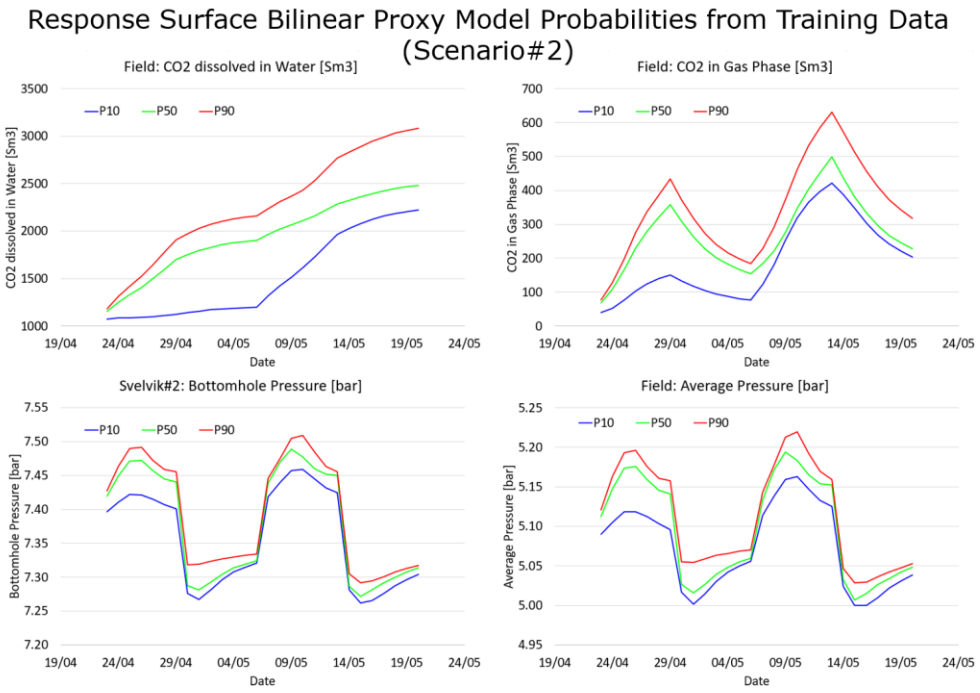

Figure 4.21: Bilinear response surface probabilities from training data (scenario#2)

The result from the probability range does not differ much from the dipping grid scenario (scenario#1), which means that the response surface proxy created for the dipping properties scenario can also imitate numerical simulation for the CO_2 injection. The result of the first validation sample is shown in Figure 4.22, and the percent error for each time step is provided in Figure 4.23.

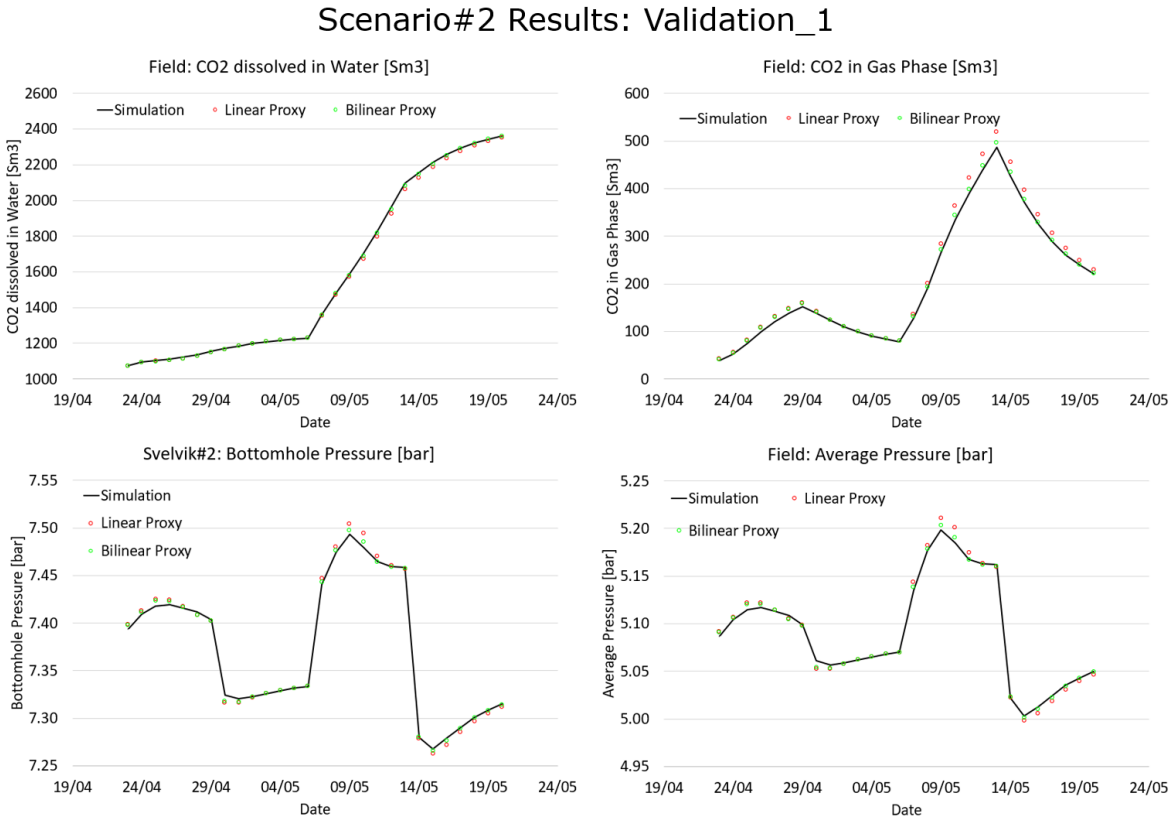

Figure 4.22: Validation_1 results for linear and bilinear proxy model (scenario#2)

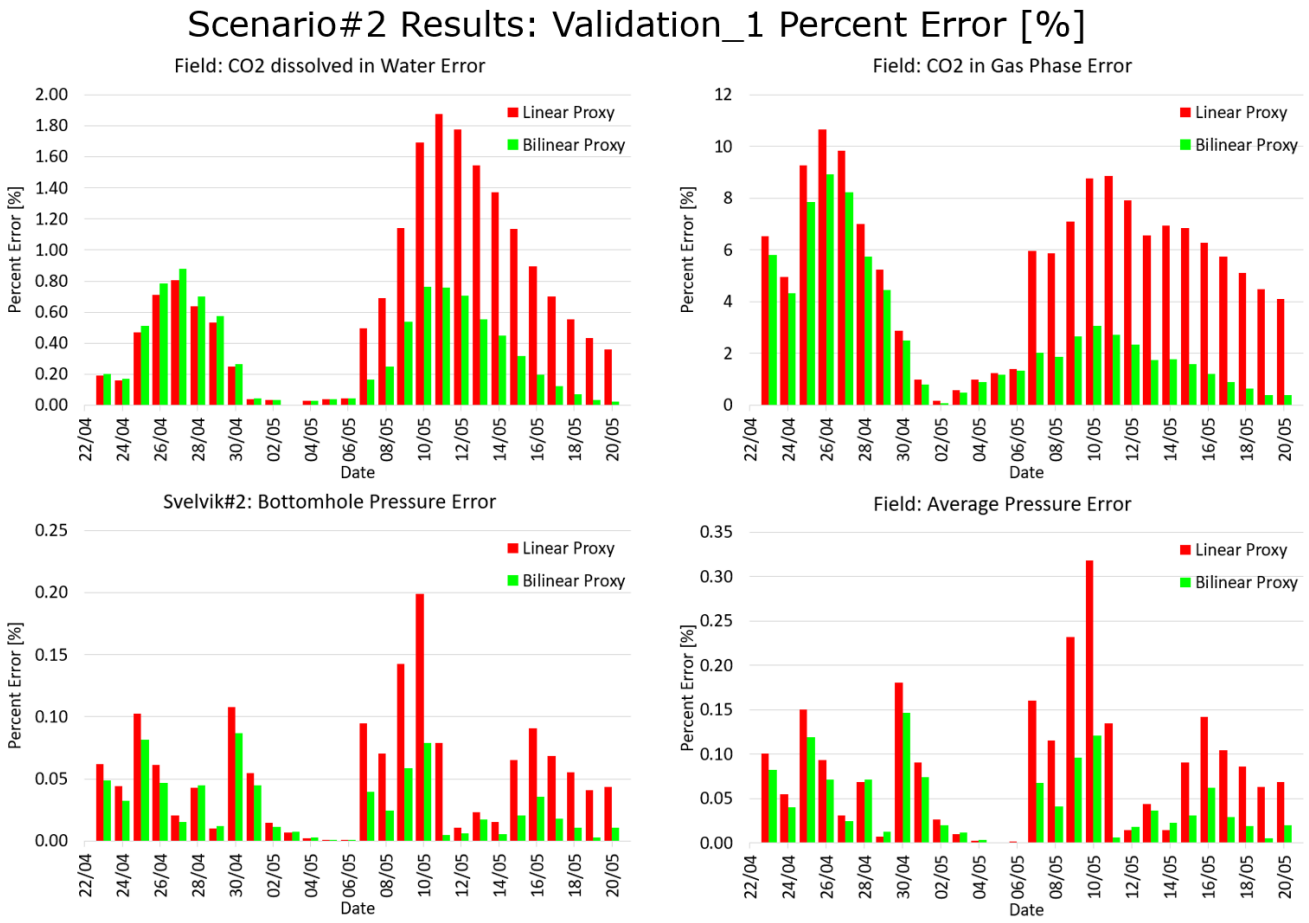

Figure 4.23: Validation_1 percent error for linear and bilinear proxy model (scenario#2)

The validation of the same case between scenario#1 and scenario#2 has similar results. In the dipping properties scenario, the CO_2 in gas phase can follow the trend of the simulation result but has a higher percent error than the other parameters. Since the proxy model is built with the polynomial regression model, the value of the predicted variable will be limited to the linear and bilinear formula. A summary of errors for all validation cases for the dipping properties scenario is presented in Table 4.7 for the linear proxy model and Table 4.8 for the bilinear proxy model.

Table 4.7: Linear proxy model validation cases error summary (scenario#2)

Linear	Svelvik#2 Bottomhole Pressure			Field: CO2 Dissolved in Water			Field: CO2 in Gas Phase			Field: Average Pressure		
	Max Percent Error [%]	Avg Percent Error [%]	R2 [-]	Max Percent Error [%]	Avg Percent Error [%]	R2 [-]	Max Percent Error [%]	Avg Percent Error [%]	R2 [-]	Max Percent Error [%]	Avg Percent Error [%]	R2 [-]
Validation_1	0.20	0.05	0.9980	1.88	0.66	0.9997	10.67	5.44	0.9993	0.32	0.09	0.9959
Validation_2	0.10	0.02	0.9989	0.95	0.39	0.9999	4.46	2.38	0.9990	0.15	0.04	0.9979
Validation_3	0.08	0.03	0.9991	1.07	0.28	1.0000	5.91	1.64	0.9990	0.12	0.04	0.9983
Validation_4	0.10	0.03	0.9992	0.80	0.34	0.9999	4.18	1.73	0.9993	0.16	0.05	0.9984
Validation_5	0.10	0.04	0.9988	0.97	0.28	0.9998	5.04	1.79	0.9984	0.16	0.06	0.9976
Validation_6	0.11	0.03	0.9989	0.94	0.23	0.9998	5.09	1.86	0.9977	0.18	0.05	0.9977
Validation_7	0.09	0.02	0.9993	0.21	0.09	1.0000	1.90	0.60	0.9993	0.14	0.03	0.9984

Table 4.8: Bilinear proxy model validation cases error summary (scenario#2)

Bilinear	Svelvik#2 Bottomhole Pressure			Field: CO2 Dissolved in Water			Field: CO2 in Gas Phase			Field: Average Pressure		
	Max Percent Error [%]	Avg Percent Error [%]	R2 [-]	Max Percent Error [%]	Avg Percent Error [%]	R2 [-]	Max Percent Error [%]	Avg Percent Error [%]	R2 [-]	Max Percent Error [%]	Avg Percent Error [%]	R2 [-]
Validation_1	0.09	0.03	0.9990	0.88	0.33	0.9999	8.91	2.71	0.9995	0.15	0.04	0.9978
Validation_2	0.06	0.02	0.9994	0.92	0.25	1.0000	4.92	1.34	0.9994	0.08	0.03	0.9988
Validation_3	0.08	0.03	0.9992	1.06	0.33	1.0000	6.10	1.99	0.9992	0.12	0.04	0.9985
Validation_4	0.11	0.03	0.9991	0.80	0.35	0.9999	4.20	1.80	0.9993	0.16	0.05	0.9984
Validation_5	0.11	0.04	0.9987	0.99	0.29	0.9998	5.26	1.87	0.9983	0.17	0.06	0.9975
Validation_6	0.13	0.04	0.9984	1.12	0.29	0.9997	6.41	2.40	0.9959	0.21	0.06	0.9968
Validation_7	0.10	0.02	0.9991	0.69	0.21	0.9999	4.50	1.71	0.9957	0.16	0.03	0.9982

On average, the proxy models from the response surface have a lower error in the dipping properties scenario than the dipping grid scenario. This could be due to the grid in the dipping properties scenario being a regular grid. In contrast, the dipping grid scenario consists of irregular grids that create complexity for the response surface proxy to mimic. The maximum error in the dipping properties scenario comes from the CO_2 in gas phase, which is 8-10%, with an average error of 2-5%. The other parameters yield an error of less than 1% in all validation cases. The R^2 for all cases is good (more than 0.99), similar to the dipping grid scenario result.

4.2.2 Universal Kriging Proxy

The universal kriging proxy assumes that the predicted value follows a gaussian process with a correlation function and an unknown variance determined by maximizing the outcome likelihood.

4.2.2.1 Dipping Grid Scenario Proxy Model

The probability based on the training data using the universal kriging algorithm is presented in Figure 4.24. The probability shows a similar range with the probability from the response surface proxy, which also has a similar trend to mimic the injection and shut-in of CO_2 injection.

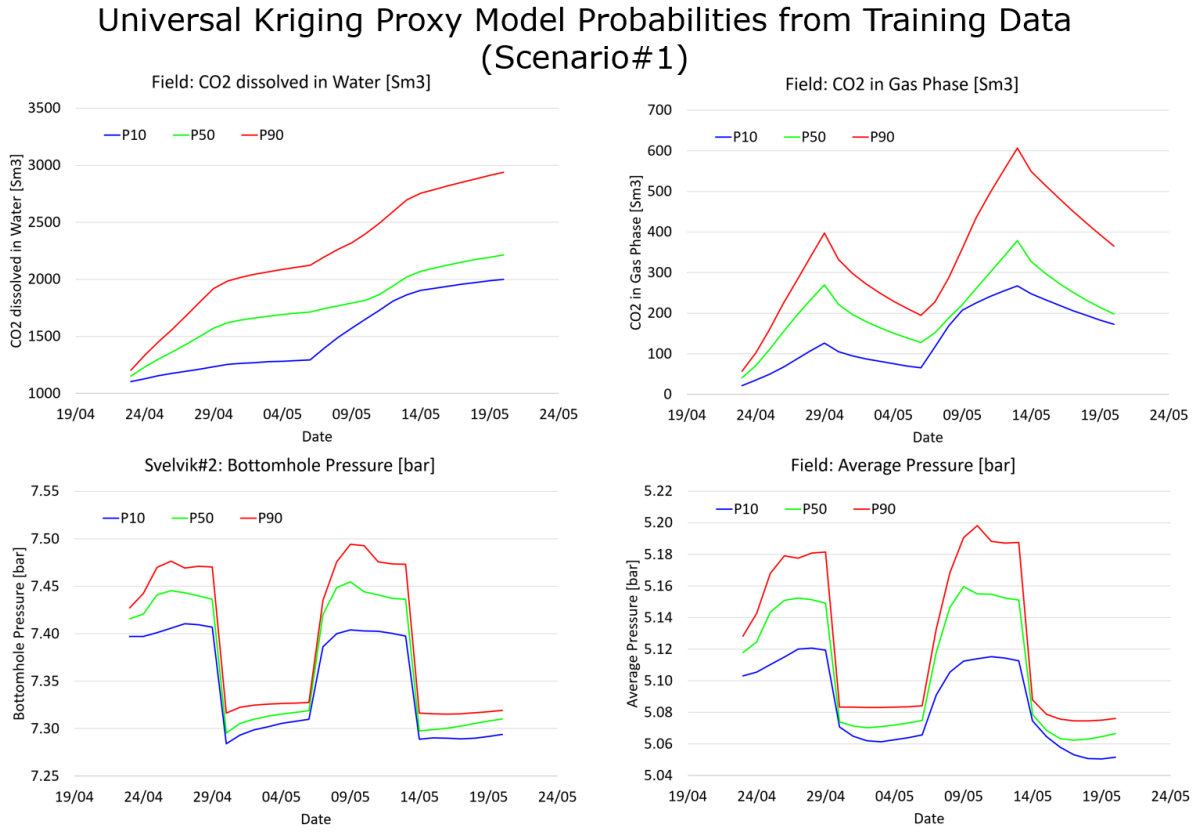

Figure 4.24: Universal kriging probabilities from training data (scenario#1)

The 1st validation result is presented in Figure 4.25. Based on the validation result, the universal kriging proxy is capable of capturing the trend and predicting the value better than the response surface proxy. The reason is that the universal kriging proxy uses the term random error addition to the linear basis over the experimental domain. This random error is determined using the Gaussian process with zero mean, unknown

variance, and correlation function determined by maximizing the outcome likelihood. Therefore, the predicted value from universal kriging tends to fit with the data and makes it possible to model a complex response with sufficient training data.

The detail of the percent error is shown in Figure 4.26. Overall, it shows a lower error magnitude than the response surface proxy model. In the universal kriging proxy, the CO_2 in gas phase also shows a little bit higher error than the other variables that the proxy model predicts. Looking at the figure between the simulated and the proxy, it seems that the error is due to the initial value of the CO_2 in gas phase being low. The error starts to diminish when the CO_2 in gas phase increases.

The summary of all validation cases is shown in Table 4.9. The universal kriging proxy model based on all validation cases is capable of predicting with high accuracy, with most of the R^2 calculated at nearly 1. The highest error from the universal kriging proxy comes from predicting the CO_2 in gas phase with a maximum error of 2.94% and an average error of 0.67% in validation sample 1. The rest of the predicted results have a minor (~0.1% percent) error.

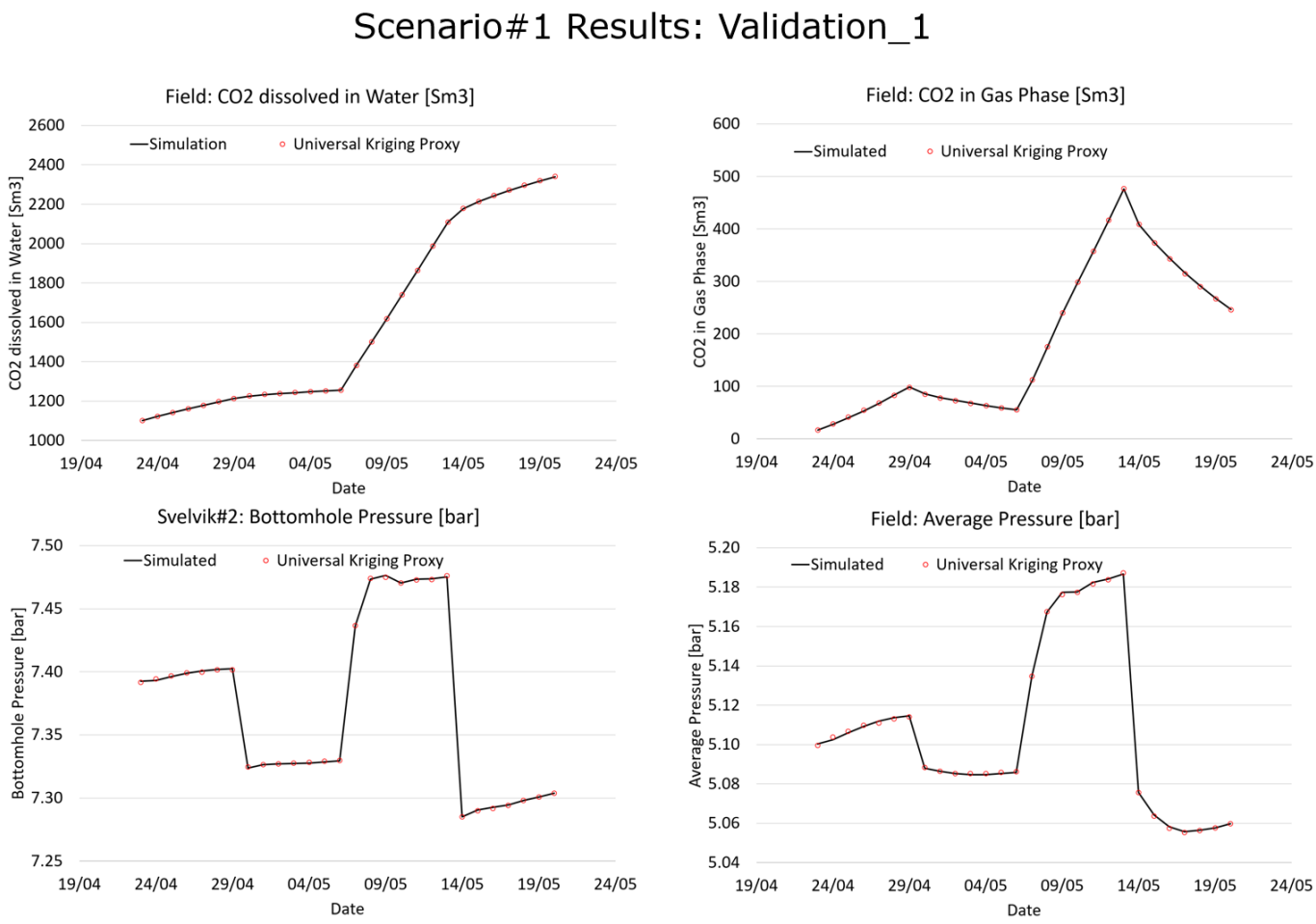

Figure 4.25: Validation_1 results for universal kriging proxy (scenario#1)

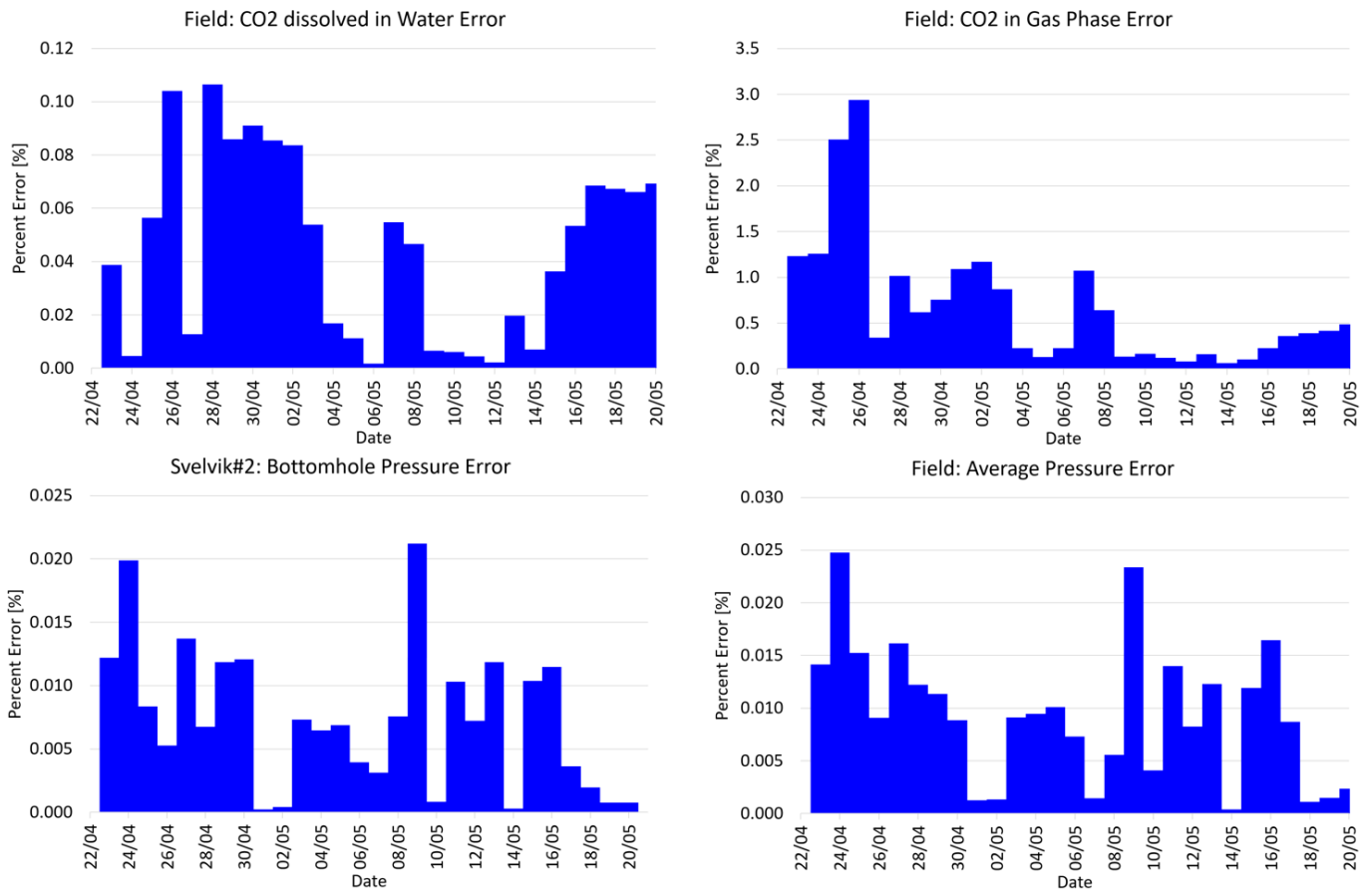

Figure 4.26: Validation_1 percent error for universal kriging proxy (scenario#1)

Table 4.9: Universal kriging proxy model validation cases error summary (scenario#1)

Universal Kriging	Svelvik#2 Bottomhole Pressure			Field: CO2 Dissolved in Water			Field: CO2 in Gas Phase			Field: Average Pressure		
	Max Percent Error [%]	Avg Percent Error [%]	R2 [-]	Max Percent Error [%]	Avg Percent Error [%]	R2 [-]	Max Percent Error [%]	Avg Percent Error [%]	R2 [-]	Max Percent Error [%]	Avg Percent Error [%]	R2 [-]
Sample_1	0.02	0.01	0.9999	0.11	0.05	1.0000	2.94	0.67	1.0000	0.02	0.01	0.9998
Sample_2	0.03	0.01	0.9999	0.09	0.05	1.0000	2.80	0.36	1.0000	0.03	0.01	0.9998
Sample_3	0.02	0.01	0.9999	0.06	0.02	1.0000	0.99	0.27	1.0000	0.02	0.01	0.9999
Sample_4	0.02	0.01	0.9999	0.10	0.02	1.0000	1.15	0.25	1.0000	0.02	0.01	0.9999
Sample_5	0.02	0.00	0.9999	0.06	0.02	1.0000	0.41	0.16	1.0000	0.02	0.00	0.9999
Sample_6	0.02	0.01	0.9999	0.12	0.07	1.0000	0.53	0.14	1.0000	0.02	0.01	0.9999
Sample_7	0.03	0.01	0.9999	0.10	0.05	1.0000	0.40	0.13	1.0000	0.03	0.01	0.9999
Sample_8	0.02	0.01	0.9999	0.07	0.03	1.0000	0.40	0.16	1.0000	0.02	0.01	0.9999

4.2.2.2 Dipping Properties Scenario Proxy Model

The universal kriging proxy for the dipping properties scenario is built to compare the performance with the dipping grid scenario. The probabilities for universal kriging with dipping properties geo-model are shown in Figure 4.27.

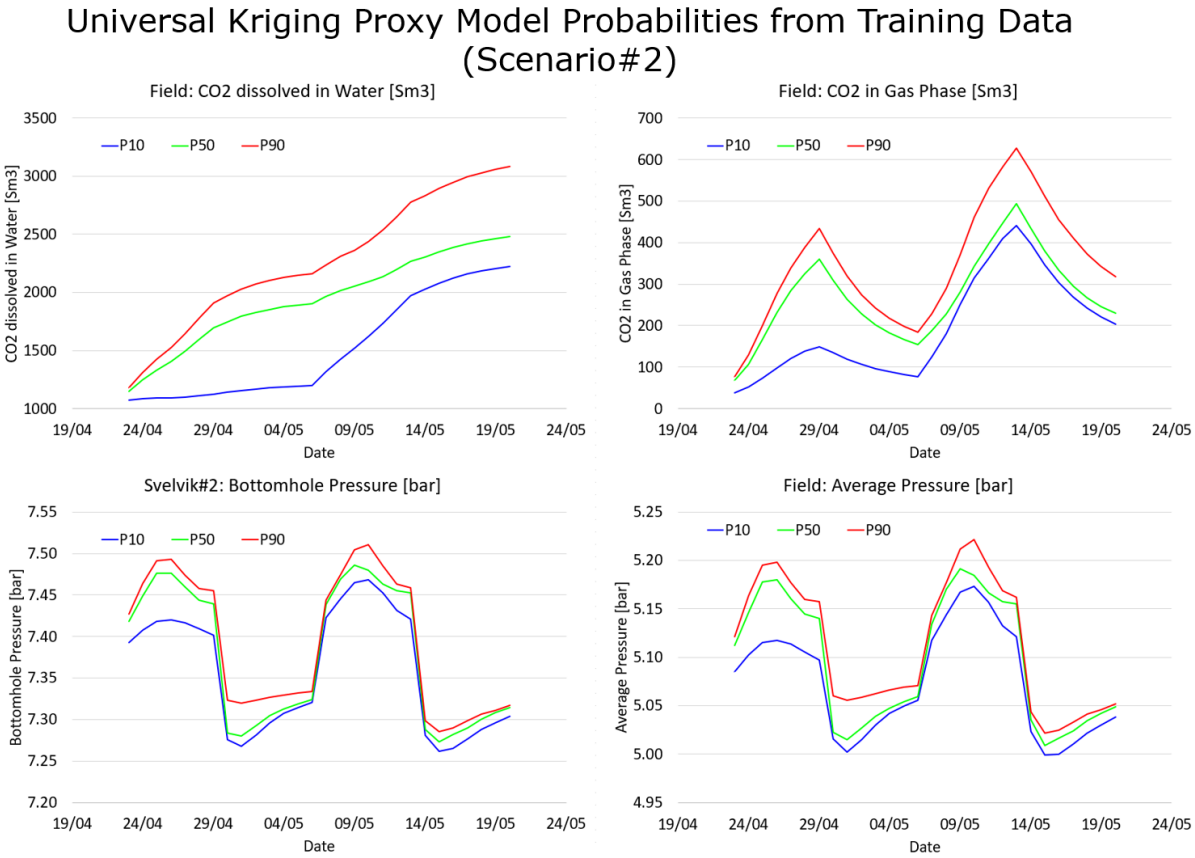

Figure 4.27: Universal kriging probabilities from training data (scenario#2)

The result from the 1st validation case with the universal kriging proxy built for the dipping properties scenario is presented in Figure 4.28 and the percent error in Figure 4.29. These two figures demonstrate that the universal kriging proxy can fit with the result from the simulation data with very little error. It means the universal kriging proxy can be used as a proxy from the numerical simulation with a similar result for predicting the new CO_2 injection.

The summary of all errors from the validation case in the dipping properties scenario is shown in Table 4.10. Overall, the predicted results by universal kriging proxy for dipping properties scenario are able to simulate the trend and the values of CO_2 injection in this type of geological model.

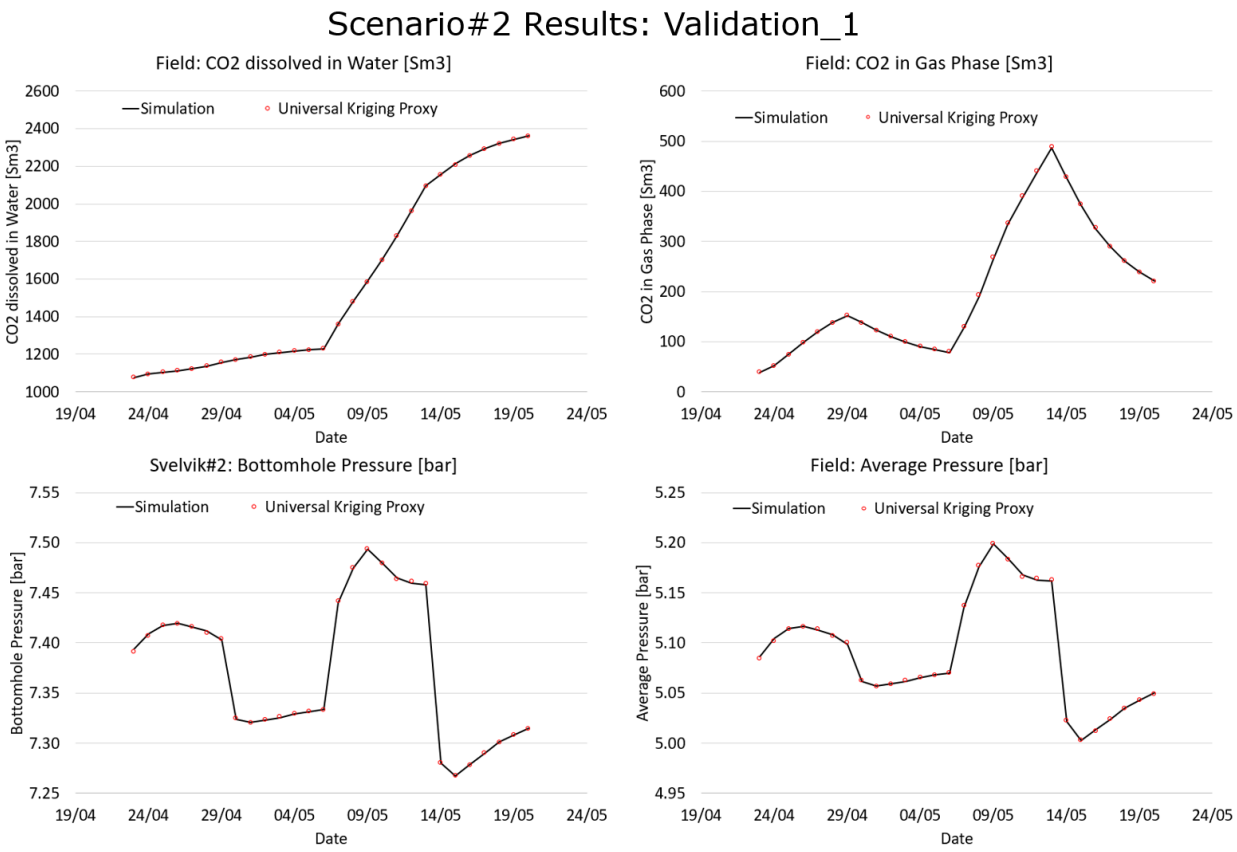

Figure 4.28: Validation_1 results for universal kriging proxy (scenario#2)

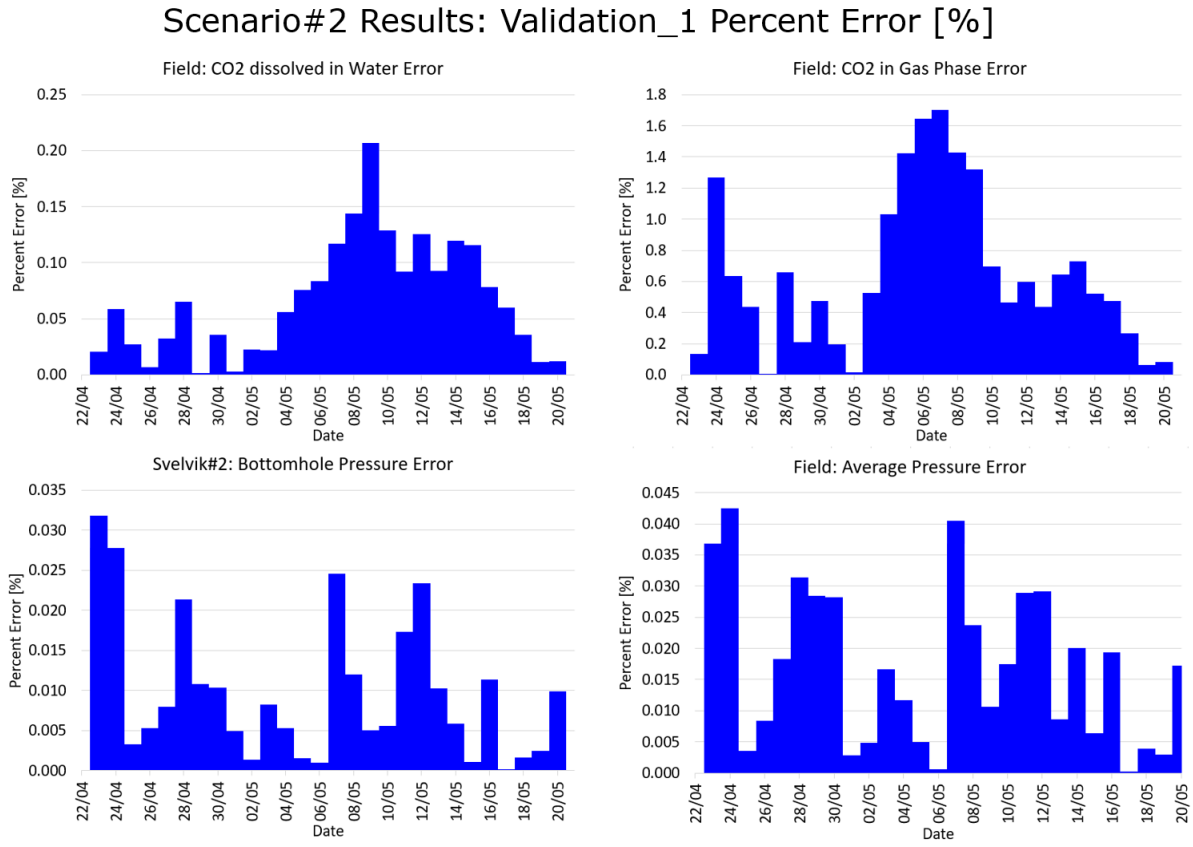

Figure 4.29: Validation_1 percent error for universal kriging proxy (scenario#2)

Table 4.10: Universal kriging proxy model validation cases error summary (scenario#2)

Universal Kriging	Svelvik#2 Bottomhole Pressure			Field: CO2 Dissolved in Water			Field: CO2 in Gas Phase			Field: Average Pressure		
	Max Percent Error [%]	Avg Percent Error [%]	R2 [-]	Max Percent Error [%]	Avg Percent Error [%]	R2 [-]	Max Percent Error [%]	Avg Percent Error [%]	R2 [-]	Max Percent Error [%]	Avg Percent Error [%]	R2 [-]
Validation_1	0.03	0.01	0.9998	0.21	0.07	1.0000	1.70	0.65	1.0000	0.04	0.02	0.9996
Validation_2	0.03	0.01	0.9999	0.15	0.09	1.0000	1.29	0.57	0.9999	0.04	0.01	0.9997
Validation_3	0.02	0.01	0.9999	0.17	0.10	1.0000	0.83	0.34	1.0000	0.03	0.01	0.9998
Validation_4	0.02	0.01	0.9999	0.16	0.08	1.0000	1.32	0.35	1.0000	0.04	0.01	0.9999
Validation_5	0.01	0.00	1.0000	0.04	0.02	1.0000	0.63	0.26	1.0000	0.03	0.01	0.9999
Validation_6	0.04	0.01	0.9999	0.08	0.03	1.0000	0.61	0.18	1.0000	0.04	0.01	0.9998
Validation_7	0.02	0.01	0.9999	0.10	0.04	1.0000	0.87	0.24	0.9999	0.03	0.01	0.9999

4.2.3 Comparison between Different Proxy Model

The proxy models from the response surface algorithm and universal kriging algorithm that have been made and validated through the cases are being compared. The proxy model is compared by using the evaluation dataset, which is not from the training and validation case. This process ensures that the proxy can emulate the numerical simulation, and unbiased comparison can be obtained.

4.2.3.1 Dipping Grid Scenario Evaluation

The result of the simulation and all the proxies for the dipping grid scenario is shown in Figure 4.30. All of the proxy models succeeded in mimicking the result from the simulation. The trend and value can be captured in the evaluation test. The percent error detail of each timestep is shown in Figure 4.31. The percent error shows that the universal kriging has the lowest error compared to the proxy from the response surface. Both response surface proxy linear and bilinear are comparable in terms of error, as seen in Figure 4.31. his is due to the response surface assuming that the predicted value follows a polynomial function, while universal kriging uses the Gaussian process and correlation function determined by maximizing the outcome likelihood. The full evaluation error is shown in Table 4.11.

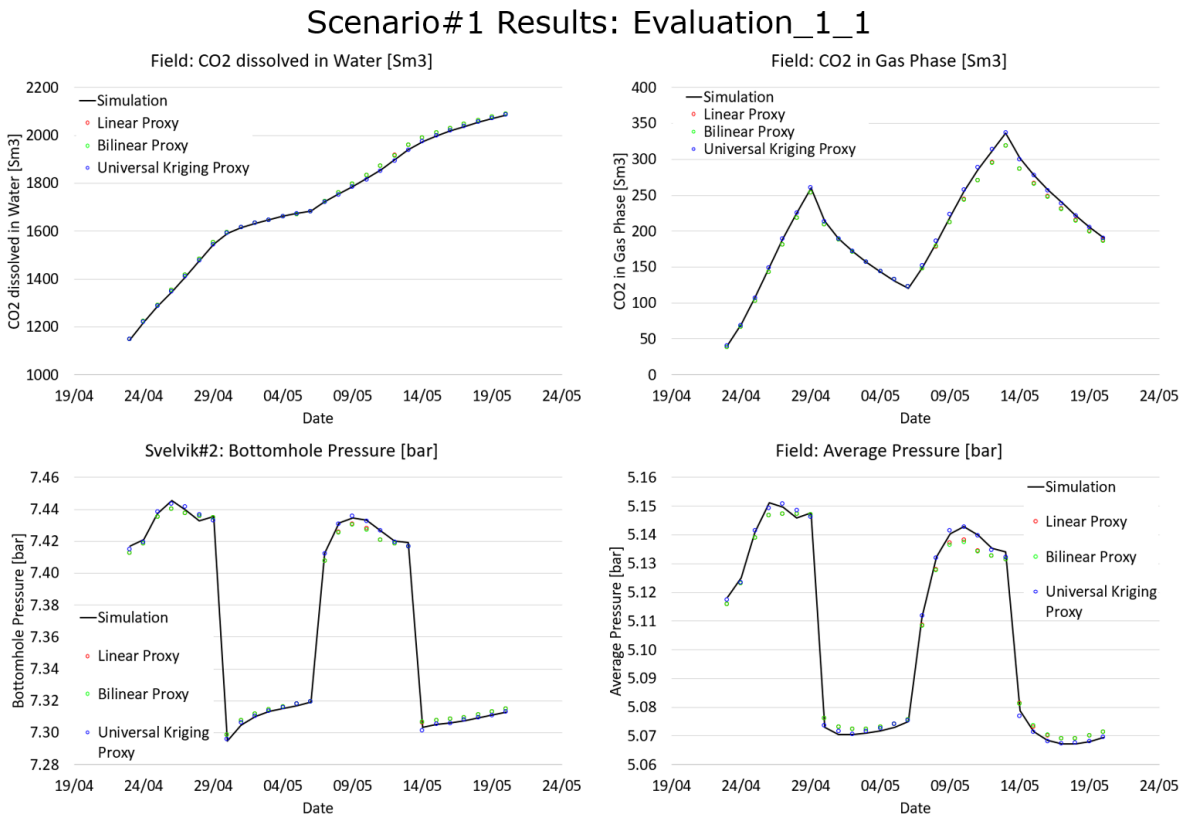

Figure 4.30: Evaluation_1_1 results of proxy models (scenario#1)

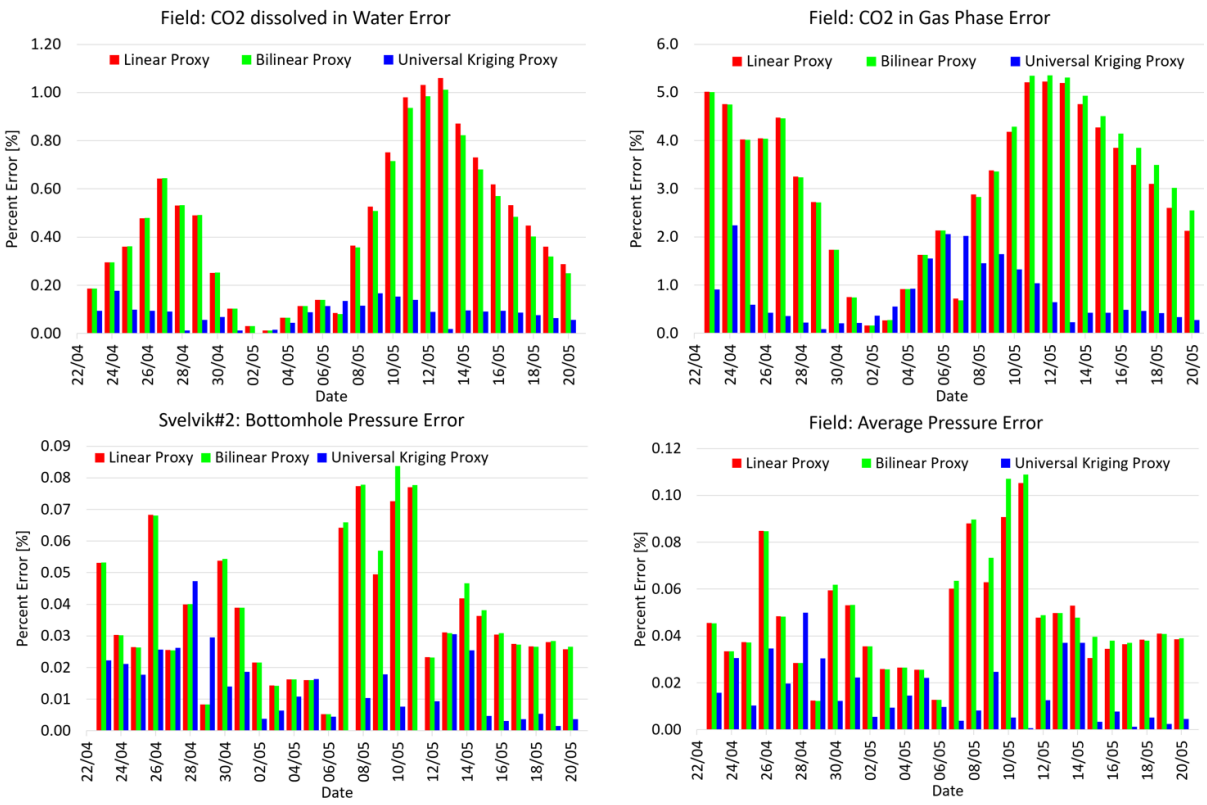

Figure 4.31: Evaluation_1_1 percent error of proxy model (scenario#1)

Table 4.11: Evaluation error for all proxy (scenario#1)

Linear	Svelvik#2 Bottomhole Pressure			Field: CO2 Dissolved in Water			Field: CO2 in Gas Phase			Field: Average Pressure		
	Max Percent Error [%]	Avg Percent Error [%]	R2 [-]	Max Percent Error [%]	Avg Percent Error [%]	R2 [-]	Max Percent Error [%]	Avg Percent Error [%]	R2 [-]	Max Percent Error [%]	Avg Percent Error [%]	R2 [-]
Evaluation_1_1	0.08	0.04	0.9991	1.06	0.44	0.9996	5.23	3.10	0.9980	0.11	0.05	0.9980
Evaluation_2_1	0.11	0.03	0.9982	0.83	0.36	0.9998	6.46	3.05	0.9984	0.11	0.03	0.9959
Evaluation_3_1	0.06	0.02	0.9987	0.55	0.17	0.9999	3.81	1.66	0.9956	0.08	0.03	0.9968
Evaluation_4_1	0.11	0.02	0.9993	0.52	0.18	1.0000	4.64	1.46	0.9988	0.16	0.03	0.9984
Evaluation_5_1	0.12	0.03	0.9993	0.61	0.26	0.9999	3.64	1.54	0.9994	0.15	0.04	0.9987

Bilinear	Svelvik#2 Bottomhole Pressure			Field: CO2 Dissolved in Water			Field: CO2 in Gas Phase			Field: Average Pressure		
	Max Percent Error [%]	Avg Percent Error [%]	R2 [-]	Max Percent Error [%]	Avg Percent Error [%]	R2 [-]	Max Percent Error [%]	Avg Percent Error [%]	R2 [-]	Max Percent Error [%]	Avg Percent Error [%]	R2 [-]
Evaluation_1_1	0.08	0.04	0.9990	1.01	0.42	0.9996	5.35	3.20	0.9979	0.11	0.05	0.9977
Evaluation_2_1	0.12	0.03	0.9982	0.78	0.32	0.9998	6.40	2.94	0.9985	0.11	0.03	0.9961
Evaluation_3_1	0.06	0.02	0.9990	0.55	0.18	0.9999	3.85	1.61	0.9970	0.08	0.03	0.9978
Evaluation_4_1	0.06	0.02	0.9998	0.33	0.11	1.0000	2.01	0.72	0.9998	0.09	0.02	0.9995
Evaluation_5_1	0.08	0.02	0.9996	0.48	0.20	1.0000	2.49	0.98	0.9997	0.10	0.03	0.9993

Universal Kriging	Svelvik#2 Bottomhole Pressure			Field: CO2 Dissolved in Water			Field: CO2 in Gas Phase			Field: Average Pressure		
	Max Percent Error [%]	Avg Percent Error [%]	R2 [-]	Max Percent Error [%]	Avg Percent Error [%]	R2 [-]	Max Percent Error [%]	Avg Percent Error [%]	R2 [-]	Max Percent Error [%]	Avg Percent Error [%]	R2 [-]
Evaluation_1_1	0.05	0.01	0.9995	0.18	0.08	1.0000	2.24	0.78	0.9995	0.05	0.02	0.9991
Evaluation_2_1	0.04	0.01	0.9997	0.21	0.10	1.0000	2.74	1.13	0.9997	0.04	0.01	0.9994
Evaluation_3_1	0.06	0.03	0.9984	0.78	0.31	0.9997	5.92	2.90	0.9911	0.07	0.03	0.9963
Evaluation_4_1	0.03	0.01	0.9999	0.12	0.05	1.0000	1.03	0.32	1.0000	0.03	0.01	0.9999
Evaluation_5_1	0.02	0.01	1.0000	0.11	0.06	1.0000	1.30	0.38	0.9999	0.02	0.01	0.9999

Based on the evaluation result, where the evaluation dataset is introduced to check the validity of the proxy, all results can reach a very high correlation with the simulation result (R^2 > 0.99). It proves that all of the proxies can be used for CO_2 injection prediction in Svelvik CO_2 Field Laboratory. The highest error also comes from the CO_2 in

gas phase, as shown in the validation result. This also could be because the value of the CO_2 in gas phase is small, and little deviation could yield a high error.

4.2.3.2 Dipping Properties Scenario Evaluation

With a different set of evaluation datasets, the dipping properties scenario is also being evaluated with the same method as the dipping grid scenario. The different set is used to ensure that the validity of the proxy is universal and unbiased. The results are shown in Figure 4.32.

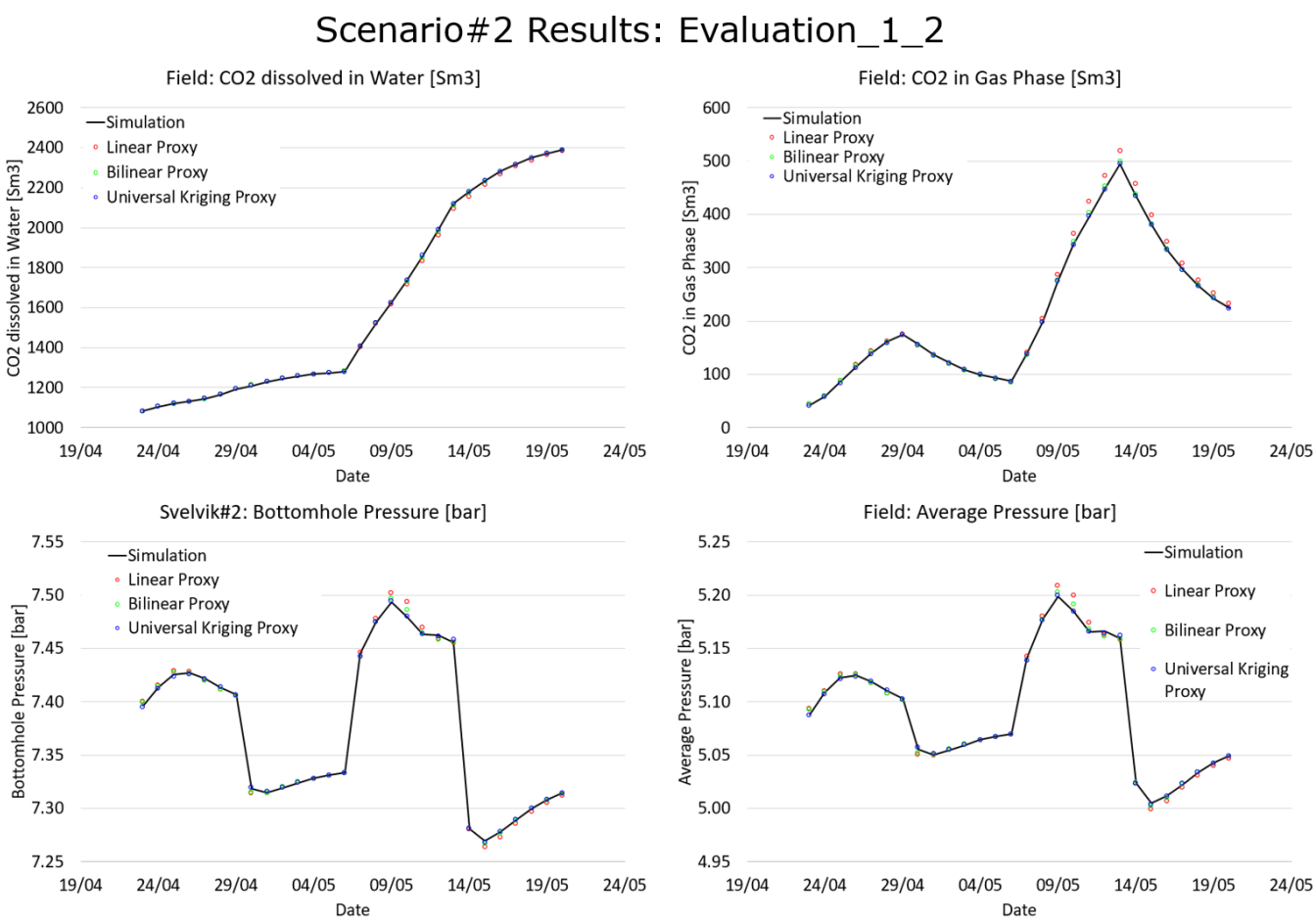

Figure 4.32: Evaluation_1_2 results of proxy model (scenario#2)

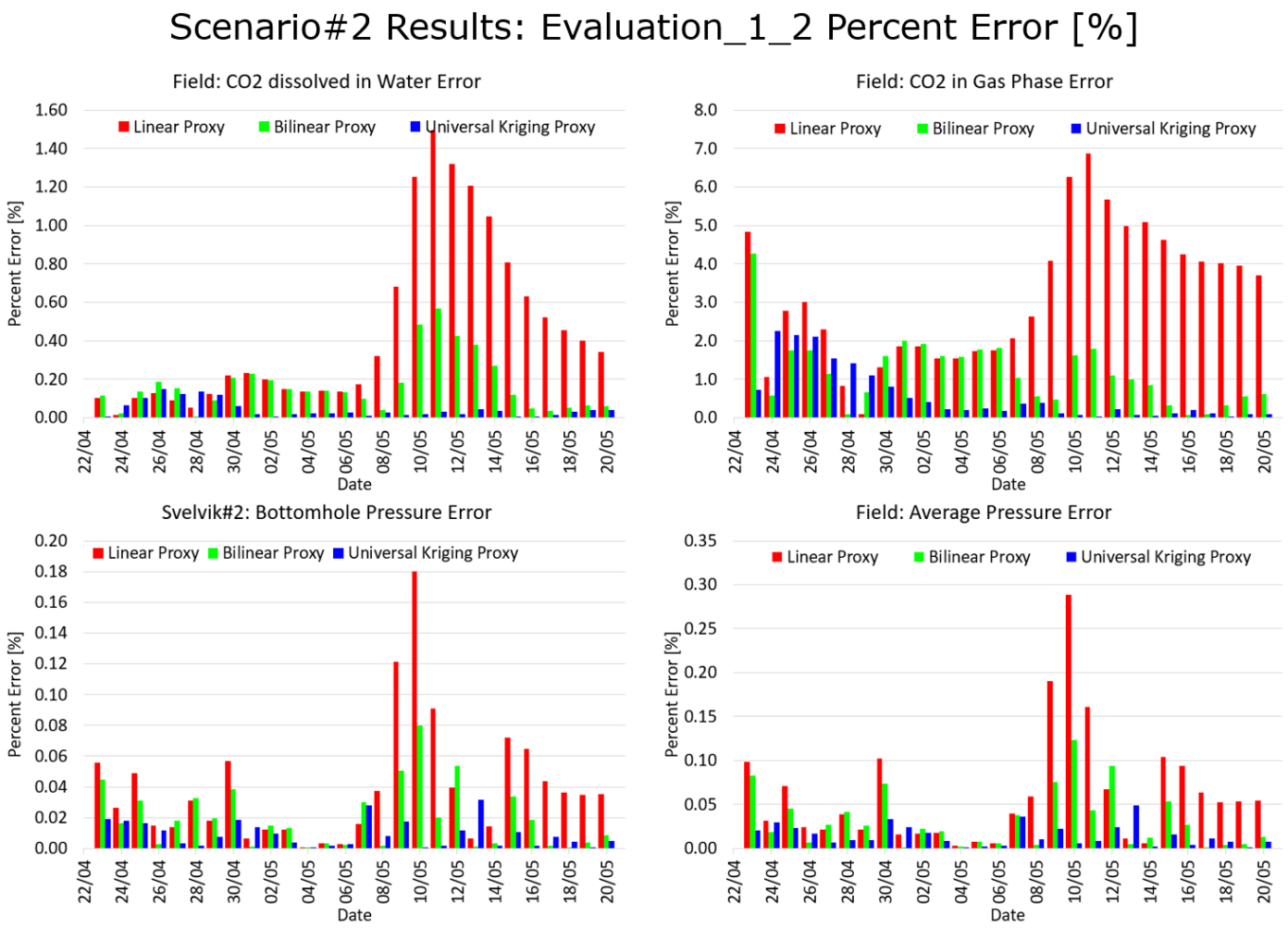

Figure 4.33: Evaluation_1_2 percent error of proxy model (scenario#2)

Table 4.12: Evaluation error for all proxy (scenario#2)

Linear	Svelvik#2 Bottomhole Pressure			Field: CO2 Dissolved in Water			Field: CO2 in Gas Phase			Field: Average Pressure		
	Max Percent Error [%]	Avg Percent Error [%]	R2 [-]	Max Percent Error [%]	Avg Percent Error [%]	R2 [-]	Max Percent Error [%]	Avg Percent Error [%]	R2 [-]	Max Percent Error [%]	Avg Percent Error [%]	R2 [-]
Evaluation_1_2	0.18	0.04	0.9983	1.49	0.45	0.9998	6.86	3.17	0.9995	0.29	0.06	0.9969
Evaluation_2_2	0.12	0.04	0.9987	0.97	0.24	0.9998	5.63	1.88	0.9978	0.19	0.06	0.9975
Evaluation_3_2	0.14	0.02	0.9994	0.30	0.14	1.0000	2.98	1.19	0.9995	0.22	0.04	0.9990
Evaluation_4_2	0.14	0.04	0.9978	0.84	0.28	0.9998	5.42	1.87	0.9960	0.22	0.07	0.9962
Evaluation_5_2	0.16	0.05	0.9977	1.41	0.63	0.9998	16.55	6.34	0.9988	0.26	0.09	0.9947

Bilinear	Svelvik#2 Bottomhole Pressure			Field: CO2 Dissolved in Water			Field: CO2 in Gas Phase			Field: Average Pressure		
	Max Percent Error [%]	Avg Percent Error [%]	R2 [-]	Max Percent Error [%]	Avg Percent Error [%]	R2 [-]	Max Percent Error [%]	Avg Percent Error [%]	R2 [-]	Max Percent Error [%]	Avg Percent Error [%]	R2 [-]
Evaluation_1_2	0.08	0.02	0.9992	0.57	0.17	1.0000	4.27	1.18	0.9998	0.12	0.03	0.9985
Evaluation_2_2	0.13	0.04	0.9985	1.05	0.26	0.9997	6.11	2.07	0.9974	0.21	0.06	0.9972
Evaluation_3_2	0.05	0.01	0.9999	0.21	0.06	1.0000	0.64	0.29	1.0000	0.05	0.01	0.9998
Evaluation_4_2	0.12	0.04	0.9982	0.78	0.26	0.9998	4.53	1.59	0.9970	0.19	0.06	0.9969
Evaluation_5_2	0.11	0.03	0.9981	1.26	0.34	0.9999	14.96	3.89	0.9987	0.19	0.05	0.9958

Universal Kriging	Svelvik#2 Bottomhole Pressure			Field: CO2 Dissolved in Water			Field: CO2 in Gas Phase			Field: Average Pressure		
	Max Percent Error [%]	Avg Percent Error [%]	R2 [-]	Max Percent Error [%]	Avg Percent Error [%]	R2 [-]	Max Percent Error [%]	Avg Percent Error [%]	R2 [-]	Max Percent Error [%]	Avg Percent Error [%]	R2 [-]
Evaluation_1_2	0.03	0.01	0.9998	0.15	0.04	1.0000	2.25	0.56	1.0000	0.05	0.01	0.9997
Evaluation_2_2	0.03	0.01	0.9999	0.13	0.05	1.0000	1.84	0.48	0.9999	0.04	0.02	0.9997
Evaluation_3_2	0.02	0.01	1.0000	0.08	0.02	1.0000	0.61	0.17	1.0000	0.03	0.01	0.9999
Evaluation_4_2	0.08	0.03	0.9990	0.44	0.18	0.9999	2.98	1.23	0.9987	0.12	0.05	0.9982
Evaluation_5_2	0.07	0.02	0.9989	1.11	0.30	0.9999	11.00	3.29	0.9991	0.11	0.04	0.9977

The evaluation result demonstrates that all of the proxies are correlated to the simulation result based on the R2 higher than 0.99 for all evaluation cases and all predicted variables.

In the case of Evaluation_5_2, it has the highest maximum percent error reaching 11 – 16%. It is further investigated that the error comes from the small initial injection rate (27.4022 Sm3/d), which initially yields a low value of CO_2 in gas phase (Figure 4.34). Therefore, even if the difference is less than 10 Sm3/d, it still has a very high calculated percent error.

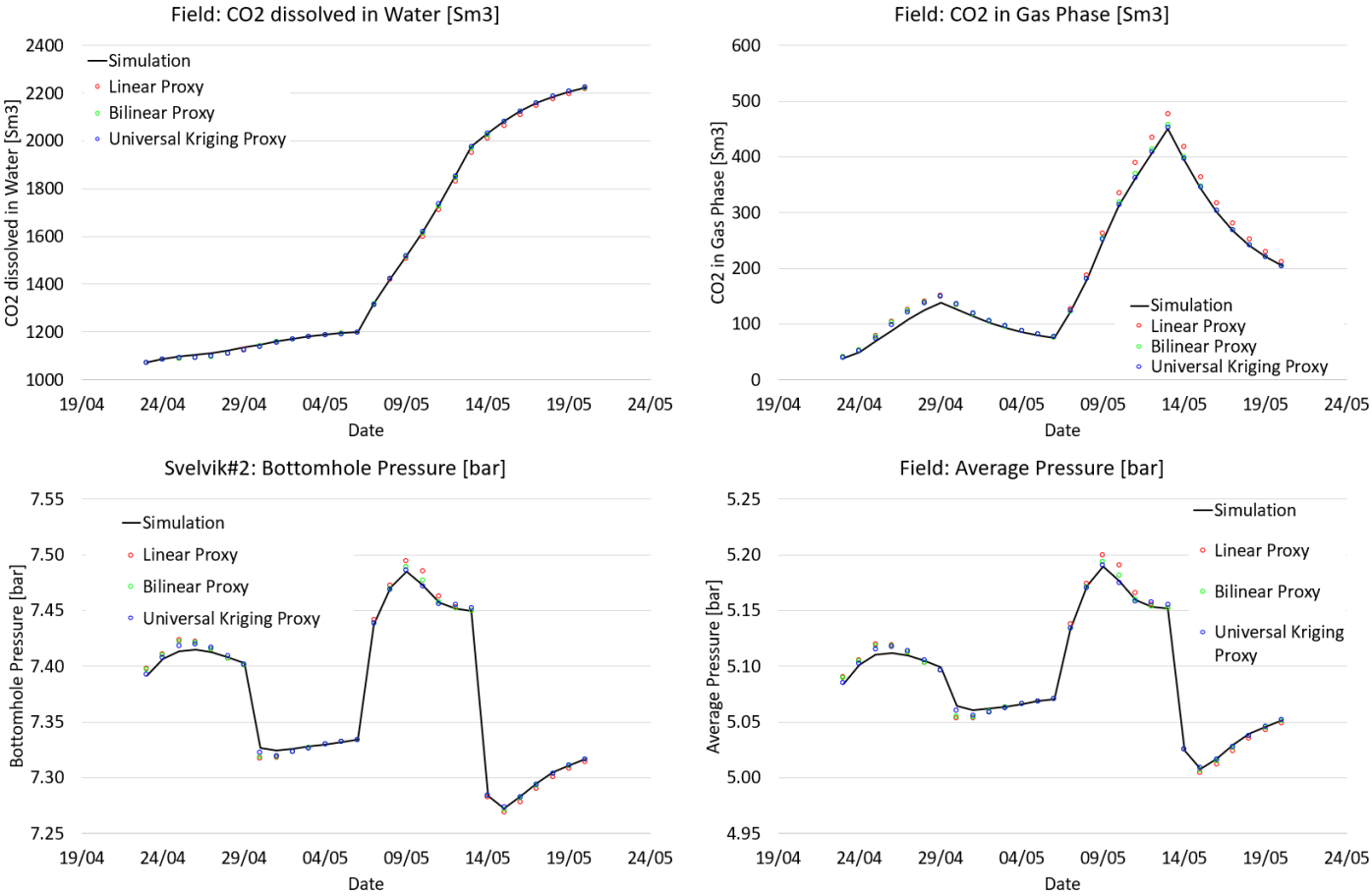

Figure 4.34: Evaluation_5_2 results of proxy model (scenario#2)

4.2.4 CO_2 Migration Prediction

As it is seen in Figure 4.10 and Figure 4.11 hat, the CO_2 has the possibility to migrate vertically from the injection depth to the upper mud layer (~38m). The proxy model also provided an interesting result, predicting the dissolved CO_2 in water and CO_2 in the gas phase for different layers (Figure 3.18). The results of the predicted layers are shown in Figure 4.35 to Figure 4.38 for evaluation sample 1 with dipping grid scenario and Figure 4.39 to Figure 4.42 for evaluation sample 1 with dipping properties scenario.

The main interest layers in this study are layer 3 as the mud layer, layer 4 as the sand layer, layer 5 as the coarse/ fine sand layer, and layer 6 as the injection layer with sand.

4.2.4.1 Dipping grid scenario

The CO_2 migrates mostly to layer 4 rapidly when the CO_2 is injected and dissolved in the water when the injection stops. The same trend is observed in layer 5 and layer 6, where the CO_2 in gas phase increases when the CO_2 is injected and declines when injection stops. Layer 3 has a different trend where the CO_2 in gas phase is accumulated in a small amount due to layer 3 being a mud layer, and the CO_2 spreads mainly in the interface between layer 3 and layer 4.

The evaluation result shows that the proxy model can mimic these effects. The response surface proxies have some difficulty mimicking the dissolved CO_2 in water for layer 6 due to the trend not following a linear model with the current input. Universal kriging proxy can have a better result in emulating the field and layered prediction since universal kriging has the advantage of increasing the likely outcome from the Gaussian process.

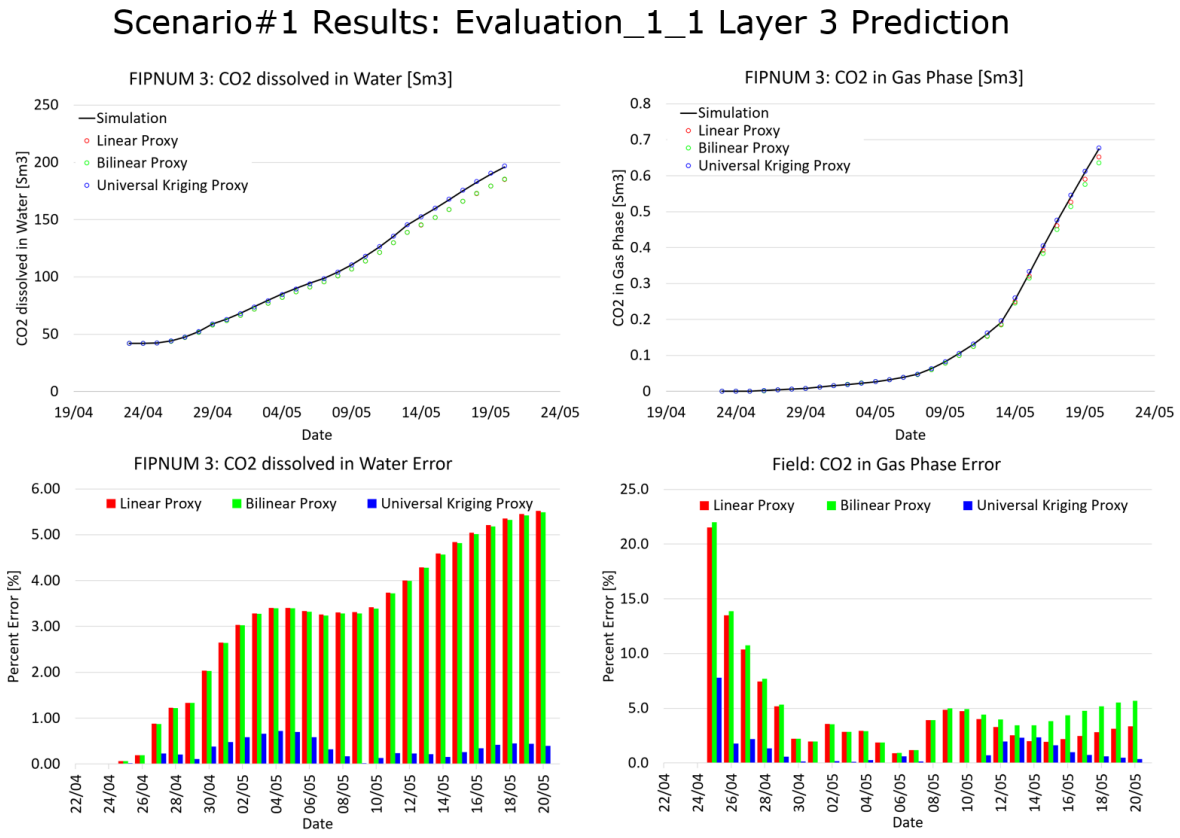

Figure 4.35: Evaluation_1_1 dissolved CO_2 and CO_2 in gas phase layer 3 prediction (scenario#1)

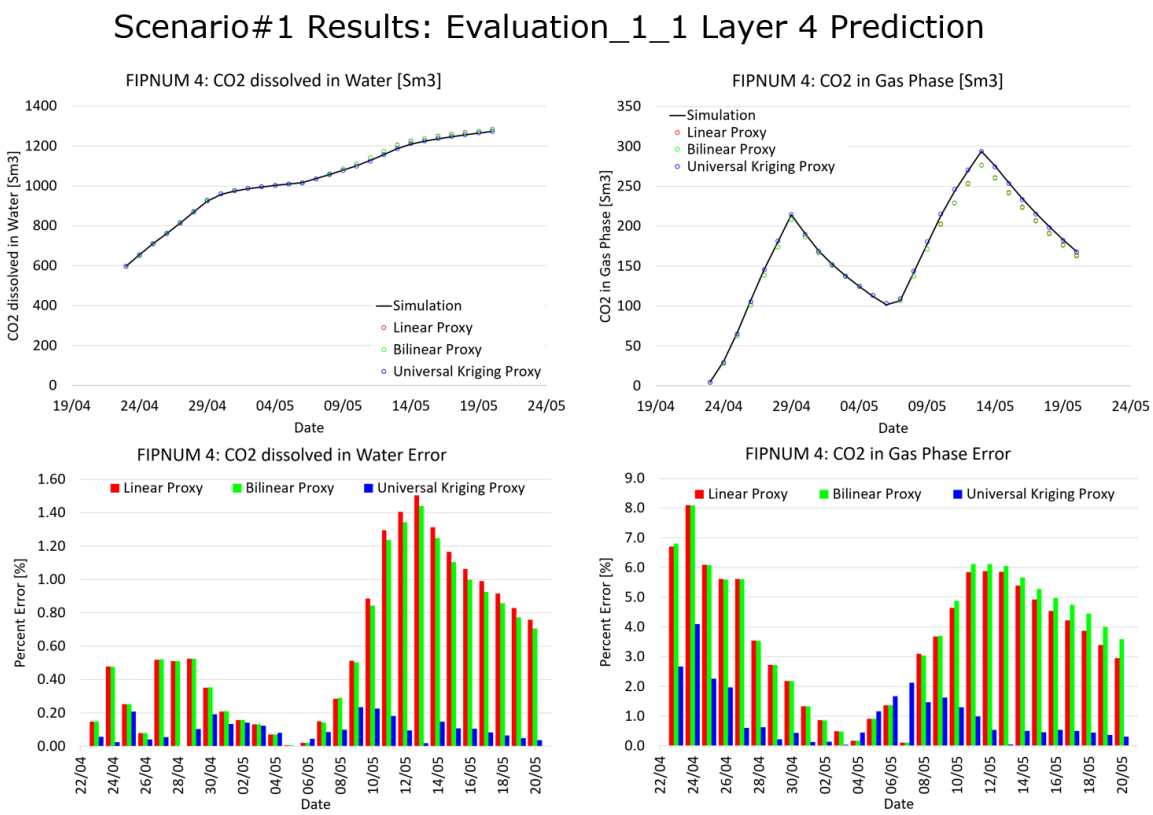

Figure 4.36: Evaluation_1_1 dissolved CO_2 and CO_2 in gas phase layer 4 prediction (scenario#1)

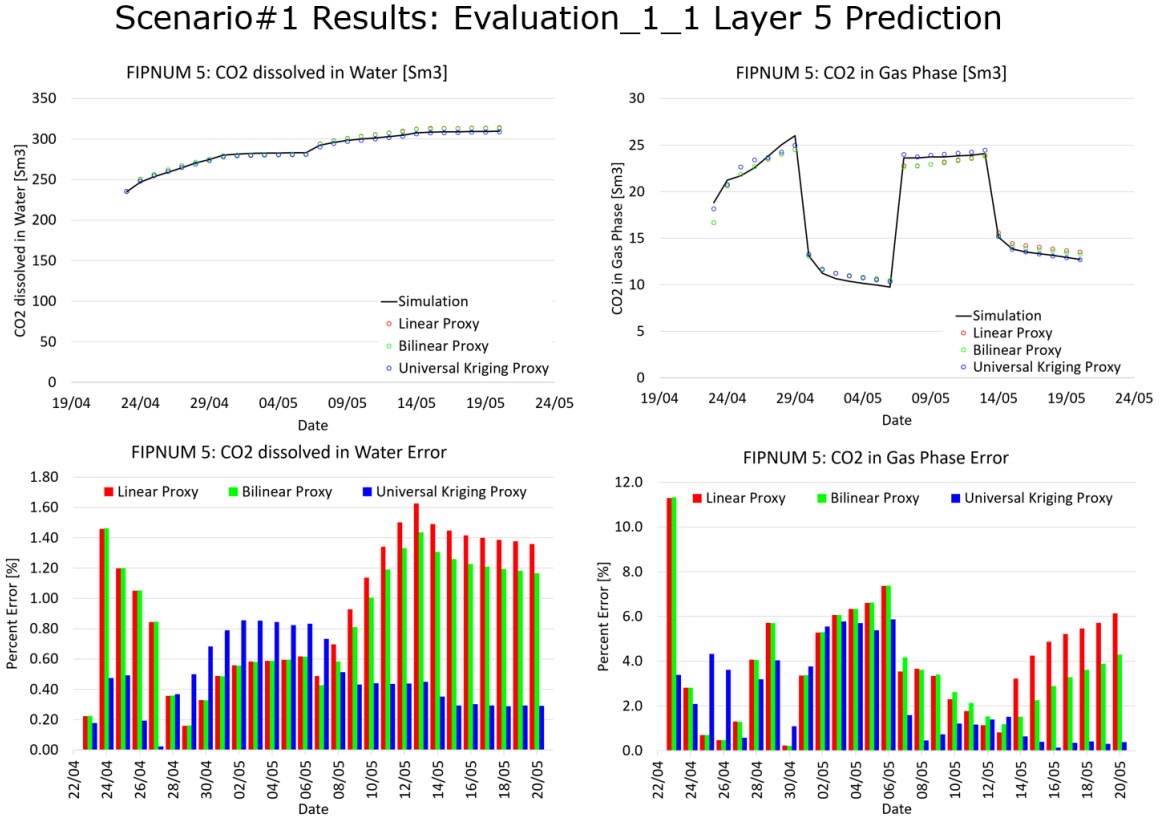

Figure 4.37: Evaluation_1_1 dissolved CO_2 and CO_2 in gas phase layer 5 prediction (scenario#1)

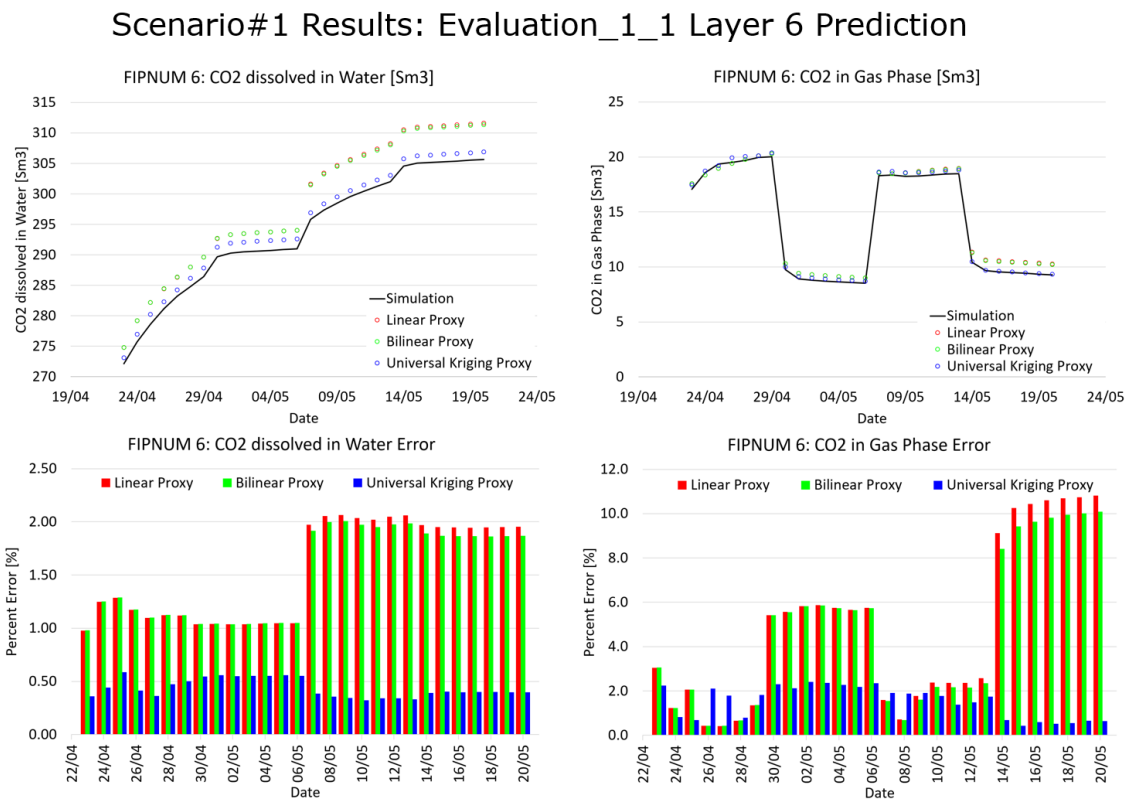

Figure 4.38: Evaluation_1_1 dissolved CO_2 and CO_2 in gas phase layer 6 prediction (scenario#1)

4.2.4.2 Dipping properties scenario

The proxy model for the dipping properties scenario is also used to predict the dissolved CO_2 in water and CO_2 in gas phase per layer to investigate the migration of the CO_2. The result of each layered zone is shown from Figure 4.39 to Figure 4.42. The proxy models are able to emulate the trend of the dissolved CO_2 in water and the CO_2 in gas phase per layer.

The dipping properties scenario shows a different migration from the dipping grid scenario due to the difference in the initial state, as shown in Figure 4.13. The same trend is shown in layer 3, where the dissolved CO_2 in water and the CO_2 in gas phase increase over time. Similar results are shown in layer 4, where most of the dissolved CO_2 and CO_2 in gas phase accumulated. This trend is also shown in the dipping grid scenario.

An interesting finding is in layer 5 and layer 6, where it differs from the dipping grid scenario. In the dipping properties scenario, when the CO_2 is injected initially, both layers show increasing CO_2 in gas phase, and while the injection stops, it declines. When injected at a higher rate, a high incremental is shown in both dissolved CO_2 in water and the CO_2 in gas phase. In layer 5, it started to decrease directly even when the injection was ongoing, while layer 6 kept the increasing trend. This happens because the migration of CO_2 from layer 5 to the upper layer happens faster than the migration from layer 6 to layer 5 since there is fine sand between layer 6 and layer 5 for this realization (Figure 3.18).

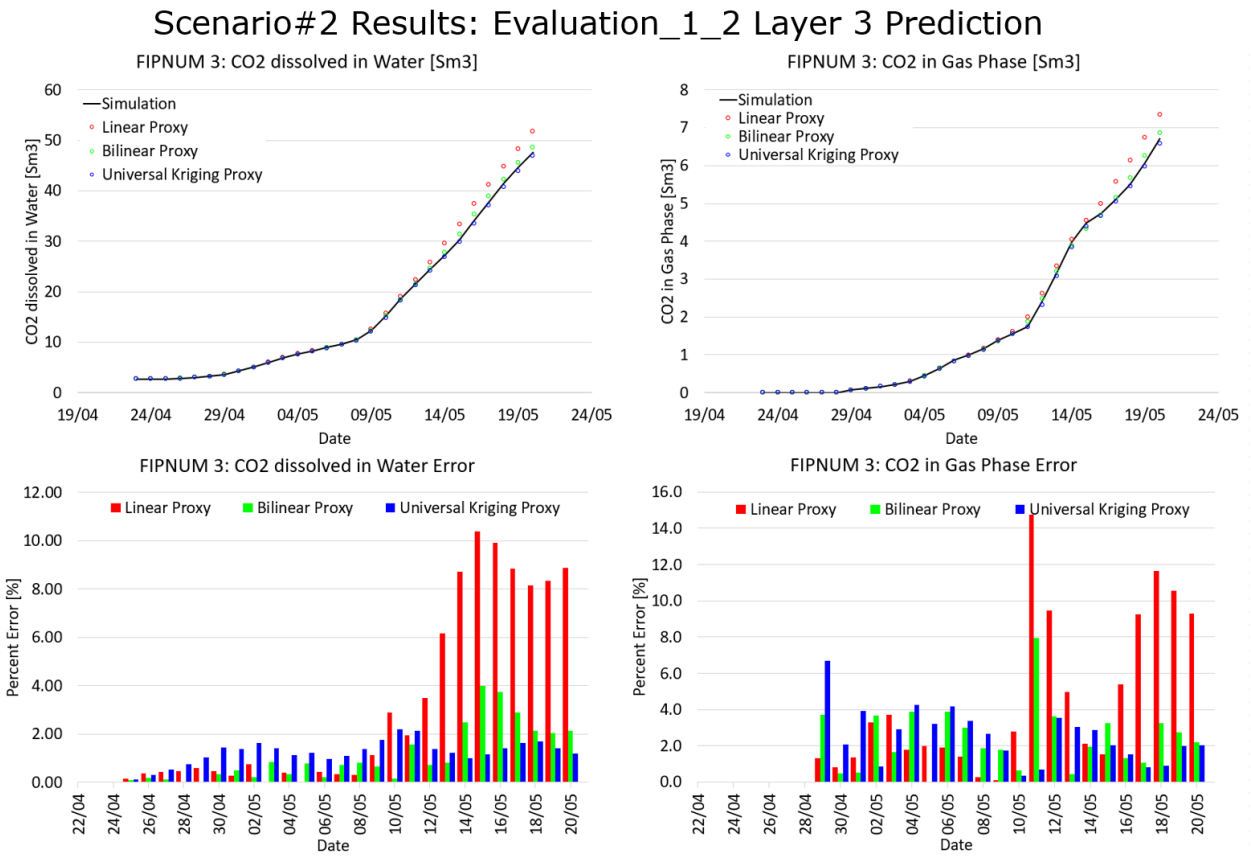

Figure 4.39: Evaluation_1_2 dissolved CO_2 and CO_2 in gas phase layer 3 prediction (scenario#2)

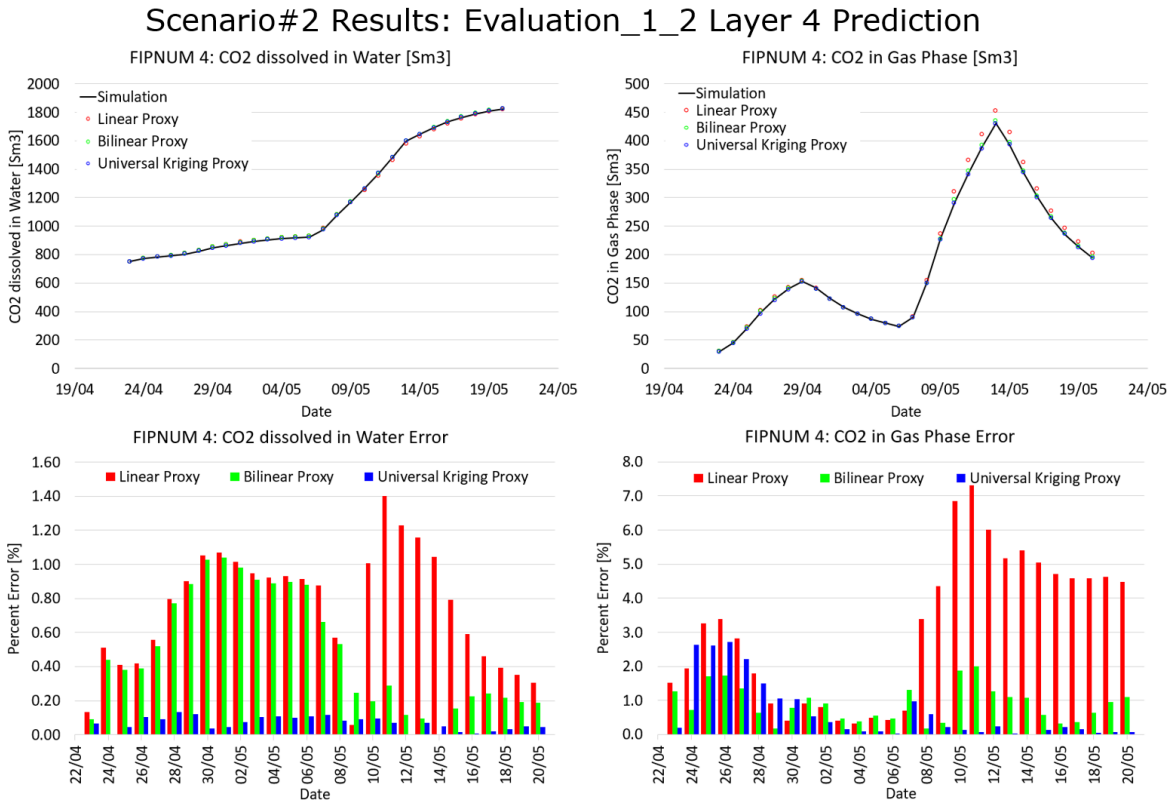

Figure 4.40: Evaluation_1_2 dissolved CO_2 and CO_2 in gas phase layer 4 prediction (scenario#2)

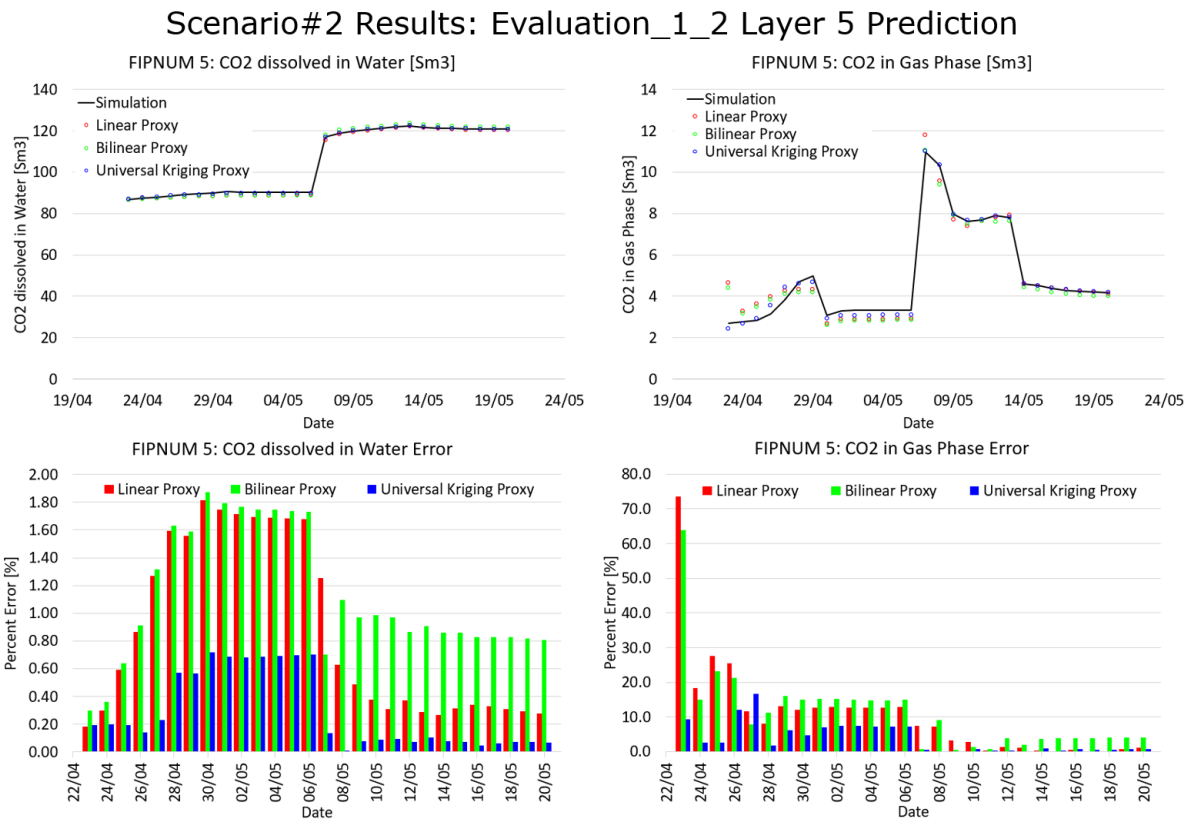

Figure 4.41: Evaluation_1_2 dissolved CO_2 and CO_2 in gas phase layer 5 prediction (scenario#2)

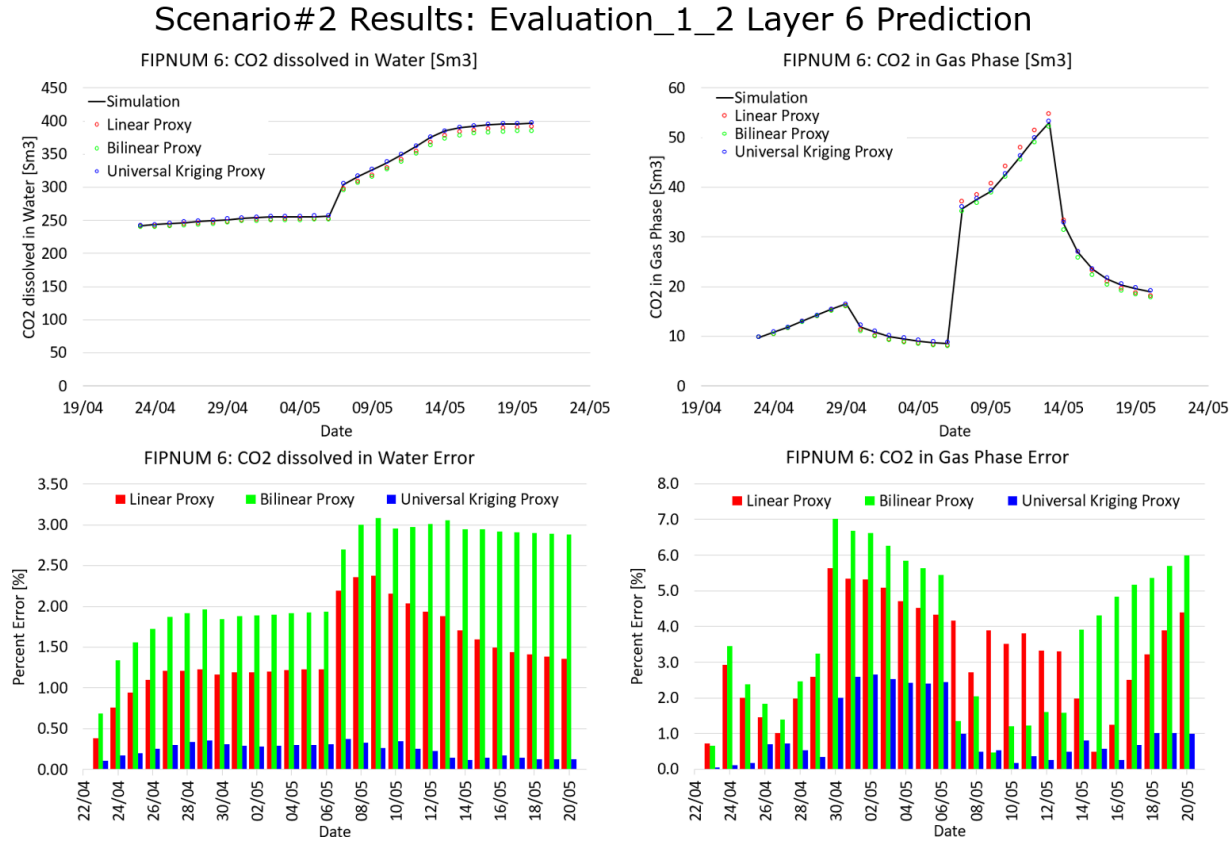

Figure 4.42: Evaluation_1_2 dissolved CO_2 and CO_2 in gas phase layer 6 prediction (scenario#2)

4.2.5 Proxy Models Limitations

With the limited training dataset and input variables for the proxy, there are several limitations when the proxy model is able to be used for prediction. The limitations are listed below:

1. The training dataset has a minimum CO2 injection rate of 21.42857 Sm3/d and a maximum CO2 injection rate of 192.8571 Sm3/d. Therefore, the proxy model cannot accurately outside the range.
2. The proxy models currently only take two inputs: the 1st CO_2 injection rate and the 2nd CO_2 injection rate. A pre-set injection design consists of two CO_2 injection cycles with 1 week of injection and 1 week of shut-in period for each cycle.
3. The CO_2 injection rate is constant through the injection period.

4.2.6 Results summarization

Chapter 4.2 describes the development, training, validation and evaluation of the proxy models to mimic the prediction of CO_2 injection in the Svelvik CO_2 Field Laboratory.

The proxy models use two independent variables as input: 1st cycle and 2nd cycle CO_2 injection rate. The predicted results from the proxy models are the Svelvik#2 bottomhole pressure, average field pressure, field dissolved CO_2 in water and CO_2 in gas phase. The proxy models are also capable of predicting layered dissolved CO_2 and CO_2 in gas phase. The layering definition is shown in Figure 3.18. The proxy models are developed for both geological scenarios.

Two types of proxy models are studied: response surface proxy and universal kriging proxy. With the results presented, it is shown that the universal kriging results have a lower percent error than the universal kriging proxy. The limitation of the response surface proxy is it only follows the general equation (Equation (1)) that is fitted to the simulation results to obtain the coefficient. Therefore, the response surface is only limited to the linear, bilinear function. The universal kriging shows a better result with the advantage of increasing the likely outcome from the Gaussian process.

Based on the evaluation results, all proxy models are highly correlated with the simulation results with R^2 above 0.99. It means that the proxy models are able to mimic the results from numerical simulation and can be used to design a further CO_2 injection in the Svelvik CO_2 field laboratory. The successful development of the proxy can save the time required to run a simulation that requires hourly per case to a matter of seconds.

The limitations of current proxy models are: the design only for 2 cycles of CO_2 injection with 1 week of injection period and 1 week of shut-in period per cycle, the CO_2 injection rate is assumed to be constant during the injection period, and finally, the input for the CO_2 injection rate is limited to the range of 21.42857 Sm3/d and 192.8571 Sm3/d since the training data is limited to that range.

5 Conclusions

A thorough study starting from understanding the Svelvik CO_2 Field Laboratory and the Pre-ACT 2019 injection campaign data, uncertainty definition based on the observed data, history matching with the monitoring results, and finally, the development of the proxy model of Svelvik to be used for the next injection campaign is completed.

Following the successful Pre-ACT 2019 injection campaign in Svelvik CO_2 Field Laboratory, several valuable insights and initial interpretation results are used to improve the reservoir model. The Pre-ACT injection campaign consists of a water injection period and CO_2 injection period with the Svelvik#2 bottomhole pressure and injection rate recorded (Figure 2.9). The initial interpretation shows that the CO_2 migrates to the upper mud layer at a depth of ~38m (Figure 2.10).

The initial history matching result shows a higher Svelvik#2 bottomhole pressure is required while injection happens in the geological model realizations (Figure 4.4). It is also shown in the water injection result, where the bottomhole pressure required to inject the amount of water is higher in the simulation than in the measure data (Figure 4.1). The best match from the history matching shows that the permeability from the geological model is multiplied by 5 with an average percent error of 0.22% (0.016 bar) and maximum percent error of 1.01% (0.074 bar) to the Svelvik#2 bottomhole pressure. The history matching results conclude that a higher permeability than the current geological model is required to match the measured data.

During the CO_2 injection, with the initial geological model, the CO_2 is spreading horizontally at the injection depth (Figure 4.5 & Figure 4.6) and it is impossible to migrate to a higher layer, as seen in Figure 2.10. This observation concludes that there is a migration path from the injection depth to the upper layer ~38m, which could be due to the discontinuation of the mud layer by sand lobes. This observation also portrays that the CO_2 is leaking to the surface through the annulus filled with bentonite slurry. With the lithofacies of the lower mud layer (50.7 – 61.2 m) being changed to sand in combination with the vertical leakage along the well, it allows the migration of the CO_2 to the upper layer (Figure 4.10 & Figure 4.11) with a result similar to the initial observation results (Figure 2.10). The dipping grid scenario spread more to the East-West direction, while the dipping properties scenario spread more to the North direction. The simulation results during CO_2 injection show a match with the measured data. However, after the CO_2 injection is stopped, the simulation results could not match with the declining measured bottomhole pressure due to the simulation result stabilizing with the initial pressure (with the assumption of an open boundary aquifer to a large extent).

Finally, two types of proxy models (response surface and universal kriging) are successfully built during the study for two geological realizations. With the input of CO_2 injection rate for each injection cycle, several parameters from the dissolved CO_2 in water, CO_2 in gas phase, average field pressure, and Svelvik#2 bottomhole pressure can be predicted with R^2 more than 0.99. The proxy models can be used for layer prediction to detect the migration throughout the layer defined. The universal kriging has better results than the response surface due to the nature being limited to polynomial function response, while universal kriging can predict a more complex trend. With the proxy models successfully developed, the simulation can be completed using the proxy model in seconds without running 2 – 3 hours of simulation.

6 Challenges and Further Work

6.1 Challenges

Several challenges that were met in this study are:

1. The small grid (1m x 1m) and the small timesteps (1 hour per timesteps) require high computational time. Upscaling the non-interest zone and timesteps are implemented to improve the time required to run a simulation case and reduce the memory usage.
2. The water injection measured data has an effect that is not following the ideal principle due to the different salinity of different tanks. Salinity measurement is suggested for water injection.
3. The measured injection and monitoring pressure data understanding are complex due to several required corrections. The parameters that can affect the pressure measured are the depth of the gauge, location of the transmitter, below packer volume, tide and water table fluctuation.
4. There is much uncertainty to be studied, and in combination with high computational time, the project will require an extensive hour to study.

6.2 Further Work

Several suggested further work that can refine this study are:

1. A further study of the injection and monitoring well bottomhole pressure data is required to apply a better correction before the next simulation study.
2. An improvement of the permeability geological model is required.
3. The relative permeability that is used in the simulation can be part of the uncertain parameter for history matching.
4. Implementation of the tubing performance relationship (TPR) model for the simulation is recommended and becomes one of the uncertainty parameters to match with the CO_2 injection behaviour.
5. With all uncertainty parameters gathered, a proxy model and optimization for history matching can be built. Building the proxy model for this study can be time-consuming.

References

Ahmadi, M., Zendehboudi, S. & James, L., 2018. Developing a robust proxy model of CO 2 injection: coupling Box–Behnken design and a connectionist method. *Fuel,* Volume 215, pp. 904-914.

Amini, S., Mohaghegh, S., Gaskari, R. & Bromhal, G., 2012. *Uncertainty analysis of a CO2 sequestration project using surrogate reservoir modeling technique.* s.l., s.n.

Assouline, S., 2005. On the relationships between the pore size distribution index and characteristics of the soil hydraulic functions. 41(7).

Bakk, A. et al., 2012. *CO2 Field Lab at Svelvik Ridge: Site Suitability.* s.l., s.n.

Benson, S. & Cook, P., 2005. *Underground geological storage,* Geneva: Intergovernmental Panel for Climate Change (IPCC).

Box, G. E. P., 1976. Science and statistics. *Journal of the American Statistical Association,* Volume 71, pp. 791-799.

Corey, A. & Brooks, R., 1964. Hydraulic Properties of Porous Media. In: s.l.:Colerado State University.

Eliasson, P. J. M. R. C. R. M. a. H. K., 2020. *A CO2 Monitoring Experiment for Pressure-Saturation Discrimination at the New Svelvik CO2 Field Lab,* Trondheim: SINTEF Industry.

Eliasson, P. et al., 2017 - 2020. *Pressure control and conformance management for safe and efficient CO2 storage - Accelerating CCS Technologies,* s.l.: SINTEF AS.

Grimstad, A.-A., 2013. *Report D4.4.1D Project NO. 7020087 Deep geomodel - final version,* s.l.: s.n.

Grimstad, A.-A., Sundal, A., Hagby, K. F. & Ringstad, C., 2018. *Modelling Medium-Depth CO2 Injection at the Svelvik CO2 Field Laboratory in Norway.* Melbourne, s.n.

Hagby, K. F., 2018. *Modelling Medium-Depth CO2 Injection at the Svelvik CO2 Field Laboratory in Norway,* Trondheim: NTNU Master Thesis.

Iman, R., 2008. *Latin Hypercube Sampling,* s.l.: Encyclopedia of Quantitative Risk Analysis and Assessment.

Jaber, A., Al-Jawad, S. & Alhuraishawy, A., 2019. A Review of Proxy Modeling Applications in Numberical Reservoir Simulation. *Arabian Journal of Geosciences,* Volume 12, p. 701.

Jaber, A., Awang, M. & Lenn, C., 2017. Box-Behnken design for assessment proxy model of miscible CO 2-WAG in heterogeneous clastic reservoir. *Journal of Natural Gas Science and Engineering,* Volume 40, pp. 236-248.

Jordan, M. & Weinzierl, W., 2020. *Svelvik CO2 Field Lab: Review of the 2019 injection campaign and interpretation of acquired data,* s.l.: Pre-ACT Webinar 6.

Krevor, S. B. M. J. B. S. M. P. C. H., Reynolds, C. & Al-Menhali, A. N. B., 2015. *Capillary trapping for geologic carbon dioxide storage - From pore scale physics to field scale implications..* s.l., s.n.

Lønne, I., 1995. Sedimentary facies and depositional architecture of ice-contact glaciomarine systems. *Sedimentary Geology,* 98(1-4), pp. 13-43.

Matthew, D. A. M., 2021. *Proxy Modeling for CO2-EOR Design Study: Water Alternating Gas and Storage,* Trondheim: MSc Thesis NTNU.

Meehan, D., 1980. A correlation for water compressibility. *Petroelum Engineer,* Volume 35, pp. 117-118.

Meehan, D., 1980. Correlation for water viscosity. *Petroleum Engineer,* Volume 56, pp. 125-126.

Melø, T., 2011. *Hydrogeology of the shallow aquifer at the Svelvik ridge,* Oslo: MSc Thesis, University of Oslo.

Naylor, M., Wilkinson, M. & Haszeldine, R., 2011. Calculation of CO2 column heights in depleted gas fields from known pre-production gas column heights. Volume 28.

Nazarian, B., 2021. *Reservoir engineering of CO2 storage (NTNU Presentation),* Trondheim: s.n.

NGU, 2018. *Maps and Data, Norges geologiske undersøkelse.* [Online]
Available at: http://geo.ngu.no/kart/minkommune/?kommunenr=628
[Accessed 06 08 2022].

R&P Geo Services AS, 2012. *D2-3-1A-2_Svelvik-well-logging-in-permeabiliy-test-well_jan-2013,* s.l.: s.n.

Ringrose, P., 2020. *How to Store CO2 Underground: Insights from early-mover CCS Projects.* s.l.:Springer.

Schlumberger, 2014. *Schlumberger Glossary.* [Online]
Available at: https://glossary.oilfield.slb.com/ja-jp/terms/a/aquifer
[Accessed 12 April 2022].

Schlumberger, 2016. *Eclipse Technical Description,* s.l.: s.n.

Schlumberger, 2019. *Petrel Guru,* s.l.: s.n.

Schuetter, J., Mishra, S., Ganesh, P. & Mooney, D., 2014. Building Statistical Proxy Models for CO2 Geologic Sequestration. *Energy Proceedia,* Volume 63, pp. 3702 - 3714.

SINTEF, 2010. *CO2 Field Lab.* [Online]
Available at: https://www.sintef.no/projectweb/co2fieldlab/
[Accessed 06 08 2022].

Sørensen, R., 1981. *Foreløpig beskrivelse til kvartærgeologisk kart SVELVIK – CL 083, M1:10 000,* s.l.: The Geological Survey of Norway, Report 1807/7.

Sørensen, R., Lie, K. & Nybakken, S., 1990. *DRØBAK 1814 II, kvartærgeologisk kart – M 1:50000,* s.l.: Norges geologiske undersøkelse.

Wiranda, W., 2021. *Simulation of Svelvik CO2 Field Laboratory Injection Experiment,* Trondheim: Specialization Project NTNU.

Zubarev, D. e. a., 2009. *Pros and cons of applying proxy-models as a substitute for full reservoir simulations.* s.l., s.n.

Appendices

Appendix 1: Svelvik CO_2 Field Laboratory Data Availability

Appendix 2: Carter-Tracy Aquifer Model

Appendix 3: Anisotropy study

Appendix 1: Svelvik CO_2 Field Laboratory Data Availability

Svelvik#1 Well Data

Svelvik#1 as an exploration well was drilled in July 2010 in the Svelvik sand ridge in Hurum, Norway. The well was drilled with the depth of 333m with several data were taken from the well.

Core analysis report

One-meter-long core samples were taken at 30, 102 and 201 m mean sea level. The water permeability and porosity were measured on these core samples and on a surface sample from 40m above mean sea level.

Core analysis report summary

Parameter	Unit	Depth 40m asl	Depth 30m msl	Depth 102m msl	Depth 201m msl
Composition	-	100% high porosity and permeability sand	70% high permeability sand 30% water	20% clay 80% silty unconsolidated sand	70% clay 30% silty unconsolidated sand
Porosity (water)	-	~0.3-0.4	0.351	0.302	0.127
Permeability	mD	2521.1	1016 – 2567	223.9	7.9

The core analysis report also reported water analysis that were extracted from cores at depth of 102 and 201 m with additional sample of the drilling mud at 232 m.

The results are summarized in **Error! Reference source not found.**. and shows that the total salt concentration is approximately 0.2% (2000 ppm) and is essentially fresh water. These results are not very related to the injection point interest.

Summary of water analysis at various depth

Specie	Result, mg/litre			PQL[1)]		Method	Uncertainty[2)]
	102 m	**201 m**	**232 m**	**Lower**	**Upper**		**Relative/absolute**
Sodium, Na	956	1080	991	0.1	100000	I-1-29	±15%/±0.1
Calcium, Ca	2.9	26.6	47.5	0.1	50000	I-1-29	±10%/±0.1
Magnesium, Mg	0.1	<0.1	3.7	0.1	50000	I-1-29	±15%/±0.1
Barium, Ba	0.1	0.1	2.9	0.05	50000	I-1-29	±10%/±0.1
Iron, free, Fe	0.6	0.1	1.7	0.1	50000	I-1-29	±10%/±0.1
Strontium, Sr	0.1	0.4	0.4	0.05	50000	I-1-29	±10%/±0.1
Potassium, K	28.8	30.1	32.4	0.1	100000	I-1-29	±15%/±0.1
Sulphur, S	131	121	218	0.1		I-1-29	±10%/±0.1
Chloride, Cl	720	810	990	1		ISO 10304-2	±10%/±0.1
Total	1839.6	2068.3	2287.6				

1) PQL, Practical quantification limits
2) Both relative and absolute uncertainties are reported. The larger argument is always the valid one

Grain size report

127 spectral gamma measurements and 27 grain size distribution analysis was carried out on selected flow line samples from Svelvik#1. The analyses revealed a silt dominated lithology with a number of sand horizons.

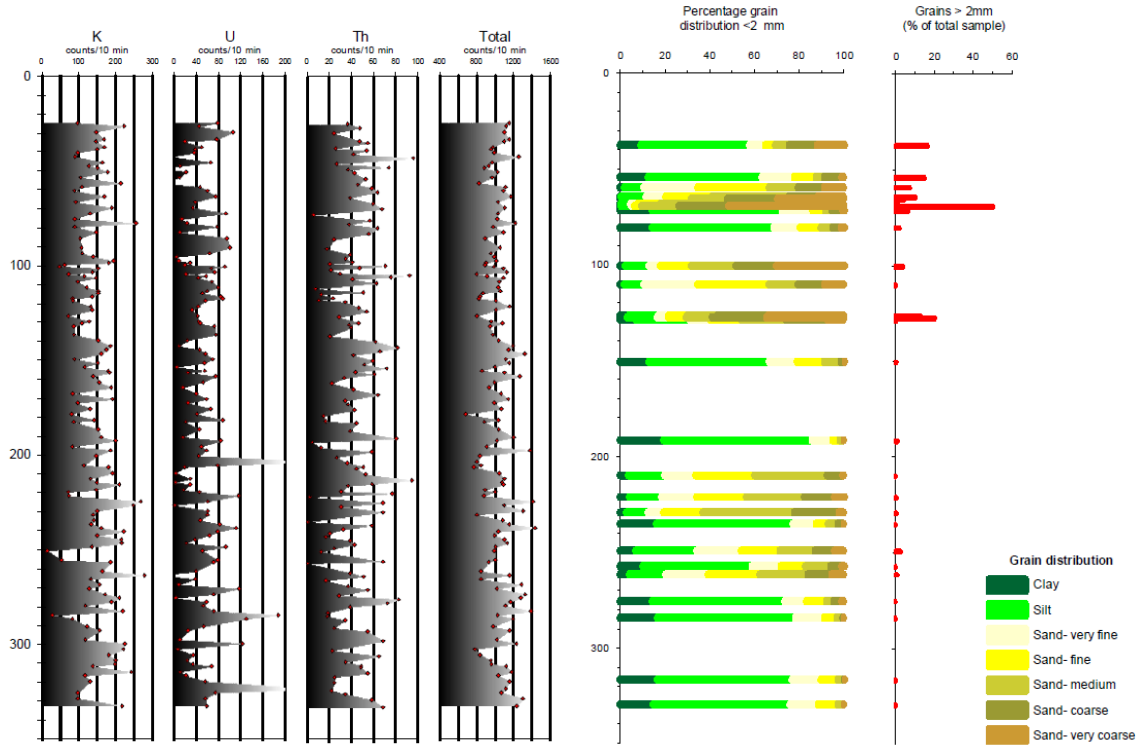

Spectral gamma measurements and grain size distribution

Sand intervals and descriptions

Intervals (m)	Sample (m)	Description
37.1 – 50.7	37 – 38	9% clay, 49% silt, and sand mainly coarse to very coarse.
61.2 – 71.2	64 – 65	Fine to very coarse sand and with about 10% coarser grains in the granule/pebble category 11% silt but clay is absent Coarser downward
	67 – 68	4% silt, medium to very coarse sand dominated
85 – 115	100 – 101	An upper sandy part from 85 to 95m A more clayey horizon at 95 – 96. Sample dominated by fine to very coarse sand (85%). In addition, 15% very fine sand and silt, almost no clay
	110 – 111	Well sorted sample dominated by very fine to fine sand (50%) 30% sand in the medium to very coarse 9% silt and 2% clay
122 – 130.8	126 – 127	Relatively poor sorted with 4% clay, 13% silt, and sand from very fine to very coarse

220 - 236	221 – 222	Sample has 4% clay and 16% silt Very fine to coarse sand
	229 – 230	Sample has 3% clay and 15% silt. Slightly better sorted than sample 221 -222. 80% sand in the range of fine to coarse.

Based on the well-logs, 7 sand intervals are defined. The intervals and description of each interval are summarized.

Well log data

Well log data available as spectral gamma ray has been reported from the grain size report shown below. The other well log data available in this well is based on the Petrel project that has been provided in which the induction and dual laterolog resistivity logs are included.

The resistivity values vary between 2 and 7ohmm for the entire log section. These observations are applicable on each layer, which were identified as high sand content.

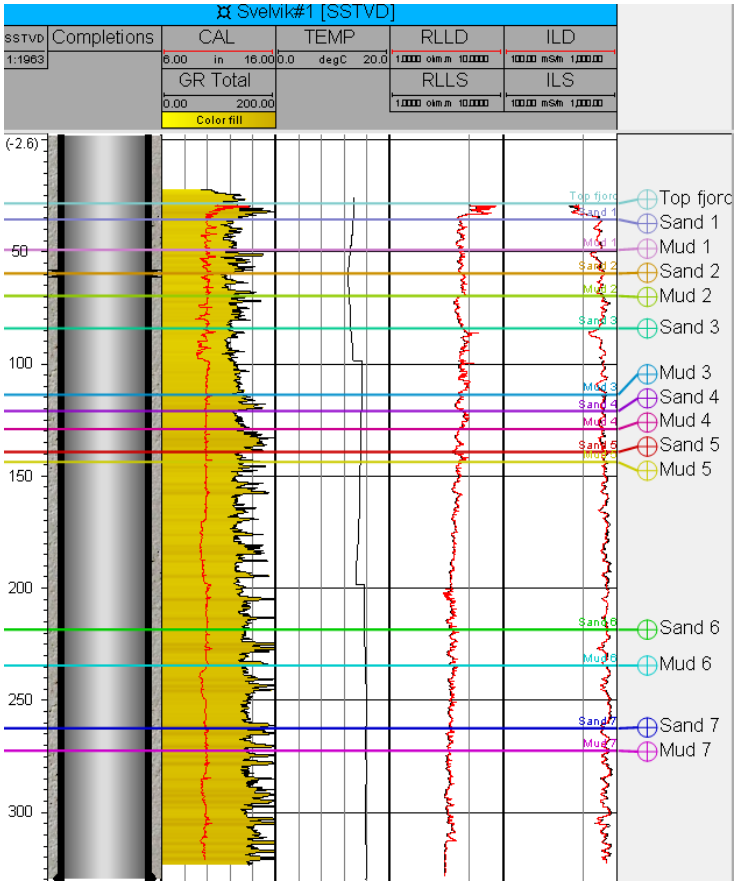

Well log of Svelvik#1

Svelvik#2 Well Data

Svelvik#2 is currently an CO_2 injection well where the well logging was performed from 15th December to 16th December 2012. The data available after the well logging are gamma ray (GR), caliper (CALI), acoustic log (TT), temperature (TEMP), and dual laterolog resistivity shallow and deep (RLLS and RLLD) from depth 20 – 80 m.

Well log data

The full well log data is available on D2-3-1A-2_Svelvik-well-logging-in-permeabiliy-test-well_jan-2013_Report (R&P Geo Services AS, 2012). Based on the interpretation of gamma and clay content logs, the sand layer can be identified are from 36.2 – 49.8 m and 60.4 – 70.9 m. These intervals very well correspond to the previous interpretation of sand layer in Svelvik#1 well which has the sand interval from 37.1 – 50.7 m and 61.2 – 71.7 m.

The summary of the well log data can be seen in the petrel project

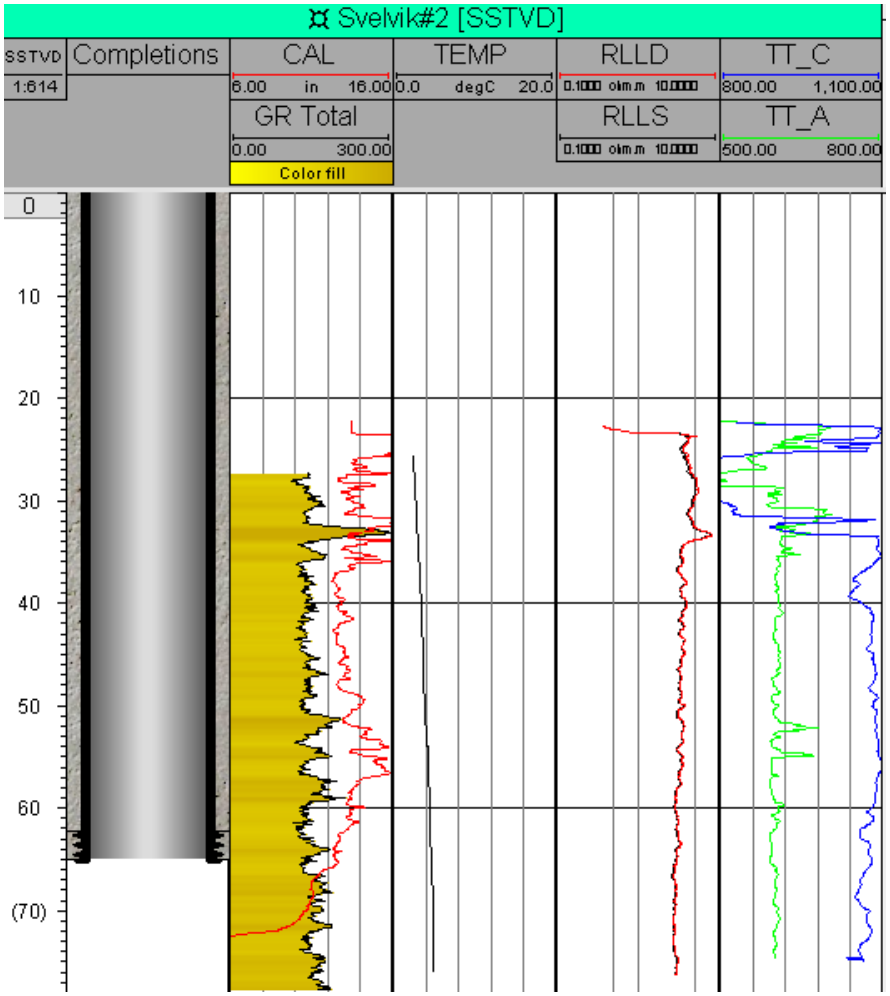

Well log of Svelvik#2

Appendix 2: Carter-Tracy Aquifer Model (Based on Schlumberger Eclipse Technical Description 2016.2) (Schlumberger, 2016)

There are two main parameters governing the Carter-Tracy aquifer model behaviour: time constant (Equation A.1) and aquifer influx constant (Equation A.2).

$$T_c = \frac{\mu_w \phi C_t r_o^2}{k_a c_1} \tag{A.1}$$

Where:

μ_w is the viscosity of water in the aquifer

ϕ is the aquifer porosity

C_t is the total (rock + water) compressibility

r_o is the outer radius of the reservoir (or inner radius of the aquifer)

k_a is the aquifer permeability

c_1 is 0.008527 (METRIC, PVT-M); 0.006328 (FIELD); 3.6 (LAB)

$$\beta = c_2 h \theta \phi C_t r_o^2 \tag{A.2}$$

Where:

h is the aquifer thickness

θ is the angle subtended by the aquifer boundary from the center of the reservoir, in degrees, divided by 360°

ϕ is the aquifer porosity

C_t is the total (rock + water) compressibility

r_o is the outer radius of the reservoir (or inner radius of the aquifer)

c_2 is 6.283 (METRIC, PVT-M); 1.1191 (FIELD); 6.283 (LAB).

The time constant (T_c) calculation is to calculate the dimensionless time and the Carter-Tracy model can expresses the pressure drop at the aquifer boundary in terms of the dimensionless pressure influence function.

$$p_{a0} - \bar{p} = \frac{Q_a}{\beta} PI_D(t_D) \tag{A.3}$$

Where:

Q_a is the aquifer inflow rate

p_{a0} is the initial pressure of water in the aquifer

$\bar{p}$ is the average water pressure on the aquifer/reservoir boundary.

The average aquifer inflow rate is calculated in grid block *i* over simulation time interval as

$$\overline{Q_{ai}} = \alpha_i \{a - b[p_i(t + \Delta t) - p_i(t)]\} \tag{A.4}$$

Where:

$$a = \frac{1}{T_c}\left\{\frac{\beta\Delta p_{ai} - W_a(t)(PI'_D)(t+\Delta t)_D}{PI_D(t+\Delta t)_D - t_D PI'_D(t+\Delta t)_D}\right\}$$

$$b = \frac{\beta}{T_c[PI_D(t+\Delta t)_D - t_D PI'_D(t+\Delta t)_D]}$$

Δp_{ai} is the pressure drop $p_{a0} + \rho g(d_i - d_a) - p_i(t)$

$PI_D{}'$ is the derivative of PI_D to t_D

α_i is the area fraction for each connection

The area for each connection is calculated by the block face communicating with the aquifer with the aquifer influx coefficient multiplier by Equation A.5.

$$\alpha_i = \frac{m_i A_i}{\sum m_i A_i} \tag{A.5}$$

Where:

$A_i$is the area of the block face communicating with the aquifer.

m_i is an aquifer influx coefficient multiplier

Appendix 3: Anisotropy Study

A previous anisotropy study is shown in figure below

The mud layer on the depth of 52 – 58m is modified to coarse sand.

Without the vertical leakage introduced along the well, the permeability anisotropy required for the CO_2 plume to migrate to the upper mud layer is 2. Permeability anisotropy of 0.1 will only gives a lateral movement, therefore a vertical path is needed when anisotropy is 0.1.

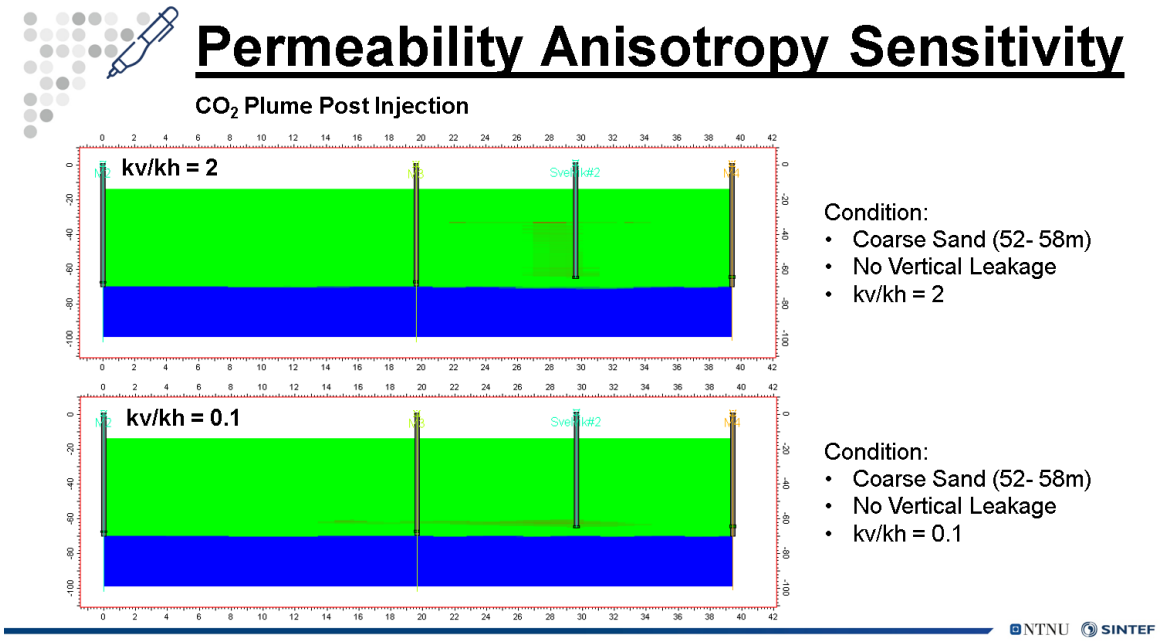

Wilson Wiranda

Simulation of Pre-ACT Injection and Development of Proxy Model for Svelvik CO2 Field Laboratory

NTNU
Kunnskap for en bedre verden